REVIEW

Check for updates

Advances in the chemical analysis of nitrite in environmental and biological samples

Nadeen Rajab, [ID] [a] Hosny Ibrahim,[b] Daohong Zhang,[cd] Ahmed F. A. Youssef [ID] *[abe] and Rabeay Y. A. Hassan [ID] *[a]

Nitrite, a potential environmental pollutant, poses a significant threat to human health. Thus, accurate and sensitive detection methods are essential for effective continuous monitoring and surveillance. In this regard, a wide range of instrumental methods for the precise determination of nitrite in different types of complex samples is collected and discussed. Besides the classical methods, chromatographic and spectroscopic techniques are included. Although these methods exhibit high sensitivity and selectivity, they involve high cost and complicated operating protocols, and warrant high caution in sample preparations. Other reported techniques, such as electrochemical and bio-electrochemical methods, could offer onsite detection and disposability, and involve handheld devices. Such features are required for simple optimization, field applicability for analysis of a large number of samples, fast response, simple device calibration, and validation. Thus, nanostructure-based electrochemical approaches are widely developed and applied in the analysis of target analytes in complex biological and environmental matrices using a few microlitres of the samples, without any prior sample preparation. Therefore, to consider the global market's needs, challenges, and perspectives on each reported method for nitrite, a comprehensive discussion has been included in this review.

[a]Biosensors Research Lab, Zewail City of Science and Technology, 6th October City, Giza, 12578, Egypt. E-mail: ahyoussef@zewailcity.edu.eg

[b]Chemistry Department, Faculty of Science, Cairo University, Giza, 12613, Egypt

[c]College of Food Engineering, Ludong University, Yantai, 264025, Shandong, China

[d]Bio-Nanotechnology Research Institute, Ludong University, Yantai, 264025, Shandong, China

[e]Environmental Engineering Program, Zewail City of Science and Technology, 6th October City, Giza, 12578, Egypt

Nadeen is a Masters candidate in Analytical Chemistry, holding a Bachelor of Science degree from Cairo University. Her graduate research focused on the development of advanced nitrite sensors, culminating in a peer-reviewed publication in RSC Advances and the successful acquisition of a patent prior to its publication. Currently, Nadeen serves as a Research Assistant at Zewail City, where her ongoing work is dedicated to pioneering novel nanosensor technologies. Her expertise lies in devising sophisticated analytical solutions for critical environmental and biological applications.

Nadeen Rajab

Dr Hosny Ibrahim is a prominent Professor of analytical chemistry in the Department of Chemistry at Cairo University's Faculty of Science, and has completed his BSc, MSc, and PhD degrees. With a career spanning several decades, he has made significant contributions to the development of spectral and electrometric analysis methods. Dr Ibrahim has authored and co-authored over 50 scientific papers published in reputable journals. His academic leadership includes supervising more than 20 masters and doctoral theses, helping to cultivate a new generation of researchers in the field and also, participating in numerous scientific conferences across Egypt, USA, etc., contributing actively to international scientific discourse.

Hosny Ibrahim

1 Introduction

Excessive use of nitrite in modern industry releases variable free nitrite ions into the environment, which disrupts our ecological life.[1] Accordingly, harmful effects on humans and animals are exerted. Nitrite can interact with hemoglobin, forming methemoglobin, by the oxidation of Fe^{2+} to Fe^{3+}, causing hemoglobin to release oxygen, which leads to tissue hypoxia and methanoglobinaemia.[2]

Free ions of nitrite can interact with secondary amines and form teratogenic nitrosamines which cause gastric cancer,[3] infertility in men by affecting sperm morphology and number,[4] activation of the synthase pathway of adenosine monophosphate protein kinase-endothelial nitric oxide in human aortic endothelial cells,[5] and apoptosis of grass carp liver cells,

which leads to endoplasmic reticulum stress.[6] For all these reasons, the World Health Organization (WHO) standards stipulate that the maximum allowed concentration of NO_2 in drinking water is 43 ppm.[7] In addition, the European Union Scientific Committee on Food (SCF) has set a daily intake of nitrite of 0.06 mg kg^{-1} for humans, while the Chinese national standard has set the maximum use of nitrite in marinated and cured meat to be 0.15 g kg^{-1}.[8] Therefore, rapid and sensitive nitrite detection has become a very critical need to protect public health and the environment.[9] In this review, the interconnection between these different detection methods is visually summarized in Scheme 1. Additionally, recent advances in nitrite detection, including various nitrite determination methods, are comprehensively reviewed as shown in Scheme 2.

2 Traditional analytical methods for nitrite detection

For decades, traditional analytical methods, relying on straightforward chemical reactions for measurable signals (e.g., color change), have been fundamental for nitrite quantification. These accessible, low-cost techniques, though still useful, often face limitations. Challenges include susceptibility to interferences from complex samples, variable sensitivity, and lengthy analysis times, impacting their overall efficiency and accuracy in modern applications.

2.1. Spectroscopic methods

The Griess method has been used for several decades for nitrite detection due to the advantages of low cost and simplicity. It employs a two-step process, nitrite-mediated diazotization of a suitable aromatic amine under acidic conditions, followed by a coupling reaction.

This results in the formation of a brightly colored azo chromophore. The concentration of this chromophore, typically

Daohong Zhang

Daohong Zhang earned her PhD from the Chinese Academy of Agricultural Sciences in 2011. She currently serves as a professor at the College of Food Engineering, Ludong University, Yantai, Shandong, China. With over 10 years of expertise in biosensors for environmental, food, and healthcare applications, her research focuses on developing on-site solutions to monitor environmental and foodborne hazards posing risks to human health. She has published over 150 papers in prestigious SCI journals. Her h-index is 42 (per SCOPUS), and she is included in Stanford University's list of the top 2% most influential scientists worldwide.

Ahmed F. A. Youssef

Ahmed Fahmy A. Youssef, PhD in Analytical Chemistry – Cairo University, visiting professor – Chemistry Department – University of Massachusetts (UMass) – Amherst, USA, JICA visiting program Hokkaido University, Japan, Safety training program – Fellow – IUPAC: Bayer CropScience, USA. Currently he is a full-time associate professor in the Environmental Engineering Program in Zewail City of Science, Technology and Innovation. He is an expert in chemical management in academic institutions, former director of the Center for Environmental Hazard Mitigation (CEHM), Cairo University, and has developed many integrated chemical management curricula and training programs in developing countries.

Rabeay Y. A. Hassan

Professor Rabeay Y. A. Hassan, Director of the Biosensors Research Centre at Zewail City of Science and Technology, Egypt, received his PhD from Braunschweig University of Technology, Germany. His experience includes postdoc. work at the University of Potsdam (2013) and UMONS (2014), plus a visiting professorship at the University of California (2015). Dr Hassan's distinctions include fellowships from the NAS, Erasmus-Mundus, DAAD, and a silver medal at the 48th International Exhibition of Inventions of Geneva. Serving as an Associate Editor for Frontiers in Chemistry, his research focuses on nanosensor development for diverse applications.
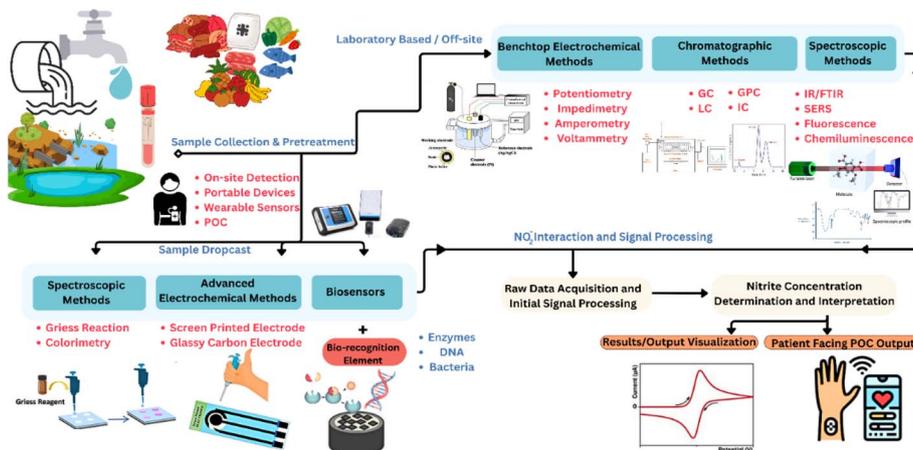
Scheme 1 Comprehensive overview of advanced instrumental methods for nitrite detection, illustrating their interconnections and diverse applications.
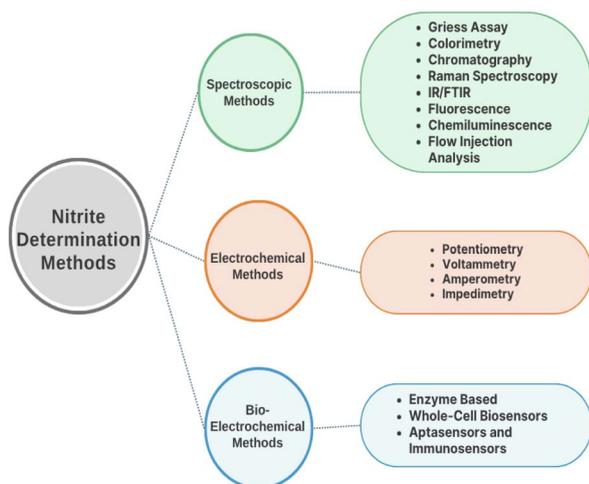
Scheme 2 Common methods used for the selective and sensitive detection of nitrite in complex matrices.

Fig. 1 Griess assay principle.

measured spectrophotometrically between 500 and 600 nm, serves as a direct indicator of the initial nitrite concentration, as shown in Fig. 1. The Griess reaction, first reported in 1879, is specific for nitrite and has been widely used for its identification in biological fluids like saliva, urine, and blood, particularly in the context of bacterial infections and the L-arginine/nitric oxide pathway. Analysis of nitrate by this reaction requires prior chemical or enzymatic reduction to nitrite, and it relies on the color produced when azo dyes react with free nitrite ions. The best coupling component of the nitrite analysis is N-(1-naphthyl)-ethylenediamine (NED), which produces a violet-red color at a wavelength of 540 nm.[10] Despite its simplicity and inexpensive feasibility, the traditional batch Griess assay faces numerous interferences in complex biological fluids.

Despite its analytical limitations and the lack of sensitivity, the Griess reaction can be employed in fluorescence, colorimetry, chromatography, and Raman spectroscopy. Hao *et al.* prepared a dual-mode colorimetric/fluorometric approach
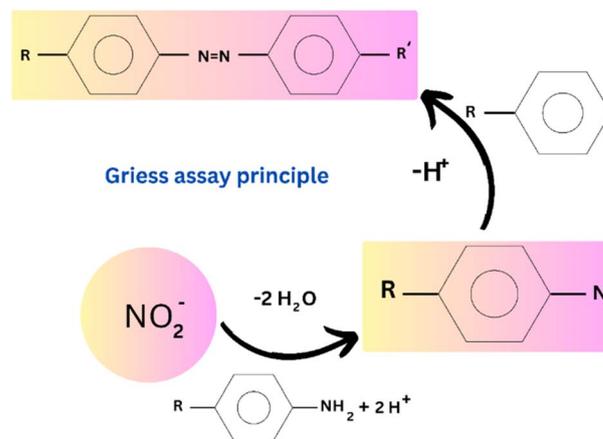
depending on the diazo-coupling reaction of m-phenylenediamine (m-PDA), which reacted with nitrite in an acidic medium and produced fluorescent primary aromatic amine derived carbon dots (PAA-CDs).[11] These PAA-CDs, obtained by a one-step solvothermal treatment of m-PDA, possess a high quantum yield (46%), good water solubility, high photobleaching resistance (enhancing stability), and low toxicity. The mechanism depends on how the PAA-CDs and nitrite interact with each other, which is dependent on how m-PDA reacts. This causes strong fluorescence quenching and clear changes in absorption. Simultaneously, a chromogenic diazo coupling reaction causes significant colour changes. This dual-signal output (fluorescence intensity and absorbance, with smartphone imaging under visible and UV light) enhances the reliability of detection results by minimizing false positives often associated with single-signal methods. The sensor was very selective and good at blocking interference. It performed well for dynamically detecting nitrite in a variety of food samples, which means it was able to tolerate matrix effects well.

Sun[12] developed a rapid, dual-mode sensing methodology for nitrite, employing N-(1-naphthalene)-ethylenediamine-derived carbon dots (NETH-CDs) as signalling probes. These NETH-CDs, synthesized through electrolysis, possess notable optical characteristics (quantum yield [QY] of 27.1%). They effectively accelerate the kinetics of the nano-interfacial Griess assay reaction, achieving completion within 1 minute. This represents a substantial improvement in reaction speed compared to conventional Griess assays, which typically require 15–30 minutes. This accelerated kinetics is attributed to synergistic interactions like electrostatic attraction, enriched localized NETH concentration, and surface adsorption on the nano surface. The carbonization of NETH not only enables the fluorescence sensing mode but also facilitates this rapid reaction. The system demonstrated high selectivity and sensitivity (LOD of 0.10 μM for colorimetry and 0.08 μM for fluorimetry). Its application was demonstrated in genuine samples such as urine, serum, sewage, and lake water, which showed accurate nitrite analysis. Furthermore, visual nitrite sensing was performed with NETH-CD-loaded test strips, demonstrating their viability for on-site applications. The dual-mode technique improves dependability and minimizes potential interferences, making it resilient for different matrices.

In another study, the Singhaphan group developed a platform made of cellulose thread modified with p-aminobenzoyl groups and a chromotropic acid reagent to ensure that diazonium ions were evenly distributed during the diazotization reaction along the thread in the presence of nitrite.[13] This was followed by a coupling reaction with a chromotropic acid, resulting in the production of a pink azo dye. To maintain the acidic conditions required for the diazotization reaction and enhance the intensity of the pink color of the azo dye, citric acid was added to the chromotropic acid and sulfuric acid solution to suppress the alkalinity of the tested samples, achieving recoveries ranging from 92.4% to 115.4%, which were confirmed by Surface-Enhanced Raman Spectroscopy (SERS).

A new colorimetric method was developed to detect nitrite levels in processed meat products.[14] Griess-doped polyvinyl alcohol G-PVA films were used for reacting nitrite with sulphanilamide under acidic conditions to produce a diazonium product, which then reacted with NED to produce a purple azo dye product. The intensity of the purple color was proportional to the nitrite concentration with the limit of detection of 12.6 μg L^{-1} for effective application in food analysis. The color intensities were analyzed using a 12 MP digital camera on an iPhone 7.0. Overall, this new method provided a quick and reliable in situ way to determine nitrite levels in processed meat products, which can help ensure food safety for consumers. The main limitation is the need for a pre-prepared film, and its long-term stability or resistance to severe fouling from complex meat matrices over extended periods would be a key consideration.

A hydrogel made of 2-naphthylacetic acid-L-phenylalanine-L-phenylalanine (Nap-FF) connected with sulfanilamide was used by Tai to detect nitrite, whereas a solution containing NED of concentration 0.033% was added to the hydrogel to change the hydrogel from transparent to yellow/orange in 10 minutes with a limit of detection of 0.72 μM.[15] In another report, a simple method was developed for detecting nitrite using a diazotization reaction between nitrite and p-aminobenzoic acid (PABA) coupled with phloroglucinol in HCl medium. This method did not require pH adjustment and the resulting azo dye turned from colorless to yellow with an absorption peak at 434 nm.[16] Also, it did not require pH adjustment or temperature control, significantly simplifying sample preparation and improving practicality.

An additional platform was made from a polymer ionogel using isopropylacrylamide (NIPAMm) as a monomer, 2,2-dimethoxy-2-phenylacetophenone (DMPA) as a photoinitiator, and an N,N'-methylenebis(acrylamide) monomer (MBAAMm) as a crosslinker. The platform containing Griess reagent was combined with a paper based microfluidic PMMA device to enable the onsite detection of nitrite ions.[17] Embedded carbon dots with citric acid and ethylenediamine were used to form a platform for detecting nitrite in Chinese food. Naphthalene ethylenediamine hydrochloride (NETH) was used for the coupling reaction of nitrite. The diazotization reaction was initiated by sulfanilic acid (SA), followed by the reaction between CA/EDA-CD and the nitronium ion (NO$^+$), resulting in a yellow-colored azo product obtained at 445 nm. The purple color produced from the reaction between NETH and the diazonium derivative confirmed the coupling reaction. This method showed a recovery rate of 95–105% and a limit of detection of 9.6 μg L^{-1}. Additionally, imidazole derivative [1,2-d] was used to produce the colorimetric probe 8-(4-amino-phenyl)-7H-acenaphtho[1,2-d]imidazole to rapidly detect nitrite in 20 seconds, and it exhibited diazo-like behavior. Nitrite indication was detected by the color change from colorless to intense yellow at 120 nm. The ionogel matrix can provide improved stability for reagents and potentially some resistance to matrix effects by acting as a selective barrier. Das[18] developed a colorimetric sensor for the sensitive detection of both nitrite and nitrate in agricultural products. This method utilized a Griess assay performed under organic acidic conditions, specifically employing itaconic acid. The researchers designed two distinct chemosensors: CE, composed of 4-aminobenzenesulfonohydrazide and 2-(2-(naphthalen-1-ylamino)ethoxy)ethanol, and CF, comprising 4-aminobenzenesulfonohydrazide and N-(1-naphthyl) ethylenediamine dihydrochloride. These chemosensors yielded characteristic pink azo dyes in the presence of nitrite. The sensing performance was evaluated using UV-spectroscopy, which revealed limits of detection (LODs) of 0.62 mM for CE and 0.52 mM for CF. For the preparation of agricultural product samples (e.g., vegetables), the protocol involved cleaning, peeling, homogenization, extraction with MeOH : H$_2$O (1 : 1), ultrasonication, dilution, and filtration. In contrast, lake and tap water samples required only simple filtration. The designed technique showed high recovery rates in real-world samples and was also capable of identifying nitrate after it had been reduced to nitrite using zinc dust. To improve usability, a smartphone-assisted sensing device based on RGB values and paper-based test strips were developed simultaneously for visual and on-site detection. Interference investigations demonstrated the system's strong selectivity against common

Table 1 Spectrophotometric detection of nitrite ions in biological and environmental matrices

Platform	Reagent	Method	Samples	Wavelength λ_{max} nm	Linear range (μM)	LOD (μM)	Ref.
PAA-CDs	m-Phenylenediamine (m-PDA)	Diazo coupling	Milk and food samples	515 nm fluorescence	3.0–40.0 μM	0.024 μM (fluorescence) and 0.16 μM (colorimetry)	11
Thread-based analytical device (μ-TAD)	p-Aminobenzoyl group and chromotropic acid	Griess assay	Water, Chinese cabbage and sausage samples	N/A	50–1000 μM	25 μM	13
Griess-doped polyvinyl alcohol film	Griess-doped mesoporous silica (G-MS sheets)	Griess assay	Processed meat	205 nm	147.96–2471.01 μM	0.274 μM	14
Hydrogel, 2-naphthylacetic acid-L-phenylalanine-L-phenylalanine (Nap-FF)	NED solution and 33% sulfanilamide	Griess assay	N/A	N/A	10.2 μM to 16 700 μM	0.72 μM	15
p-Aminobenzoic acid	Phloroglucinol (1,3,5-trihydroxybenzene)	Diazo coupling	Deionized, tap and river water	434 nm	1.09–2.17 μM	0.52 μM (UV-visible spectroscopy), 1.09 μM (naked-eye)	16
Ionogel-based hybrid polymer-paper	Mixture of sulphanilic acid (SAA) 1%, and N-1-naphthylethylenediamine dihydrochloride (NED)	Griess assay	Fresh and seawater	365 nm	0.0–217.34 μM	10.21 μM	17
CA/EDA-CDs carbon-dots	SA reagent	Diazo coupling	Cabbage, Chinese cabbage, spinach, lettuce, stir-fried pork, fried peas and pickled vegetable	440 nm	0.543–43.46 μM	0.209 μM	24
Cloud point extraction-Triton X-100	Sulfuric acid and KI	Catalytically enhanced reaction	Water and meat products	365 nm	0.174–2.61 μM	0.130 μM	21
Au nanoparticles–CeO$_2$ nanoparticles–graphene oxide hybrid nanozyme	3,3′,5,5′-Tetramethylbenzidine (TMB)	Catalytically enhanced reaction	Tap water	633 nm	100–5000 μM	4.6 μM	22
Perphenazine (PPZ)	Bromate in a phosphoric acid medium	Catalytically enhanced reaction	Rain, polluted well and formulated waste waters	525 nm	Up to 0.0978 μM	0.00152 μM	23
NETH-CD nanoprobe	NETH-CDs + p-aminobenzene sulfonic acid (Sa)	Dual-mode (colorimetry and fluorimetry) Griess assay	Urine, serum, sewage, lake water	Colorimetry: N/A (visual); fluorimetry: ex 359 nm, em 431 nm	0.2–100 μM (both modes)	0.10 μM (colorimetry), 0.08 μM (fluorimetry)	12
Chemosensors CE and CF	4-Aminobenzenesulfonohydrazide (C) + 2-(2-(naphthalen-1-ylamino)ethoxy)ethanol (E) or N-(1-naphthylethylenediamine dihydrochloride (F); itaconic acid; Zn dust (for nitrate)	Colorimetric Griess assay (smartphone-assisted, paper-based)	Agricultural products (vegetables), lake water, tap water	UV-spectroscopy (pink azo-dyes)	CE: 5–421 μM; CF: 10–453 μM	CE: 620 μM; CF: 520 μM	18

anions. The determination of nitrite could be carried out using two methods, Griess assay and Raman spectroscopy. By utilizing both methods, a more comprehensive understanding of the nitrite content in the sample can be achieved. Thus, a modified version of the Griess method[19] was used to detect nitrite using Raman, fluorescence, and colorimetry techniques. To detect nitrite using fluorescence and colorimetric methods, a mixture of *p*-aminothiophenol-capped gold nanorods and 1,8-diaminonaphthalene-modified gold nanoparticles was utilized to detect the nitrite. The limits of detection for fluorescence, colorimetry, and Raman methods were 0.01 μM, 0.05 μM, and 0.8 nM, respectively. Another approach was developed to identify nitrite using surface-enhanced resonance Raman scattering (SERRS) with silver nanoparticles (Ag NPs).[20] The method involved a modified diazo coupling reaction with 4-ATP and NED in an acidic environment. A deep red azo dye was formed and detected at the 532 nm wavelength in just two minutes. The integration of gold nanorods and nanoparticles provided significantly enhanced signal due to plasmonic effects and allows for multimodal detection, which can improve robustness and reduce false positives by cross-validation. These nanomaterials also contribute to the stability of the sensing platform. Various species, including iodide ions, artificial enzymes, and perphenazine, have been monitored to observe the catalytic reaction caused by nitrite.[21-23] Nitrite was detected indirectly through cloud point extraction, using the reaction between nitrite and iodide ions in an acidic medium.[21] The produced tri-iodide ion was extracted into non-ionic Triton X-100. The extracted surfactant was diluted and measured spectrophotometrically, resulting in an absorbance signal at 365 nm and a limit of detection of 6.0 ng mL^{-1}. An additional method for colorimetric determination of nitrite was developed using synthetic artificial enzymes.[22] The enzyme-like AuNP–CeO$_2$ NP@GO catalytic nano-hybrid acted as the substrate in the proposed mechanism, where nitrite acted as an oxidizing agent and 3,3′,5,5′-tetramethylbenzidine (TMB) acted as an electron donating reducing agent. The modified nanohybrid reacted with TMB in the presence of the oxidizing agent and converted the colorless TMB into a green color by the formation of the oxidized species [AuNP–CeO$_2$ NP@GO], confirming the presence of nitrite. This reaction occurred in a prepared buffer with pH 2.0. A kinetic method for determining nitrite based on the red color produced from the oxidation of perphenazine (PPZ) was reported by Mubarak.[23] PPZ reacted with bromate in the presence of phosphoric acid and was oxidized into the cation PPZ*, resulting in a red color and a strong absorbance peak at 525 nm within just 30 seconds, indicating the presence of nitrite. PPZ* was then irreversibly oxidized into the colorless PPZSO with an absorbance peak of 342 nm.

Spectroscopic techniques surpass the Griess assay for nitrite detection, especially in intricate samples like food and biological fluids. Some techniques, like the rhodamine SERS sensor, achieve specificity by monitoring signal decrease of a target molecule upon reaction with nitrite. Additionally, combining modified Griess assays with fluorescence or Raman spectroscopy expands the range of detection methods. Some

techniques require specialized equipment and expertise, increasing the complexity. Additionally, certain methods may be susceptible to interferences from other sample components, and some might not be ideal for direct analysis of complex matrices. To sum up the contents of this section, Table 1 has been prepared.

2.2. Chromatographic methods

As a common instrumental analytical technique, chromatography includes different modes such as gas chromatography (GC), liquid chromatography (LC), gel permeation chromatography (GPC), and ion exchange chromatography (IC). Chromatography has been used for nitrite detection by direct and indirect analysis.

2.2.1. Gas chromatography (GC). Gas chromatography (GC) is primarily used for the analysis of volatile organic compounds, making it a solution for nitrite determination in food and herb samples.[25] Since nitrite itself is not very volatile, its detection often requires derivatization or headspace techniques for indirect analysis. GC is a useful method for quickly, precisely, and accurately analyzing nitrite in various types of samples, particularly food samples. GC includes gas adsorption chromatography, capillary gas chromatography, and gas–liquid partition chromatography (GLPC).[26]

To determine nitrite levels in urine, food, and environmental samples, GC-Mass Spectrometry (GC-MS) and liquid chromatography with fluorescence detection (LC-FL) were developed by Akyüz and Ata,[27] with the aid of aqueous nitrite derivatization using 2,3-diaminonaphthalene (DAN). Nitrite reacts with DAN under acidic conditions to form the highly fluorescent and volatile 2,3-naphthotriazole (NAT). For nitrate analysis, it was enzymatically converted to nitrite prior to derivatization. Sample preparation for solid samples involved extraction with 0.5 M aqueous NaOH by sonication, followed by derivatization and extraction with toluene. The method demonstrated high sensitivity (LOD of 0.02 pg mL^{-1} for nitrite by GC-MS in SIM mode), good precision (RSD 1.00% for nitrite), and high recoveries (98.40% for nitrite), highlighting its reliability and selectivity for trace-level detection in complex biological, food, and environmental matrices.

A new gas chromatographic method was reported by Zhang,[28] implementing the high-throughput headspace (HS-GC) to indirectly detect nitrite in water. The mechanism relies on the specific reaction between nitrite and cyclamate in a closed vial in the presence of sulfuric acid, which forms volatile cyclohexene. The volatility of cyclohexene makes it easy to be monitored by the GC with a well-separated peak. This method is simple, accurate, and sensitive (LOD of 0.46 μg L^{-1}), with good precision (RSD <3.5%) and recoveries (94.8–102%). Its automated and high-throughput sampling mode makes it very efficient for batch sample testing, particularly for surface water samples. This approach effectively converts a non-volatile analyte into a volatile one, circumventing direct GC limitations.

Aslani and Armstrong[25] provided a comprehensive review on the hyphenation of GC with various high-information spectroscopic techniques, including Fourier Transform Infrared (FTIR)

spectroscopy, Nuclear Magnetic Resonance (NMR) spectroscopy, Molecular Rotational Resonance (MRR) spectroscopy, and Vacuum Ultraviolet (VUV) spectroscopy. While these combinations provide valuable qualitative and structural information, they also present challenges. For instance, VUV spectroscopy faces significant background absorption from virtually all molecules in the 115–185 nm range, which historically required high-intensity synchrotron sources. FTIR relies on changes in dipole moment for absorption, providing unique vibrational fingerprints. The complexity of interfaces and the inherent information provided by each spectroscopic detector vary, with MRR and NMR offering the most detailed structural information. These hyphenated techniques, while powerful, often involve more complex instrumentation and data interpretation compared to simpler GC detectors, and their fouling resistance would depend on the specific interface design and sample matrix.

2.2.2. Liquid chromatography (LC). Different types of liquid chromatography, including high-performance liquid chromatography (HPLC), supercritical fluid chromatography (SFC), and size exclusion chromatography (SEC), are also reported for the chromatographic analysis of nitrite. LC techniques, particularly HPLC, offer high sensitivity and fast analysis in various samples (*e.g.*, blood, food, drugs, water).

Lin and Fuh[29] developed a method for the simultaneous determination of nitrate (NO_3^-) and nitrite (NO_2^-) in vegetables using poly(1-vinylimidazole-*co*-ethylene dimethacrylate) (VIM-EDMA) monolithic capillary liquid chromatography with UV detection. This monolithic column offers advantages such as a relatively simple synthetic process, good thermal stability, and mechanical strength under high pressure, contributing to enhanced column stability and robustness. The method demonstrated good linearity (0.5–100 µg mL^{-1}), intra-day/inter-day precision (0.06–6.93%), and accuracy (90.33–103.32%). Importantly, no obvious carry-over or decline of separation performance was observed for more than 200 analyses of real samples, indicating excellent fouling resistance and long-term stability of the monolithic column in complex vegetable matrices. Although the detection limits (0.06 µg mL^{-1} for NO_2^-) were relatively higher than some other LC-UV techniques, the method provided satisfactory sensitivity for monitoring nitrite levels in vegetables according to the Acceptable Daily Intake (ADI) levels set by the EU.

Yenda[30] developed a simple isocratic LC method using reversed-phase HPLC coupled with a UV detector for the quantification of trace-level inorganic degradation impurities, including nitrite, in sodium nitroprusside (SNP) drug substance and liquid dosage form. The method's stability-indicating nature was demonstrated by its ability to accurately quantify impurities under forced degradation conditions (thermal, acidic, alkali, photolytic, and oxidative stress), showcasing its robustness and reliability in challenging pharmaceutical matrices. Nitrite anions were retained and separated using an anionic ion pair reagent in the reversed phase. The quality-by-design (QbD) approach was used for robustness checks, varying multiple factors simultaneously to ensure method reliability.

Furthermore, a vortex-assisted (VA) hydrophobic deep eutectic solvent (DESs) was used in nitrite determination in water and biological samples.[31] HPLC was combined with a photodiode array detector to detect nitrite through a diazotization–coupling reaction of diphenylamine and *p*-nitroaniline. Nitrite was indirectly quantified through the enrichment of the azo product by DES-based VA-DLLME.

2.2.3. Ion exchange chromatography (IC). Additionally, ion exchange chromatography was applied for nitrite detection in infants' meat foods.[32] The method was evaluated in a concentration range of 0.46–36 mg L^{-1}, with a retention time of 7.5 minutes and a detection limit of 0.13 mg L^{-1}. The matrix effect originated from the interferences of the sample components with nitrite and decreased by 14% with the usage of ultrapure water in calibration standards. In another study, Mazumdar[33] analyzed nitrite in meat products using ion exchange chromatography with a retention time of 2.6 to 3.0 minutes, LOD of 0.10 mg L^{-1}, and a recovery of 96% at 80 °C. Chiesa[34] successfully developed a high-performance ion-exchange chromatography (HPIEC) method equipped with a conductivity detector (SCD) for nitrite detection in seafood samples. In this protocol, nitrite was oxidized into nitrate by hydrogen peroxide at pH 3.6 in order to be detected.

A compact low-cost optical UV detector was fabricated and integrated with a 235 nm LED and low back pressure ion chromatography IC unit for the direct determination of nitrite in natural waters in less than 2.5 min.[32] The low operating current is used to aid in performing the analysis at stable LED temperatures, thus there is no need for heat dissipation.

The enhanced capillary ion chromatography (CIC) method was developed based on ion chromatography (IC).[35] The CIC was coupled with a conductivity detection device for nitrite determination in meat products to provide higher sensitivity, better selectivity towards the matrix interferences, and less waste production compared to IC. Real meat samples containing nitrate and chloride ions were tested to prove the applicability of the suggested method; however, large concentrations of chloride led to a strong reduction in the nitrite signal.

2.2.4. Capillary electrophoresis (CE). On the other hand, capillary electrophoresis (CE) offers rapid analysis times (often under a minute) and highly efficient separation of analytes, making it suitable for high-throughput nitrite detection. It was implemented to determine nitrite ions using microchip capillary electrophoresis (MCE) conjugated with zone electrophoresis (ZE) and isotachophoresis (ITP) techniques on the microchip.[36] ITP was performed first to eliminate the matrix in the sample, then ZE was used to enhance the sensitivity. MCE had the advantages of high speed, highly efficient separation of analytes, and a low amount of waste produced. This technique generates minimal waste compared to other chromatography methods, contributing to a more environmentally friendly approach.

Furthermore, Wang[37] developed a fluorometric capillary electrophoresis method that could detect nitrite in human plasma. The proposed mechanism was based on the direct reaction between nitrite with 2,3-diaminonaphthalene (DAN) yielding the fluorescent 2,3-naphthotriazole. Troška[38] modified

another method to determine nitrite in cerebrospinal fluid (CSF) using capillary electrophoresis coupled with iso-tachophoresis (ITP) on a poly(methylmethacrylate) chip provided with contact conductivity detectors and a coupled separation channel (CC). The CC chip included a column-switching method to electrophoretically eliminate the chloride in CSF samples.

Della Betta[39] proposed a capillary zone electrophoresis (CZE) for nitrite quantification in baby foods with an analysis time of 30 seconds. The nitrite signal was directly detected with a UV-spectrophotometer at wavelength 210 nm. Freitas[40] demonstrated a microchip electrophoresis device (ME-C4D) for the electrophoretic separation of nitrite in environmental samples, built on the basis of the nitrification process that occurred in water owing to the presence of *Nitrosomonas* and *Nitrobacter* bacteria without the need for fish's urea. As ammonium was introduced and oxidized by *Nitrosomonas* bacteria into nitrite, nitrite was oxidized by *Nitrobacter* into nitrate, thus the nitrogen cycle can be monitored. ME-C4D showed a fast separation of 60 s of nitrite, nitrate, chloride, and sulfate with a simple and cost-effective methodology. Conjugating electrophoretic PDMS microchips with electrochemical separation was introduced by Siegel[41] for the detection of nitrite in lipopolysaccharide (LPS)-stimulated RAW 264.7 and native macrophage cells with the detection limit of 0.5 mM. Gottardo[42] constructed a spectro-photometric CE method for the direct detection of nitrite in biological samples. The reported system used the applied potential of −15 V and tetraborate as a running electrolyte. The UV absorption of nitrite was measured at 214 nm. Lucas (2022)[43] developed a portable analytical methodology based on microchip electrophoresis coupled with amperometric detection for the determination of nitrite in environmental water samples (aquarium and fish breeding dam water). The mechanism involves electrophoretic separation of nitrite followed by amperometric detection using integrated Ti/Pt thin-film electrodes. Water samples were collected, filtered (0.22 μm nylon filters), and stored, with no further pretreatment necessary apart from dilutions. This highlights a minimal sample preparation strategy. The system achieved separations within 60 s and demonstrated satisfactory linear behavior (20–80 μmol L^{-1}) with an LOD of 1.3 μmol L^{-1}. The methodology showed good recovery values (83.5–103.8%) and agreement with a reference technique, indicating its robustness and reliability. Its low sample consumption, portability potential, and high analytical frequency make it promising for environmental monitoring. While specific fouling resistance was not detailed, the minimal sample preparation and fast analysis time contribute to practical applicability in real-world matrices.

Tembo (2020)[44] presented a selective and simple capillary electrophoresis method to determine nitrite in black, green, and herbal teas. The mechanism relies on nitrite anions moving in the opposite direction of the electroosmotic flow, with cations eluting last, which prevents interferences from other inorganic anions with nitrite anions, thus enhancing selectivity. Tea samples were prepared by boiling the teas in deionized water for 5 minutes, followed by filtration (0.45 μm filter) and refrigeration. A three-factor full factorial experimental design was employed to systematically investigate the effects of three key variables: capillary temperature, buffer concentration, and applied voltage. This statistical approach is highly efficient for detecting factor interactions with a minimum number of experiments. Prior to the full factorial analysis, stable preliminary conditions were established, including a constant pH of 3.5 for the phosphate buffer. The three factors were then studied over a specific range based on preliminary experiments: buffer concentration (50 to 70 mM), capillary temperature (20 to 40 °C), and applied voltage (−15 to −20 kV). The primary response measured was the corrected peak area (analyte peak area divided by migration time), with data analysis performed using Minitab 18. This systematic optimization was crucial for achieving the sharp, high-resolution nitrite peaks observed within 7 minutes.

Table 2 Chromatographic detection of nitrite ions in biological and environmental matrices

Principle	Reagent	Separation time	Matrix	Range (μM)	LOD (μM)	Ref.
Zone electrophoresis (ZE) and isotachophoresis (ITP)	MCE method	10 min	Deionized water activated plasma	32.60 to 280.37	20.21	36
Fluorometric capillary electrophoresis	2,3-Diaminonaphthalene (DAN)	1.4 min	Human plasma	0.002 to 0.5	0.0006	37
Isotachophoresis (ITP)	3-(N,N-Dimethyldodecylammonio)-propanesulfonate	20 min	Cerebrospinal fluid CSF	0.006–0.009	0.0089	38
Capillary zone electrophoresis CZE	BGE composed of perchloric acid and β-alanine	0.5 min	Baby foods	108.67–1195.39	3.26	39
Microchip electrophoresis	Lactic acid and L-histidine (His)	60 s	Environmental samples	0–120	4900	40
Electrophoretic PDMS microchips and isotachophoresis (tITP)	Borate + TTAC	30 s	Lipopolysaccharide (LPS) and macrophage cells	2000–9000	500	41
Spectrophotometric CE	Tetraborate	N/A	Biological samples	N/A	N/A	42
Microchip electrophoresis	Lactic acid and L-histidine (His) mix	60 s	Water samples	20 and 80	1.3	43
Capillary electrophoresis	Sodium phosphate monobasic	7 min	Black, green and herbal tea	30.00–499.89	21.52	44
Sample-stacking capillary electrophoresis	Formic acid	2 min	Honey bee pollens	1.5 to 10	0.31	45

Table 3 Flow injection techniques used for the determination of nitrite ions in biological and environmental matrices

Detection principle	Reagent	Sample rate/h	Matrix	Wavelength	Linear range (μM)	LOD (μM)	Ref.
Spectrophotometry	N-(1-Naphthyl)ethylenediamine dihydrochloride (NED) and sulfanilamide	18	Soil	543 nm	0.435–34.775	1.000	46
Spectrophotometry	N-[1-Naphthyl]-ethylenediamine	32	Natural waters	610 nm	2.17×10^{-5}–1.087×10^{-3}	6.5×10^{-6}	47
Flame atomic absorption spectrometry (FAAS)	Manganese(IV) dioxide oxidant micro-column	90	Food and waste water	279.5 nm	0–391.22	1.521	48
Spectrophotometry	Sulfonazo III and potassium bromate	60	Environmental samples	570 nm	0.174–6.520	0.130	49
Reverse flow injection analysis (rFIA) with a spectrophotometer	NED solution	5	Sea water samples	540 nm	0.002–0.5	0.0006	50
Amperometry	(NH$_2$-IL/SiCNP) GE	N/A	N/A	N/A	0.05–0.35	0.02	51
Amperometry	Prussian blue–carbon paste electrode	N/A	Water and sausage samples	N/A	N/A	9	52
Spectrophotometry	Sulfanilamide and N-1-naphthylethylenediamine dihydrochloride	20	Environmental samples	540 nm	0–100	0.1	53

Consequently, Kalaycıoğlu[45] introduced a new sample-stacking capillary electrophoresis technique for the simultaneous detection of nitrate and nitrite in honey-bee pollen. The sensitivity was enhanced by the sample stacking technique due to the increase in the buffer conductivity (by adding 30 mM sodium sulfate to the separation buffer), which effectively concentrates the analytes. This resulted in sharp nitrite peaks. The developed method was validated with a nitrite calibration curve in the range of 1.5 to 10 μM and resulted in an LOD of 0.31 μM. Sample preparation for honey-bee pollen involved preparing a solution where the buffer conductivity was adjusted for stacking, a strategy to overcome matrix effects and improve detection in complex samples. CE offers a promising technique for analyzing nitrite due to its speed, efficiency, low waste generation, and versatility. Addressing limitations in sensitivity and potential interferences can further improve the applicability and reliability of CE for nitrite detection in diverse samples. To sum up the contents of this section, Table 2 is prepared.

2.3. Flow injection analysis

A simple online heterogeneous flow injection method was reported to determine nitrite, nitrate, and ammonium ions in the soil.[46] Nitrite was detected by the Griess–Ilosvay reaction, and the formed azo product was detected at a wavelength of 543 nm. In this approach's mechanism, samples were injected and passed into three streams. The first stream was the Griess–Ilosvay diazotization reaction through the coupling between N-(1-naphthyl) ethylenediamine dihydrochloride (NED) and sulfanilamide. The second stream detected nitrite and nitrate by the reaction between the sample and NH_4Cl + EDTA. The third stream detected nitrite and ammonium. Therefore, three absorbance peaks were obtained. FIA can be coupled with various detection methods, including spectrophotometry, amperometry, and atomic absorption spectrometry, providing flexibility for nitrite analysis. Yue[47] reported a simultaneous determination of nitrite and nitrate using a catalytic FIA system. The corresponding peak appeared with a shoulder; the shoulder height corresponded to the nitrite. The decrease in the shoulder height at 610 nm is attributed to the absorbance of crystal violet through its reaction with potassium chromate in the presence of nitrite. Noroozifar[48] developed a method by combining FIA with flame atomic absorption spectrometry (FAAS). Nitrite reduced manganese(IV) dioxide to give Mn(II) as a product that was detected by the FAAS in acidic medium. The nitrite analysis rate was 90 samples per hour, which makes it applicable for the routine analysis of meat and water samples.

In another model, the 60-sample per hour method was constructed by Nouroozi.[49] The developed FIA technique was based on the influence of nitrite on the reaction between sulfonazo III and potassium bromate. Nitrite was detected and measured by the decrease of sulfunazo III absorbance peak height at a wavelength of 570 nm, in the presence of bromate as a strong oxidizing agent. In this report,[50] nitrite was detected in seawater with the reverse flow injection (rFIA) method. rFIA was developed with the aid of a long path-length liquid waveguide capillary cell (LWCC). The system contained two channels, one

for nitrite determination and the second for the nitrate and nitrite combination.

Salimi[51] used an amperometric method combined with the FIA. In this regard, silicon carbide (SiC) nanoparticles were conjugated with (1-(3-aminopropyl)-3-methylimidazolium bromide) to form the NH_2-IL/SiC nanocomposite, which was then electrodeposited on a glassy carbon electrode. The FIA configuration showed an LOD of 0.3 μM, a correlation coefficient of 0.9945, and a nitrite concentration range of 1–24 μM. A similar approach was developed by Pradela-Filho[52] through developing an amperometric-based FIA method utilizing Prussian blue (PB) and modified carbon paste electrode for the recirculation of the carrier solution to be applied for the nitrite analysis. The PB worked as a redox mediator and electron shuttle in this electrochemical system.

Wang[53] demonstrated an automatic flow injection analysis system for nitrite quantification using VCl_3 as a reducing agent, while Griess reagent was utilized with the sulfanilamide, and N-1-naphthylethylenediamine dihydrochloride. A pink azo dye was produced with a characteristic peak signal at wavelength 540 nm. Some FIA methods may require careful optimization to minimize interferences from other sample components that could affect the chosen detection reaction; also, the sensitivity of FIA might be lower compared to some chromatography techniques like HPLC. To sum up the contents of this section, Table 3 has been prepared.

3 Advanced spectroscopic techniques for nitrite detection

3.1. Chemiluminescence

Chemiluminescence is a captivating natural phenomenon that occurs during specific chemical reactions. It results in the emission of light or heat from electrons in an excited state, releasing heat during exothermic reactions.[54] This characteristic of chemiluminescence is valuable for identifying nitrite in organic and inorganic substances with low detection limits. Chemiluminescence methods comprise gas-phase and luminal techniques, with certain considerations due to the drawbacks of

Fig. 2 Gas-phase chemiluminescence.

the gas-phase and luminal techniques. Thus, it is important to carefully evaluate whether chemiluminescence is the most appropriate method for a particular application and to use it in conjunction with other analytical techniques when necessary.

3.1.1. Gas-phase chemiluminescence. Gas-phase chemiluminescence occurs when nitrite is reduced to nitric oxide to react with ozone, producing the excited state of nitrogen dioxide (NO_2^*) and molecular oxygen, as shown in Fig. 2. The excited nitrogen dioxide decays rapidly into nitrite, emitting a chemiluminescence signal at a wavelength of 600 nm. Nagababu[55] measured nitrite levels in blood plasma by reducing nitrite to NO in a mixture of glacial acetic acid/ascorbic acid to enhance the chemiluminescence signal intensity. NO reacted with ozone and generated a chemiluminescence signal that had a linear relationship with nitrite concentrations, which was detected using a nitric oxide analyzer (NOA). The signal was reduced by adding sulfanilamide, confirming the suggested mechanism. No signal appeared in the presence of nitrate or any other nitrated interference, such as nitrated lipids, proteins, RSNOs, or RNNOs. Fu[56] proposed a dual-electrode to sense nitrite and ascorbic acid by measuring the emission spectrum of Eu-SiMoW in sulfuric acid and sodium sulfate, relying on the fast oxidation of Eu-SiMoW (reduced form) by the free nitrite ions. According to the nitrite concentration, the absorbance of the reduced Eu-SiMoW decreased at a wavelength of 517 nm. From these linear decreases in the absorbance levels, LOD was calculated to be 1.16 μM. On the other hand, fluorescence intensities were recovered by the increase of NO_2 concentrations in a linear relationship $R^2 = 0.992$ at a wavelength of 592 nm, giving an LOD of 5.39 μM. This assay was optimized to determine nitrite using a UV-vis spectrophotometer in real food samples such as spinach. The results were validated with the HPLC as a standard method.

3.1.2. Luminal chemiluminescence. For chemiluminescence emission to occur, luminal must be mixed with an appropriate oxidizing reagent. The reaction, known as luminal chemiluminescence, leads to the release of light, as demonstrated by Ding[57] in the creation of a luminescent terbium metal–organic framework for nitrite detection. A suggested composite $(K_{13}Eu(SiMoW_{10}O_{39})_2 \cdot 28H_2O)$ was prepared by the solvo-thermal technique. The photo-luminescence responses were investigated by using different anions in addition to nitrite, such as SCN^-, CO_3^{2-}, Br^-, Cl^-, ClO_3^-, and HPO_4^{-2}. Nitrite exhibited a luminescence quenching effect at a wavelength of 549 nm. With the increase of NO_2^- concentration (from 3.0 μM to 1000 μM), the photoluminescence intensity of the composite decreased, and the light blue color of the composite changed to dark blue color under UV light, which ensured the applicability of the assay.

Yaqoob[58] proposed a chemiluminescence detection method for peroxy-nitrite anion using a simple flow injection analysis technique. NO_2^- was oxidized by H_2O_2, forming peroxy-nitrous acid in an acidic medium, which was further converted into peroxy-nitrite anion in an alkaline medium. Peroxy-nitrite had a catalytic effect on luminal, which, when oxidized, produced a chemiluminescent emission. Also, Co(II) and Fe(II) had a catalytic effect on luminal oxidation, thus improving its

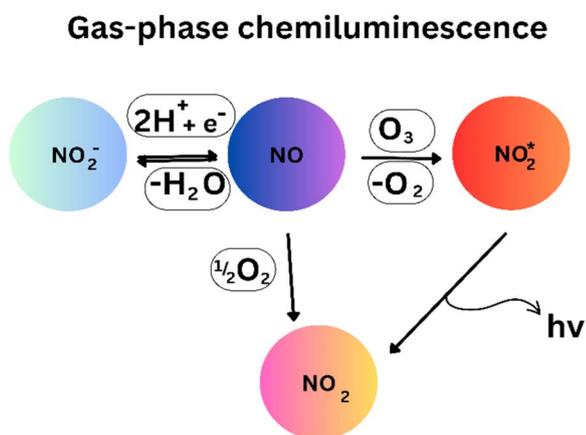**Table 4** Chemiluminescence detection of nitrite ions in biological and environmental matrices

Platform	Co-reagent	Cl method	Samples	Linear range (μM)	LOD (μM)	Ref.
Reaction of NO with ozone	Ascorbic acid and glacial acetic acid reagent	Gas phase CL (ozone based)	Fasting human plasma	0.056–0.210	0.010	55
Eu-containing polyoxometalate $K_{13}Eu(SiMoW_{10}O_{39})_2 \cdot 28H_2O$ (Eu-SiMoW)	Ascorbic acid (AA)	Gas phase CL	Spinach	0–600	2.82	56
Nano-porous terbium luminescent metal–organic framework	N/A	Luminal phase	Deionized water	3–1000	0.54	57
Luminol (5-amino-2,3-dihydrophthalazine-1,4-dione)	Hydrochloric acid and hydrogen peroxide	FIA-luminal phase	Rain, fresh and mineral waters	7.14×10^{-4}–3.569	7.14×10^{-4}	58
Orange luminescent nitrogen doped carbon dots (N-CDs)	N/A	Luminal phase	Sausage, pickle and tap water samples	8–100	0.65	59
Cyanine dye IR-790-NaYF4:Yb,Tm@NaYF4	N/A	Luminal phase	Tap water and Huojin river water	0.20–140	0.030	60
3,6-Di(2-thienyl)-2,5-dihydropyrrolo[3,4-c]pyrrole-1,4-dione (TH-DPP) polymeric films (PTH-DPP)	$S_2O_8^{2-}$	Electrochemiluminescence (ECL)	Tap water, milk, ham and sausages	0.3–1000	0.08	61

signal. To avoid their interfering effects, Co(II) and Fe(II) were masked by EDTA. Copper(II) depressed the signal of the blank; however, it didn't affect the nitrite signal. A salinity value above 8.7 had a quenching effect on the chemiluminescence signal, hence the proposed method was perfectly applied to fresh water, while Jing[59] developed orange luminescent carbon dots (N-CDs) for nitrite monitoring in food and water samples. The N-CD suspension had an orange luminescence absorbance peak at 365 nm, and it showed stability over the pH range 3.0–12. In addition, the intensity increased with the increase of nitrite concentration from 8.0 to 100 μM in a linear relationship and resulted in an LOD of 0.65 μM.

Chen[60] proposed a quantitative imaging analysis method based on (IR-790)-NaYF4:Yb, Tm@NaYF4. The luminescent nano-probe relied on the energy transferred from the up-conversion nanoparticles to the cyanine dye (IR-790), reducing the fluorescence intensity while adding nitrite to recover the luminescence. Luminescence recovery was visualized by IR-790 color change from dark blue to yellow. Additionally, a new approach based on the luminescent polymer [3,6-di(2-thienyl)-2,5-dihydropyrrolo[3,4-c]pyrrole-1,4-dione (TH-DPP)] was proposed in which it was converted into conductive (PTH-DPP) polymeric films.[61] With the addition of nitrite, the chemiluminescence signal increased by a factor of 3.8 more than the signal detected before the addition of nitrite. While luminescence methods offer attractive features for nitrite detection, some limitations need to be addressed. The requirement for specific oxidizing agents can introduce complexity, and ensuring complete selectivity for nitrite across diverse samples remains a challenge. Furthermore, the sensitivity of some methods might come at the cost of increased complexity or limitations in applicability. To sum up the contents of this section, Table 4 has been prepared.

3.2. Fluorescence spectroscopy

Fluorescence spectroscopy examines the fluorescence of samples by using a light beam to excite the electrons in molecules, causing them to emit light, usually in the visible range. Nitrite itself does not emit fluorescence, but it can be detected through its chemical reactivity with non-fluorescent reagents in nitrosation or diazotization reactions, which produce highly stable fluorescent compounds. To detect nitrite, Ali[62] modified α-MnO$_2$ nanorods with fluorescein dye (FLR) to be quenched when it was added to MnO$_2$, forming a nanoprobe FLR@MnO$_2$ NRs. Nitrite reduced the formed nanocomposite to soluble Mn^{2+}, and the FLR was liberated as a fluorescent species to be measured at 518 nm, producing an LOD of 0.27 μM. This approach was applied to real water samples, tap water, and conduit water. However, the probe relies on quenching by Mn^{2+} ions, which might be susceptible to interference from other reducing agents. In contrast, Doroodmand[63] focused on developing a fluorescence nitrogen carbon dot (N-CD) probe that could effectively sense the presence of nitrite, nitrate, and NO$_x$ gas. The study found that the C-dot fluorescence emission intensities were detectable from 350 nm to 465 nm in a universal buffer at pH 2.0. When carbon dots interacted with

Table 5 Fluorescence spectroscopic detection of nitrite ions in biological and environmental matrices

Platform	Turn off/on	Matrix	λ_{ex} and λ_{em}	Reaction time	Range (µM)	LOD (µM)	Ref.
α-MnO$_2$ nanorods (FLR@ α-MnO$_2$ NRs)	Turn on	Natural waters	490/518 nm	15 min	0.83–67.0	0.27	62
UiO-66-NH$_2$	Turn off	Food samples	320/448 nm	120 s	0–10000	77	64
BODIPY-probe	Turn on	Living cells	470/532 nm	2 min	0–8	0.015	65
N/S doped carbon dots	Turn off	Deionized water	400/480 nm	N/A	0–500	30	66
CTAB@AuNPs	Turn on	Forensic samples	415/575 nm	5 min	0–60	0.07	67
AAC probe	Turn on	*Escherichia coli*	567/656 nm	7 min	0–1	0.0067	68
Near-infrared fluorescent probe	Turn on	Living HeLa and V79 cells	630/542 nm	N/A	0.0–26.0	0.045	69

nitrite, an azo dye was formed, which caused a quenching effect on the fluorescence intensities. The probe was synthesized by the microwave carbonization of citric acid. While this approach offers multi-analyte detection, the quenching mechanism might be less selective compared to other studies focusing solely on nitrite. Furthermore, metal organic frameworks (MOFs) were used in the fluorescence determination of nitrite by the UiO-66-NH$_2$ turn-off fluorescence probe.[64] This probe was fabricated and applied to detect nitrite through diazotization and reduction chemical reactions. The fluorescence intensity increased with the increase of nitrite concentration, with intensity at 448 nm and good linearity ($R^2 = 0.9994$). The estimated LOD was 77 µM with a short response time of 120 s to make the probe valid for tap water and food sample analysis.

Another method for detecting nitrite and NO involved the use of BODIPY dye.[65] This was achieved through the attachment of BODIPY with the amino group of *o*-phenylenediamine at the *meso*-position to fabricate a turn-on fluorescence probe. With the addition of nitrite concentration, the absorption peaks increased at 412 nm, while the fluorescence intensity was observed at 532 nm. The LOD of this approach was calculated to be 15 nM, calculated from the linear calibration range of 0–8 µM. MOFs might offer higher selectivity due to their well-defined pore-like structures, but BODIPY dyes could be advantageous for higher sensitivity. On the other hand, Deng[66] used the one-step solvo-thermal method to prepare blue-green fluorescent carbon dots (CDs) from *p*-aminobenzenesulfonic acid. CDs contained hydroxyl (–COOH), amino (–NH$_2$), and sulfuric acid (–HSO$_3$) functional groups. The sulfuric acid group interacted with nitrite ions, causing fluorescence quenching. The quenching may be attributed to a static quenching effect. The fluorescent film was prepared by combining the CDs with methylcellulose, which could be quenched with sodium nitrous acid to be used in portable sensors. The fluorescence spectrum was obtained at an excitation wavelength of 400 nm, but the intensity decreased with the increase of nitrite concentration at 480 nm in a linear relationship, showing an LOD of 30 µM. Although CDs offer simple preparation methods, their quenching mechanisms might be less specific compared to other approaches. A new protocol was presented by Chaien-doo.[67] It involved the use of gold nanoparticles stabilized by cetyltrimethyl ammonium bromide (CTAB@AuNPs) to detect nitrite ions through oxidative etching, which results in the production of gold ions (Au^{3+}). Furthermore, Au ions were used

to catalyze hydrogen peroxide to react with fluorogenic *o*-phenylenediamine (OPD) and yield the fluorescent 2,3-diaminophenazine (DAP). Nitrite could be indirectly detected by tracing the change levels in the DAP intensity. This method was suitable for gunshot residue GSR applications. Yu[68] developed a novel near-infrared fluorescent probe (AAC probe) to quantitatively detect nitrite levels in *Escherichia coli* through turn-on fluorescence imaging. Nitrite in food samples and river water was also detected using this method, and the results were confirmed by the Griess assay. The mechanism of the sensor developed relied on the diazotization reaction that occurred between nitrite and 4-(2-aminophenyl) in an acidic medium with a pH of 1.0. This reaction produced 7-(diethylamino) coumarin (activated aromatic ring) and aryldiazonium in the form of an orange azo dye ACC intermediate. Furthermore, the ACC intermediate reacts with nitrite to form a new compound, a purple-colored NIR-Nit product. This product was detected with a mass-to-charge ratio (*m/z*) of 320.1393. The assay showed a linear relationship between nitrite addition and the emission intensity at 656 nm, and the LOD was 6.7 nM. Zhan[69] investigated a near-infrared-fluorescent probe based on benzo[*a*] phenoxazine and *o*-phenylenediamine for the selective cellular imaging of exogenous nitrite. The probe responded colorimetrically to nitrite, with absorption signals at 630 nm and 542 nm in the presence of 30% DMSO, with an emission spectrum in the 590–820 nm range. Due to the action of photoinduced electron transfer (PET), the developed probe showed very faint fluorescence under weakly acidic circumstances. However, by generating benzotriazole derivatives, it can hinder the quenching process *via* PET. Thus, the fluorescence spectrum was enhanced by 9-fold with an excitation strike of 580 nm. Fluorescence spectroscopy for nitrite detection is highly effective due to its high sensitivity with specific probes. However, limitations include complex probe design for some methods and potential interference from other analytes in complex samples. But it's a promising technique with room for development in probe universality and robustness. To sum up the contents of this section, Table 5 has been prepared.

3.3. Infrared spectroscopy (IR/FTIR)

The process of infrared spectroscopy involves the interaction of infrared light with molecules. Different molecules absorb light at varying frequencies depending on the functional group of the molecule. Each functional group has a unique structure,

molecular potential energy surface, and atomic mass, which correspond to a specific vibrational frequency. Different molecules absorb infrared light at unique frequencies based on their functional groups. This allows for targeted detection of a nitrite's specific vibrational frequencies. Thus, infrared (IR) spectroscopy is a vibrational spectroscopic technique that probes the interaction of infrared radiation with matter. Molecules absorb IR light at specific frequencies corresponding to their characteristic vibrational modes (stretching and bending of chemical bonds).

Additionally, Fourier Transform Infrared (FTIR) spectroscopy is a widely used type of IR spectroscopy that employs an interferometer to collect a broad range of spectral data simultaneously. FTIR offers several advantages over traditional dispersive spectrometers, including a wider spectral range, a superior signal-to-noise ratio (due to the multiplex advantage), and reduced stray radiation, enabling more rapid and precise measurements.

While direct IR detection of nitrite in complex matrices can be challenging due to overlapping signals, various strategies have been developed to enhance its applicability. Huang utilized near-infrared (NIR) spectroscopy combined with chemometrics for the determination of total nitrogen, ammonia nitrogen, and nitrite nitrogen in river water during intermittent aeration.[70] They produced a back-propagation neural network model that, after using principal component analysis to get rid of extra spectral information, showed a correlation coefficient of 0.9524 for nitrite. The spectral range that was looked at ranged from 4000 to 12 500 cm^{-1}. This method showed that multivariate analysis could be used to get useful information from complicated NIR spectra for monitoring the environment. The method showed that the amount of nitrite in river water could be measured between 0.05 and 31.40 mg L^{-1} (about 1.09 to 682.6 μM). It was very important to employ a back-propagation neural network to deal with the complicated spectral data and reduce any possible interference from the natural river water matrix. This made it possible to accurately measure nitrite together with total nitrogen and ammonia nitrogen.

In a different application, FTIR spectroscopy, alongside laser micro-Raman spectroscopy, was employed by Ma to characterize the effects of low-dosage sodium nitrite on yak meat myoglobin in a hydroxyl radical oxidation environment.[71] Rather than directly measuring nitrite, the main goal of this work was to comprehend how nitrite protects myoglobin structure and oxidation. It underlines how useful FTIR is for examining molecular alterations brought on by nitrite in intricate biological systems like meat. By tracking changes in disulfide bonds, carbonyls, and total sulfhydryl groups, as well as modifications to atomic/molecular interactions and the secondary structure of myoglobin, the researchers were able to identify and describe the degree of protein oxidation. According to the core sensing mechanism, nitrite has an antioxidative function because it protects sulfhydryl groups and significantly decreases the formation of carbonyls and disulfide bonds.

Furthermore, the spectroscopic data provided crucial insights into how nitrite inhibits the expansion of the heme center size and the transition of iron (Fe) from a low-spin to a high-spin state, both being characteristic markers of oxidative damage.

Attenuated Total Reflection Infrared (ATR-IR) spectroscopy has also been explored, particularly for mechanistic studies in catalysis. For instance, Ebbesen used ATR-IR spectroscopy with a Pd/Al$_2$O$_3$ catalyst layer deposited on a ZnSe internal reflection element to investigate the mechanism of nitrite hydrogenation.[72] They found that the H–Pd/Al$_2$O$_3$ surface had nitrite (NO$_2^-$(aq)) adsorbed at 1235 cm^{-1}. They also found other evolving peaks at 1450, 1510, and 1705–1720 cm^{-1} that corresponded to chemical intermediates such as adsorbed NO. Although it is not a direct quantitative method for biological or environmental samples, this *in situ* approach presents substantial understanding into the chemical transformations of nitrite on catalytic surfaces. Through the adsorption of palladium acetylacetonate on precalcined γ-Al$_2$O$_3$ powder, ball milling, and deposition on the ZnSe IRE, the Pd/Al$_2$O$_3$ catalyst was prepared. Other functional groups, however, may have overlapping absorption peaks in typical biological or environmental samples, requiring cautious interpretation and frequently required chemometric analysis to deconvolve the nitrite signal. The direct application of ATR-IR for quantitative nitrite detection in highly complex, unpurified real samples remains challenging due to these interferences.

Further advancing spectroscopic methods for nitrite detection, Gallignani[73] established a unique approach for detecting nitrite that combines flow analysis (FA), vapor phase generation (VPG), and FTIR, notably in high concentration samples (frankfurters/sausages). In this redox system, the addition of ascorbic acid or potassium iodide to an acidic solution converted nitrite quantitatively into gaseous nitric oxide (NO). The produced NO has a distinct absorbance band at 1876 cm^{-1} (with baseline correction between 1879 and 1872 cm^{-1}). This analytical system stood out for its simplicity, as it did not require temperature or pH control and was successfully tested on sausage food samples. The vapor phase generating stage effectively separates the analyte (NO gas) from the complex food matrix, reducing common spectrum interference and improving selectivity. The FA-VPG-FTIR system efficiently separated the analyte from the solid/liquid food matrix components, which would otherwise cause significant spectral interference. This method significantly improved selectivity and allowed for robust detection in real food samples without necessitating extensive matrix removal. The system's stability was demonstrated by the consistent spectra over many scans.

Beyond direct quantitative detection, Paydar[74] utilized infrared spectral analysis to investigate the relationship between nitrite and nitrate content and the color of edible bird's nests (EBNs). While not a direct quantitative method for environmental monitoring, their study demonstrated that red/brown cave-EBNs contained higher intensities of C–N and N–O bonds (red/brown) compared to white house-EBNs, correlating with increased nitrite and nitrate levels. This highlights IR's utility in characterizing nitrite's presence and its impact on material properties in complex food-related matrices.

In another related spectroscopic application, Yilmaz[75] published a new colorimetric assay for nitrite that used the near-

infrared (NIR) absorption dye IR780 and revealed an unexpected colorimetric response to nitrite ions. While it is primarily a colorimetric method, the use of an NIR-absorbing dye, as well as the outline of its application in processed meat products and tap water, is pertinent to the larger spectroscopic context. The probe demonstrated great sensitivity (LOD = 227 nM or 0.227 μM), fast response (<5 s), and excellent selectivity against common ions. This method also investigated smartphone-based imaging for real-time and on-site visual detection, illustrating the potential for portable applications. The results revealed good recovery rates (85–113%) and repeatability (RSD < 5%), indicating strong performance in complicated matrices. The distinct color change and potential for smartphone-based detection make it highly relevant for on-site, real-time monitoring. Ozmen[76] developed a simple, sensitive, and specific spectrophotometric approach detecting nitrite in water that employs a synthetic azo dye, 4-(1-methyl-1-mesitylcyclobutane-3-yl)-2-(p-N,N-dimethylazobenzene)-1,3-thiazole. The dye was characterized using the UV-vis spectrophotometric method, and infrared (IR) examination revealed an absorption maximum at 482 nm, suggesting the complementing role of IR in verifying molecular structure and reaction products in nitrite detection chemistry. The approach successfully detected 0.012 μg mL^{-1} (approx. 0.26 μM) in both tap and lake water.

To sum up the contents of this section, Table 6 has been prepared.

3.4. Raman spectroscopy

Raman spectroscopy depends on the detection of the scattered light excited from a photon-struck molecule; the excited molecule returns to its ground state at a different vibrational or rotational state, and emits a photon. Nitrite itself doesn't have a strong Raman signal; however, indirect Raman detection could be applied by observing the Raman signature of reaction products formed with specific reagents. This enables targeted detection by choosing appropriate reagents. In addition, surface-enhanced Raman spectroscopy (SERS) significantly amplifies the Raman signal, allowing for detection of very low nitrite concentrations, separating the low-intense scattered light signals, and has great potential for the onsite detection of nitrite.

3.4.1. Nanomaterial-enhanced SERS platforms. Recent advancements have focused on developing highly efficient SERS substrates for nitrite sensing, often integrating novel nanomaterials. Yang developed a novel enhanced SERS sensor based on a diazo reaction between urea and nitrite.[77] Their platform utilized Au arrays, obtained by self-assembling gold nanoparticles onto functionalized glass surfaces and subsequently modifying them with urea. The uniformly propagated Au nanoparticles produced an extremely stable SERS signal. The diazo reaction in acidic environments resulted in Raman peak suppression at 1003 cm^{-1} due to the N–C–N stretching of urea, allowing for nitrite measurement. The sensor detected nitrite in human saliva at a linear range of 20 to 120 μM. The method was commended for its speed, sensitivity, and selectivity in this complex biological matrix, as well as the fact that it does not

Table 6 IR/FTIR spectroscopic detection of nitrite ions in biological and environmental matrices

Platform	IR/FTIR	Sample	Wave number	Range (μM)	LOD (μM)	Ref.
Near-infrared spectra with a spectrophotometer	IR	River water	4000–5100 cm^{-1}, 6500–7500 cm^{-1}, 8000 to 8500 cm^{-1} and 10 400 cm^{-1}	1.087–682.46	N/A	70
Fourier transform infrared spectroscopy and laser micro-Raman spectroscopy	FTIR	Yak meat	1335–1650 cm^{-1}	N/A	N/A	71
Flow analysis-vapor phase generation-Fourier transform infrared (FA-VPG-FTIR)	FTIR	Food samples	1875 cm^{-1}	N/A	N/A	73
Pd/Al$_2$O$_3$ using ATR-IR spectroscopy	IR	Water	1720 cm^{-1}, 1510 cm^{-1}, 1235 cm^{-1}	N/A	N/A	72
Flow analysis-vapor phase generation-Fourier transform infrared (FA-VPG-FTIR)	FTIR	Food samples (sausage)	1876 cm^{-1} (for gaseous NO)	N/A (high concentration samples)	N/A	73
Infrared spectral analysis	IR	Edible bird's nests (EBNs)	C–N and N–O bonds (characterization)	N/A	N/A	74
Near-infrared (NIR) absorbing dye IR780 colorimetric assay	Colorimetric (NIR-based)	Tap water, processed meat products	775 nm (absorption wavelength)	N/A	0.227	75
Spectrophotometric method with azo dyes	UV-vis (IR characterization)	Tap water, lake water	482 nm (absorption wavelength)	1.087–43.469	0.26	76

require a pretreatment process for saliva samples. This direct analytical capability provides a considerable benefit in biological diagnostics by reducing frequent sample preparation problems.

Further exploring chemical reaction-based SERS methods, Wang[78] proposed a one-step chemical reaction method for nitrite determination based on the reaction between 2-thiobarbituric acid and nitrite using SERS. *S*-Nitrosothiol was generated through the nitro–thiol reaction, and it showed a characteristic band at 685 cm^{-1} generated from the C–S stretch. The calibration curve was constructed between the increased nitrite concentration levels and SERS intensity. Due to their optical properties, gold nanoparticles were used to enhance the quality of SERS signals by using KCl as an aggregating agent.

Focusing on highly structured nanomaterials for enhanced SERS, Wang[79] developed a highly structured hollow ZnO@Ag nanosphere as a SERS substrate for sensing nitrite. This system relied on the significant SERS enhancement achieved by traces of nitrite interacting with 4-ATP and 1-NA on the nanosphere surface, leading to a new enhanced peak at 1281 cm^{-1}. The hollow structure and specific morphology of the ZnO@Ag nanospheres contributed to their high sensitivity and selectivity. The sensor has an ultra-low limit of detection (LOD) of 0.3 $\times 10^{-8}$ mol L^{-1} (0.003 μM) and a large linear range (1.0 $\times 10^{-8}$ to 1.0 $\times 10^{-3}$ mol L^{-1}). Its excellent selectivity has been noted for nitrate and nitrite measurement in foods. This methodology was successfully used to analyze nitrite in pickled radish samples, which are a particularly demanding food matrix due to their high salt content and complex chemical composition. Validation against national standard techniques (GB 5009.33-2016, PR China) and strong statistical analysis (RSD <14%) confirmed accuracy and precision in real food samples.

Building on the use of nanocomposites, Chen[80] developed another SERS model using a bifunctional nanocomposite (Fe$_3$O$_4$@SiO$_2$/Au NPs) to detect nitrite. The nanocomposite was used to purify the nitrite ions in different samples, and to enhance the Raman characteristic peak by by using a magnetic field to aggregate the nanocomposite. Thus, the Fe$_3$O$_4$ and Au NPs were conjugated with the 4-ATP to react with nitrite forming a diazonium salt, which reacted with aromatic amines, giving azo compounds. The core Fe$_3$O$_4$@SiO$_2$ Au MNPs were stimulated by an exciting laser at a wavelength of 780 nm. The corresponding Raman signals, which appeared at 1436, 1391, and 1140 cm^{-1}, were assigned to the formed azo compounds and showed a linear relationship with nitrite concentrations. This SERS model was tested in pond water, pickles, and synthetic urine samples. The developed SERS platforms demonstrate their ability to detect nitrite at low concentrations. This makes it suitable for applications where sensitivity is crucial, like environmental monitoring or medical diagnostics. However, the instrumentation required for SERS is often bulky and not suitable for on-site detection. Thus, developing portable SERS platforms is essential for broader applicability.

Further innovations in SERS platforms include the development of dual-mode sensors. For example, Tan[81] introduced a novel dual-mode SERS/colorimetric detection method for nitrite in food products, utilizing a multifunctional gold nanoparticle-doped covalent organic framework (Au@COF) composite. In this system, the diazo reaction between nitrite and toluidine blue (TB) under acidic conditions leads to the attenuation of TB's characteristic SERS signal and absorption peak. The Au@COF composite not only improved SERS and reproducibility, but it additionally enhanced reaction rates and sensitivity due to its superior adsorption capacity and stability. The dual-mode nature enables both visual screening (colorimetric) and highly sensitive quantification (SERS), increasing the reliability of the results. It showed high sensitivity and excellent recovery rates in food samples like luncheon meat, cured meat, and sausage. Its excellent selectivity has been confirmed against common ions such as Br^-, $H_2PO_4^-$, CO_3^{2-}, and NO_3^-. The intrinsic simplicity of the colorimetric mode, along with the increased sensitivity of SERS, makes it ideal for practical food safety applications.

For multi-analyte detection, Gu constructed a miniature multi-channel SERS sensor on a polydimethylsiloxane (PDMS) platform.[82] This system enables rapid delivery of polluted water and specific identification of multiple components, including sodium nitrite, by incorporating different probes (*e.g.*, urea for nitrite) in corresponding detection areas. The PDMS-based microchannel design facilitates simultaneous and rapid analysis. The system achieved an LOD for sodium nitrite of 5.0 $\times 10^{-7}$ M (0.5 μM). It exhibited excellent sensitivity and specificity for the simultaneous detection of multiple water pollutants. The method demonstrated excellent recovery rates for water pollutants ranging from 82.1% to 115.8%, highlighting its reliability in environmental water matrices.

Li developed a SERS method for nitrate and nitrite detection in aquaculture water using β-cyclodextrin-modified gold nanoparticles (SH-β-CD@AuNPs).[83] This platform addresses limitations of single metal nanoparticles by combining AuNPs with cyclodextrin supramolecular compounds, resulting in ultrahigh selectivity and enhanced Raman activity. Nitrate is first converted to nitrite using vanadium(III) chloride, and then both are detected *via* the SERS signal of benzotriazole (BTAH) formed from the reaction of *o*-phenylenediamine (OPD) with nitrite. The cyclodextrin modification ensures stable AuNP substrates. This approach provides LODs as low as 0.0105 μM for nitrite, with a linear range of 0.1–30.0 μM. The "ultra-high selectivity" was attributed to the cyclodextrin modification. It was also confirmed in a variety of genuine water samples, including tap water, aquaculture water (fish tanks and land-based industries), and ocean. Sample preparation required simple filtration (0.45 μm microporous membranes). Spiked recovery trials demonstrated good accuracy, ranging from 96.8% to 103.4%, with low relative standard deviations (1.89% to 4.21%), proving the robust detection accuracy under challenging aquaculture conditions.

Zhao[84] introduced a novel approach using an NiFe$_2$O$_4$@Ag sensor where an external magnetic field significantly enhances Raman detection of nitrite. This enhancement is attributed not only to magnetic aggregation of the nanoparticles but also to a magnetic field-induced dielectric polarization effect, leading to improved sensitivity. It also achieved an ultra-low LOD of 1.25

Table 7 Raman spectroscopic detection of nitrite ions in biological and environmental matrices

Platform	Reagent	Sample	Raman emission signal cm⁻¹	Range (μM)	LOD (μM)	Ref.
Au-SERS	2-Thiobarbituric acid	Tap water and pickled brine	685 cm^{-1}	10.87–369.48	4.56	78
Au-SERS	Urea	Human saliva	1003 cm^{-1}	20–120	N/A	77
A silver nano-pyramid array was used coupled with plasmonic gold nanostars-SERS	4-Aminothiophenol 4-ATP@Au and 1-naphthylamine (1-NA@Ag)	River water	1140 cm^{-1}, 1389 cm^{-1}, and 1434 cm^{-1}	2.17×10^{-5}–21 734.40	1.30×10^{-5}	20
Fe$_3$O$_4$@SiO$_2$/Au NPs-SERS	4-Aminothiophenol	Pond water, pickles and synthetic urine samples	1436, 1391, and 1140 cm^{-1}	10–100	15.63, 13.69, and 17.77	80
ZnO@Ag nanospheres	1-Naphthylamine (1-NA) and 4-aminothiophenol (4-ATP)	Pickled food	1281 cm^{-1}	0.01–1000	0.003	79
Au@COF composite	Toluidine blue (TB)	Luncheon meat, cured meat, sausage	N/A (attenuation of TB signal)	N/A	N/A	81
PDMS multi-channel SERS sensor	Urea (for nitrite)	Water pollutants	N/A (specific identification)	N/A	0.5	82
β-Cyclodextrin-modified AuNPs	o-Phenylenediamine (OPD) (forms BTAH)	Tap water, aquaculture water, seawater	N/A (SERS signal of BTAH)	0.1–30.0	0.0105	83
NiFe$_2$O$_4$@Ag sensor (magnetic field enhanced)	N/A	Real samples (environmental water)	N/A	0.01–1000	0.00125	84
3D composite SERS substrate (cysteamine/gold/cysteamine on anodic aluminum oxide)	N/A (direct detection)	Water	N/A	N/A	2.17	85
Alginate hydrogel substrates with SERS	Phenosafranin	Meat extracts	N/A	N/A	81.50–176.26	86
Au@Ag nanoparticles	4-Aminophenylthiophenol	Pickled food	N/A (PATP bridging)	5.00–100.00	0.17	87

$\times 10^{-9}$ mol L^{-1} (0.00125 μM) with a wide linear range from 10^{-8} to 10^{-3} mol L^{-1} (0.01 to 1000 μM). It demonstrated "superior detection ability towards NO$_2^-$ in real samples," suggesting its robustness in environmental water matrices.

Lai[85] proposed a three-dimensional (3D) composite SERS substrate consisting of a cysteamine/gold/cysteamine structure self-assembled onto anodic aluminum oxide. This 3D porous structure aims to improve the sensitivity for direct detection of nitrite and nitrate in water without any sample pretreatment. It showed LOD for nitrite of 0.1 mg L^{-1} (approx. 2.17 μM) in water samples. Importantly, this method allows for direct detection without any pretreatment, simplifying the analytical process. It also demonstrated equivalent detection limits for mixed nitrite and nitrate solutions, indicating its potential for multi-analyte analysis, though with a weaker Raman signal in mixed solutions.

In another development for food analysis, Liang combined alginate hydrogel substrates with SERS for the quantitative analysis of sodium nitrite in meat products.[86] This method utilizes phenosafranin as a single-molecule probe and focuses on optimizing the hydrogel properties for robust and consistent SERS signals. The study also explored the use of machine learning algorithms (Support Vector Machine) for more accurate data prediction and recovery rates in complex food matrices. This method reported LODs for sodium nitrite in meat extracts ranging from 3.75 mg kg^{-1} to 8.11 mg kg^{-1} (approx. 81.5 to 176.3 μM). The method showed low interference from the food matrix and achieved high recovery rates (98.6–99.8%) when combined with a Support Vector Machine algorithm for data prediction, outperforming traditional linear regression. This highlights the potential of integrating machine learning to enhance accuracy in complex food samples.

Finally, Wang developed a robust and sensitive SERS method for nitrites in pickled food using Au@Ag nanoparticles.[87] This platform leverages the high enhancement effect of silver and the good stability of gold. Nitrites are anchored to the substrate surface *via* bridging with 4-aminophenylthiophenol (PATP), which also aids in Raman scattering cross-section amplification and internal calibration, leading to high selectivity and precision. It was tested in pickled food and achieved an LOD of 0.17 μM with a linear range of 5.00–100.00 μM. This method demonstrated high selectivity and good precision (RSD < 7.00%) with satisfying recovery rates (101.42–107.35%) in real pickled food samples, proving its robustness in a challenging food matrix. The use of PATP for internal calibration further contributed to its reliability.

To sum up the contents of this section, Table 7 has been prepared.

4 Electrochemical detection methods

Electrochemical determination of nitrite achieved low cost, fast analysis, and applicability to different materials, giving many options for nitrite detection. Electrochemical methods could be classified into potentiometric and non-potentiometric

methods. Non-potentiometric methods include voltametric, amperometric, and impedimetric methods. In all electrochemical methods, working electrode surface functionalization and modification with organic and inorganic catalysts are strongly recommended to support high selectivity, high sensitivity, and robust analysis with fast electron transfer kinetics.[88]

4.1. Potentiometric methods

The potentiometric method for nitrite detection involves measuring the potential difference between a working electrode and a reference electrode at zero current. This technique often relies on ion-selective electrodes (ISEs) designed to selectively bind nitrite ions.

A nitrite potentiometric method was developed by Hassan et al.[89] using a polymeric membrane made of (4-sulphophenylazo-)1-naphthylamine (SPAN) to support the ion exchange of tris(bathophenanthroline) Ni(II)-SPAN. Nitrite was converted into a lipophilic SPAN ion with the use of a Griess reagent. In another potentiometric study, Shamsipur[90] prepared a longlifetime potentiometric method to detect nitrite in foods. Three different ionophores were constructed from the parasubstituted derivatives of (tetraphenylporphyrinato) cobalt(III) acetate and used for the preparation of a nitrite-selective electrode. Ganjali[91] introduced a sensitive and highly selective nitrite ion-selective electrode based on the Co(II)–salophen complex (CSC). The electrode's membrane was composed of the CSC complex, PVC, orthonitrophenyloctyl ether, and hexadecyltrimethylammonium bromide. Complexation–decomplexation kinetics of nitrite ions with the CSC complex resulted in a fast dynamic response time of less than 10 s, while the internal solution concentration didn't affect the potential response of the electrode. The plasticizer PVC affected the mobility of the CSC complex and its ionophore. This platform showed high simplicity in setup, rapid response times, and the potential for miniaturization for portable devices. Dana[92] prepared a nitrite selective electrode based on the metalloporphyrin Co(III) tetraphenylporphyrins (ClCoTPP) in o-nitrophenyloctylether plasticized PVC membranes. The potentiometric procedures involved the synthesis of chloro-(5,10,15,20-tetraphenylporphyrinato)–cobalt(III) ClCo(III)TPP to be used as the sensing element. The electrode showed near Nernstian response and great selectivity towards nitrite over different anions except for the lipophilic anions of thiocyanate and perchlorate. Thus, susceptibility issues to interferences from other ions were reported; hence, certain considerations were recommended for the electrode preparation, including the use of ionophores and more selective sensing elements. Additionally, another ionophore composed of a lipophilic derivative of cobalt(II) salophen was reported.[93] The Co(II) complex contained tertbutyl groups to monitor the nitrite. However, the leaching of the PVC-embedded ionophore was a big challenge for the applicability of this approach in real sample analysis. The undesired leaching of the Co(II) salophen ionophore could be prevented by enhancing its lipophilicity with the addition of tertbutyl groups (aliphatic terminal groups). Moreover, the tertbutyl groups improved the stability of the ionophores in the PVC membrane. Another ion-selective electrode was designed by Feng[94] to detect urinary tract infections in older people by measuring nitrite in fresh urine samples. Soares[95] produced a simple hydrophobic and hydrophilic ion-selective electrode based on laser-induced graphene (LIG) to detect nitrite in food samples. LIG was used for disposable printed electrodes. The hydrophobic electrode surfaces had less water between the electrode and the ion-selective membrane, which enhanced the potential stability, and provided a broad range of nitrite concentration from 10^{-5} to 10^{-1} M. According to these findings, potentiometric methods are generally fast, relatively inexpensive, and can be miniaturized for portable applications, and surface modification allows for tailoring the selectivity and sensitivity towards nitrite.

4.2. Voltammetric methods

In voltammetric methods, a voltage (V) is applied, and the resulting current (I) is measured. Linear sweep voltammetry involves a linear increase in potential. Cyclic voltammetry involves potential that has a triangular wave shape. Various materials are used in voltammetric methods, including nanomaterials. Nanomaterials have a large surface area and small particles, which increase the absorptivity of the electrode. Nanomaterials include metals (Pt, Ni, Ag & Au), metal oxides (Fe_2O_3, CoO_2, ZrO_2, MoO_6), or carbon-based materials such as graphene and multi-walled carbon nanotubes.[96–99]

Electrodes enhanced with metallic nanoparticles exhibited excellent performance in areas such as catalysis, mass transfer augmentation, high effective surface area, and biocompatibility.[88] Herein, Cao[100] synthesized the composite of iron porphyrin ($FeTMP_yP$) restacked and inserted into niobium molybdate laminates $[NbMoO_6]^-$ forming a $FeTMP_yP/NbMoO_6$ sandwich-shaped nitrite sensor, applied on a glassy carbon electrode through the exfoliation/restacking method. Using this nanocomposite, the differential pulse voltammetry technique (DPV) was used for testing nitrite in water samples, giving a limit of detection of 7.4 μM, and a small range of RSD% (0.013–1.340%), proving a high accuracy and strong applicability of the proposed sensor towards real sample analysis. In addition, high selectivity features were obtained when different species such as NaCl, $NaNO_3$, Na_2CO_3, and glucose were tested.

Yanalak[101] constructed a black phosphorus/molybdenum disulfide semiconductor doped with Ni and Co metals (BP/MoS_2-Y (Y: Ni, Co)). It was used in the dual applications of nitrite and photocatalytic hydrogen evolution sensing. The fabricated heterojunctions were tested on a glassy carbon electrode (BP/MoS_2–Co/GCE) for nitrite monitoring by linear sweep and differential pulse voltammetry. Because of their multiple intriguing features, carbon nanostructures have shown considerable promise in the development of high-performance electrochemical sensors. Carbon nanomaterial-enabled electrochemical sensors have been rated as one of the most promising technologies. With their great sensitivity, ease of use, and outstanding selectivity, nitrite detection methods seem promising. Silver sulfide nanoparticles combined with hierarchical porous carbon (HPC), in addition to fullerene C_{60}

and Nafion, formed a successful composite (C_{60}–Ag_2SNP–HPC–Nafion). The composite was mounted on a glassy carbon electrode and tested for nitrite by the DPV method.[102] HPC and silver sulfide were synthesized by the co-precipitation method. The coupling of HPC–silver sulfide with fullerene and Nafion was achieved by using Nafion as an immobilizer and the electrode deposition of fullerene solution on the electrode surface. The addition of fullerene enhanced the peak currents and the sensitivity of the electrode. HPC has excellent porosity, which was suitable for modification with silver nanoparticles.

Graphene and graphene oxide (GO) have a special chemical structure in which sp^3 carbons attached to different functional groups are separated by sp^2 carbons.[103] These properties made it an excellent material for electrode fabrication in sensing nitrite with low LODs. A nanocomposite made of reduced graphene oxide (rGO) and a mixture of manganese–vanadium oxide and gold nanoparticles (MnO_x–VO_x–AuNPs@rGO) was exploited for the effective voltammetric analysis of nitrite and hydrazine in sausages and river water.[104] The developed nanocomposite had many electroactive sites and nanoholes that improved the overall voltammetric performance of the modified electrode. Linear sweep voltammetry was the voltammetric technique used in reporting the oxidation process, resulting in an LOD of 10 μM. Nethravathi[105] developed a nanocomposite of reduced graphene oxide (rGO) and mixture of Bi_2O_3 and silver nanoparticles (Ag–Bi_2O_3–rGO) to be utilized for the voltammetric detection of nitrite in biological samples.

Mounesh and Venugopala Reddy[106] reported a reliable electrochemical method of nitrite detection using the thermally stable tetra L-methionine cobalt(II) phthalocyanine (CoTL-MethPc) coupled with MWCNTs. The process was validated by cyclic voltammetry, differential pulse voltammetry, and chronoamperometry techniques. Multiwalled carbon nanotubes increased the proton conductivity of the formed composite and the electron transfer rate. The catalytic process was diffusion-controlled with light absorption of the intermediate products

on the electrode surface. Mounesh[107] also synthesized tetra-4-(2-methoxyphenoxy) carboxamide cobalt(II) with amide-bridged phthalocyanine (CoTMePhCAPc) to analyze the nitrite in drinking water and leaf lettuce. The composite was further embedded with MWCNTs on the surface of a glassy carbon electrode.

Hybrid organic frameworks such as covalent-organic frameworks (COFs), metal organic frameworks (MOFs), and zeolitic imidazolate frameworks (ZIFs) exhibit porous coordinated structures showing high porosity, high chemical functionality, and tunable pore size. MOFs are suitable for electrochemical catalysis. But they have poor stability, so they should be modified with other heat- and water-stable nanomaterials.[108] Ambaye[109] prepared a metal–organic framework to develop an electrochemical sensor for nitrite in wastewater samples using carbon black/copper metal–organic framework (CB/Cu-MOF) nanocomposites. The CB/Cu-MOF was employed in flexible screen-printed carbon electrodes (SPCEs). The modified electrode demonstrated a fivefold increase in current response over the bare-SPCE with the LSV technique. Imidazole zeolites (ZIFs) combine the properties of MOFs and zeolites, with higher thermal and chemical stability. They are rich in nitrogen, carbon, and transition metals.[110]

Saeb[111] suggested a novel electrochemical sensor for nitrite detection based on the ZIF-8@ZIF-67/Au nanocomposite. The electrode was modified with Au nanoparticles to enhance the active surface area and the conductivity, so that the current response was improved. DPV was conducted in a phosphate buffer (pH 7.0) to determine the nitrite concentrations, providing an LOD of 2.0 nM and LOQ of 6.7 nM to be suitable for water and food analysis. Accordingly, nanomaterials are revolutionizing the field of voltammetric nitrite detection. Their unique properties enable the development of highly sensitive, efficient, and versatile sensors. By exploring novel materials and optimizing composite design, this technology holds immense promise for diverse analytical applications.
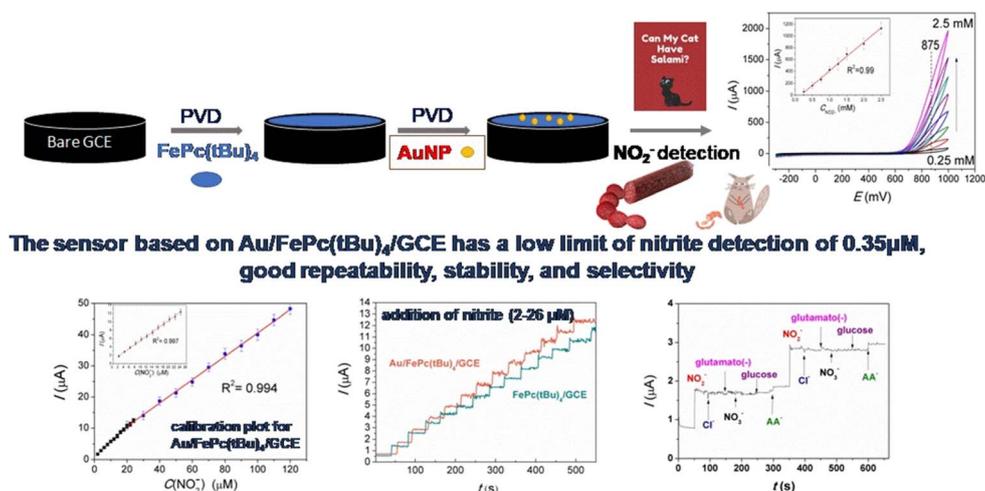

Fig. 3 The use of laser-induced graphene (LIG) to fabricate flexible screen-printed carbon electrodes and disposable nitrite ion-selective electrodes (reproduced from: S. I. Dorovskikh, D. D. Klyamer, A. D. Fedorenko, N. B. Morozova and T. V. Basova, *Sensors*, 2022, **22**, 5780), open access with permission from MDPI. Licensed under CC BY 4.0, 2022.
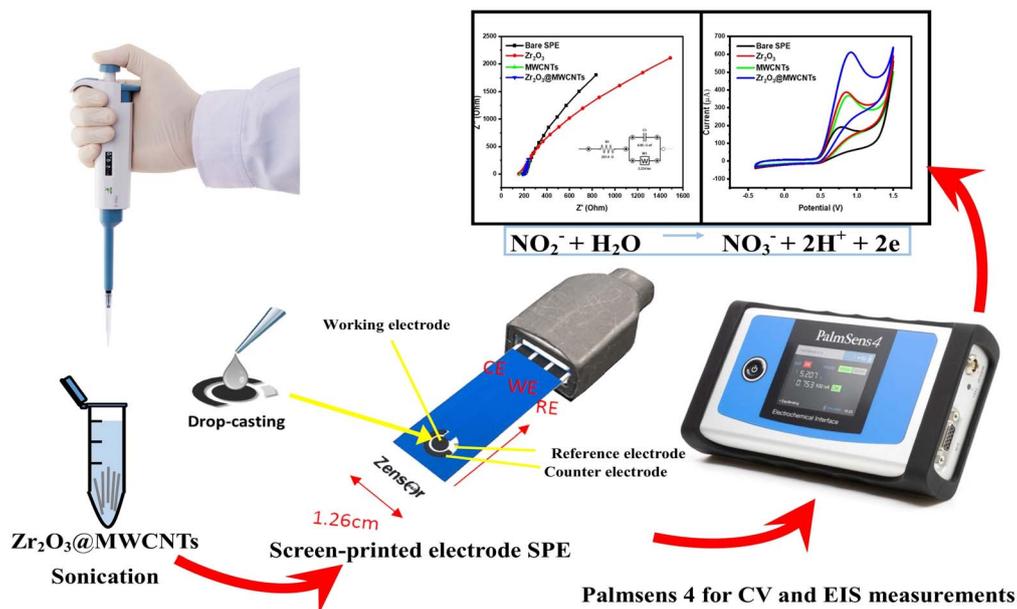
Fig. 4 Construction of a portable and disposable sensing system for the continuous monitoring of nitrite in food and environmental samples (reproduced from: N. Rajab, H. Ibrahim, R. Y. A. Hassan and A. F. A. Youssef, *RSC Advances*, 2023, **13**, 21259–21270), open access with permission from the Royal Society of Chemistry. Licensed under CC BY-NC 3.0, 2023.

4.3.   Amperometric methods

The amperometric method is highly suitable for measuring nitrite traces, due to the fast and direct oxidation of nitrite into nitrate in air. Such a fast and sensitive method is needed for real sample analysis. Amperometry allows for sensitive detection of nitrite by directly measuring the oxidation current. The continuous nature of the measurement enables real-time monitoring of nitrite concentration changes. In this regard, electrode surface modification with reduced graphene oxide or nanogold was used for the direct amperometric detection of nitrite in meat and lake water samples.[112,113] Chang[114] adapted a zirconium-based MOF (UiO-66)-iridium nanocomposite for the electrocatalytic amperometric determination of nitrite. Using an applied potential of 1.1 V, the LOD, linear range, and sensitivity were 0.41 μM, 5.0–120 μM, and 167 μA mM^{-1} cm^{-2}, respectively. Li[115] integrated the nano-organic framework MOF of UiO-66 with the expanded graphite (UiO-66/EG) by a solvothermal method and detected nitrite in the range of 0.20 μM–13 mM, giving an LOD of 0.06 μM. Yang[116] designed a nitrite sensing material based on Co@N-doped carbon nanorods and nanosheets derived from MOFs, which were extracted from the carbonization of Co-ZIF-L (2-MIM). For application in real water and sausage sample analysis, the optimized amperometric technique provided a wide range of nitrite from 0.5 μM to 8.0 mM, and LOD of 0.17 μM.

Dorovskikh[117] analyzed the nitrite in meat products by using a mixed composite of iron(II) tetra-*tert*-butyl phthalocyanine and Au nanoparticles to produce a thin film of Au/FePc(*t*Bu)$_4$ for the sensitive amperometric detection of nitrite, as shown in Fig. 3. Saraiva[118] reported another amperometric procedure using carbon fiber microelectrodes. Three-pulse amperometry was

applied at a constant potential of 0.8 V and the current decay decreased from 47% to 0%. Additionally, metal oxide-based electrodes were used to improve the electronic properties of the modified nanocomposites in conjunction with MWCNTs. Rajab[119] modified a disposable screen-printed electrode with a ZrO$_2$@MWCNT nanocomposite, as shown in Fig. 4. The catalytic activity was enhanced by a factor of 6 compared to the bare electrode. MWCNTs improved the conductivity while zirconium oxide increased the peak current. Chronoamperometry was used in evaluating the sensor, and the calibration curve resulted in an LOD of 0.94 μM. The electrode was applied to several food and water samples, such as burgers, chicken, cooler–sheller water, and tank water. Another disposable carbon electrode modified with bismuth selenide-carboxylic multi-walled carbon nanotubes (Bi$_2$Se$_3$@MWCNTs-COOH) was implemented.[120] The use of MWCNTs provided a wide network connection that allowed Bi$_2$Se$_3$ to disperse between them, thus increasing the active sensing area.

A group of metal oxides (CuO, NiO, and SnO$_2$) was conjugated onto a transparent conductive Fluorine-doped Tin Oxide electrode (FTO) for application in the nitrite amperometric analysis.[121] First, CuO was allowed to build up on a clean pre-treated FTO electrode uniformly. The nickel nitrate was drop cast on the CuO-FTO electrode and oven dried at 400 °C, giving the resulting CuO–NiO@FTO electrode doped with fluorine SnO$_2$. The drop-casting of NiO on CuO decreased the diffusion resistance and increased the electron transfer rate. This electrode was tested on real tap water samples. Cheng[122] fabricated a non-enzymatic amperometric nitrite sensor synthesized from the nanomaterial ZnO, and modified it with the conductive copolymer on a glassy carbon electrode. The hybrid coupling of Co$_3$O$_4$ and MoO$_3$ with a glassy carbon electrode was carried out

for the sensing of nitrite in food and water samples.[123] The composite was prepared by electrodeposition of $(NH_4)_6$-$Mo_7O_{24} \cdot 4H_2O$ and $Co(NO_3)_2 \cdot 6H_2O$ and rinsed with deionized water. The proposed electrode was tested in sausage and water samples. The LOD showed up to be 0.075 μM with a high sensitivity of 1704 μA mM^{-1} cm^{-2}.

Manibalan[124] used electrodes modified with CeO_2 doped with Sn for nitrite detection. This electrode was fabricated by facile precipitation on a glassy carbon electrode. Cyclic voltammetry and amperometry were used for nitrite investigation, resulting in an LOD of 16 nM. This $Sn–CeO_2$ electrode was applicable in a spiked pond lake with RSDs of 2.43% and 2.62%. Sudhakara[125] suggested a platform made of ZnO conjugated with tetra-amino-cobalt(II) phthalocyanine, which was mixed with polyaniline (PANI) to form PANI-TaCoPc@ZnO. As the author claimed, the existence of PANI increased the active surface area. In another report, GO was modified with PANI and Au nanoparticles.[126] In this regard, the existence of PANI prevented the aggregation of the Au nanoparticles and supported the electrical conductivity of the modified electrode. The sensing platform was applied for the amperometric analysis of nitrite in tap water with an LOD of 0.17 μM, with an extremely short time of analysis (2.0 seconds as a response time).

Additionally, other introduced materials, such as poly-3,4-ethylenedioxythiophene, exhibited promising features due to their ease of polymerization, low cost of preparation, and high conductivity.[127] Thus, Kumar[128] modified a working electrode with the PEDOT-rGO to be applied for the electrochemical detection of nitrite. The PEDOT-rGO-based electrode provided numerous active sites and high electrocatalytic activity.

To exploit the advantages of GO, CNTs, and metal oxides, Zhao[129] developed an electrochemical sensor based on Co_3O_4-rGO@CNTs. Graphene oxide nano-sheets were produced by the Hummers' method before they were physically mixed with the CNTs through a one-hour sonication. Eventually, the collected mixture was annealed at 350 °C for 2 h. This sensor did not generate amperometric responses with different interferents such as Na^+, SO_3^{2-}, NO_3^-, Cl^-, and alcohol. Thus, the sensor was applied to water samples spiked with different concentrations of nitrite and showed high recoveries between 96 and 102%. Furthermore, the growth of Au nanoparticles on graphene and carbon nanofibers achieved a high sensitivity (8361 A cm^{-2} mM^{-1}), with an LOD of 1.24 μM over a wide linear range of 1.98 μM–3.77 mM. Feng[130] constructed an electrochemical sensing platform for amperometric detection of nitrite using ZIF-67C@RGO/NiNPs loaded on a glassy carbon electrode for application in food, ham, and sausage analysis. Silicon was also exploited for nitrite determination.[131] The modified silicon-based electrode was fabricated by the microfabrication method and demonstrated high stability and reproducibility of 94%. River water, seawater, and deionized water spiked with nitrite were analyzed using this electrode material. Annalakshmi[132] suggested the sonochemical synthesis of strontium ferrite (SF) nanochain architecture, and the sonochemical process improved the electrochemical performance of the electrode. Accordingly, real water samples of rain, river, and tap water

were analyzed with a very small RSD that varies between 0.02 and 0.15%.

A hybrid combination between organic and inorganic materials was developed for the detection of nitrite,[133] a keg-ging-type cluster of $[SiMo_{12}O_{40}]^{4-}$ combined with $[Cu(pic)_2]$ units forming a 2D framework arrangement. The reported sensor wasn't tested in real samples, but the test experiment approved its sensitivity, selectivity, and LOD. Cai[134] proposed a 2D transistor sensor for the amperometric detection of nitrite, showing an excellent LOD of 0.01 nM. The sensor was based on the highly conductive ultrathin $Ti_3C_2T_x$-MXene prepared by the direct etching of $Ti_3C_2T_x$ in the presence of LiF and HCl. Then the ultrathin $Ti_3C_2T_x$-MXene was doped with Au nanoparticles. The advantage of the transition metal used is amplifying the signals produced, thus providing a high sensitivity of the sensor in addition to the electrocatalytic properties of the gold nanoparticles. Zhang[135] designed a novel 3D CeO_2 nanosheets/CuO nanoflower p–n heterostructure supported on carbon cloth (CeO_2 NSs/CuO NFs/CC) for electrochemical nitrite sensing. This unique architecture, synthesized by electrodeposition, combines the p-type CuO nanoflowers with n-type CeO_2 nanosheets, creating a p–n heterojunction. The morphology optimization (nanoflowers and nanosheets) significantly increases the electrochemically active surface area and availability of active sites, while the p–n heterojunction promotes efficient charge transfer and carrier separation, enhancing electrocatalytic activity and reducing the required oxidation potential. This leads to a high sensitivity of 11 610 μA mM^{-1} cm^{-2}, a wide linear range of 0.1–4000 μM, and an LOD of 0.037 μM. The prepared electrode can rapidly and accurately detect nitrite residues in food samples, indicating excellent anti-fouling properties and stability due to the robust 3D structure and strong electronic interactions within the heterostructure, which minimize non-specific adsorption and maintain the performance in complex food matrices. Promsuwan[136] devised a gunshot residue (GSR) screening flow injection nitrite with a high throughput of 165 samples per hour. The sensor was modified with Pd and glassy carbon microspheres (GCMs) to enhance the electrocatalytic activity as well as the amperometric responses. For further enhancements, Promsuwan[137] developed a portable FI-amp system. Screen-printed carbon electrodes were altered with silver nono-prisms and phosphorus CNTs (AgNPr@P-CNTs/SPCE) and nitrite was detected in the presence of GSR. The kinetics were studied using chronoamperometry and cyclic voltammetry. Amperometry's future in nitrite detection is bright. New materials like 2D TMDCs and optimized hybrid materials promise even better performance. Integration with microfluidics can create miniaturized, automated analysis systems. While voltammetry offers valuable information, amperometry's simplicity, real-time analysis, and high sensitivity make it ideal for nitrite detection, especially when combined with advanced materials and microfluidics. Despite the advantages, amperometric techniques require careful consideration of factors like applied potential, electrode fouling, and interferences from other analytes in the samples.

Table 8 Developed electrochemical methods used for the nitrite ions in biological and environmental matrices

Sensing element(s)/transducer	Method	Real sample	Detection range (μM)	LOD (μM)	Ref.
Tris(bathophenanthroline) Ni(ii)/(4-sulphophenylazo)-1-naphthylamine (SPAN)@polyvinyl chloride (PVC)	Potentiometry	Wastewater and meat products	$1–1 \times 10^4$	0.5	89
(Tetraphenylporphyrinato) cobalt(iii) acetate@polymeric membrane (PME)-coated graphite (CGE)	Potentiometry	Milk, cheese, flour, and sausage	PME: $1–1 \times 10^5$; CGE: $0.05–5 \times 10^4$	PME: 0.8; CGE: 0.02	90
Co(ii)–salophen complex (CSC)	Potentiometry	Water, milk, cheese, wheat, sausage, and flour	$1–1 \times 10^5$	0.8	91
Co(iii) tetraphenyl porphyrins (TPP) in o-nitrophenyloctylether polyvinyl chloride PVC	Potentiometry	Beef, sausage, pate, and salami	$50–1 \times 10^5$	40	92
Co(ii) tert-butyl-salophen	Potentiometry	Human urine	$10–1 \times 10^4$	2	93
Urinary tract infection (UTI) screening point of care testing POCT device	Potentiometry	Human urine	N/A	N/A	94
Laser-induced graphene (LIG)	Potentiometry	Bacon, ham, and sausage	$10–1 \times 10^5$	2.17	95
SA/NEA/MHA/Au	Impedimetry	Blood serum	0.1–4	0.02	141
Embedded ion-imprinted polymer (IIP)	Impedimetry	Milli-Q water	217.34–869.37	N/A	139
CPE/Ru(iii)-BSAP-PLA	Impedimetry	Tested in NaCl solution	$0–1.38 \times 10^4$	1.39	142
Au@Chrome-Black T	Impedimetry	Tested in purified water	0.5–100	10	140
CR-GO/GCE	Amperometry	River, tap & rainwater	8.9–167	1	112
Nanoporous gold	Amperometry	Processed meat and lake water	$1–2 \times 10^3$	0.01	113
Ir-UiO-66	Amperometry	Tested in $HClO_4/NaClO_4$ aqueous solutions	5–120	0.41	114
CoN-CRs/MGCE	Amperometry	Sausages and tap water	$0.5–8 \times 10^3$	0.17	116
Au/FePc(tBu)$_4$/GCE	Amperometry	Meat products	2–120	0.35	117
Carbon fiber microelectrodes	Amperometry	Tap water and synthetic saliva	$15.21–1.999 \times 10^3$	5.43	118
CuO/NiO/FTO	Amperometry	Milk, apple juice and pickles	$1–1.8 \times 10^3$	0.013	121
MoO$_3$/Co$_3$O$_4$/CC	Amperometry	Water and sausages	$0.3125–4.514 \times 10^3$	0.075	123
GO-PANI-AuNPs/GCE	Amperometry	Tap water and sewage	0.0005–2.58	0.17	126
Ni$_{2.5}$Mo$_6$S$_{6.7}$/PEDOT-rGO/GCE	Amperometry	Tap water and pickled vegetables	$1–1 \times 10^4$	0.33	127
Bi$_2$Se$_3$@MWNTs-COOH	Amperometry	Tap water and moat water	$0.01–7 \times 10^3$	0.002	120
Co$_3$O$_4$-rGO/CNTs	Amperometry	Tap water	$8 \times 10^3–5.6 \times 10^4$	0.016	129
ZIF-67C@RGO/NiNPs/GCE	Amperometry	Ham sausage	0.2–473	0.086	130
Si@Ag/AgCl@ Au WE/CE	Amperometry	Sea water & river water	$500–2.5 \times 10^3$	27	131
SF/GCE	Amperometry	Rain, river and tap water	$0.02–3.6 \times 10^3$	0.0063	132
[SiMo$_{12}$O$_{40}$]$^{4-}$	Amperometry	Tested in $H_2SO_4 + Na_2SO_4$	100–900	0.22	133
Sn–CeO$_2$	Amperometry	Pond water	$10–6 \times 10^3$	0.016	124
PA-TaCoPc@ZnO	Amperometry	N/A	0.2–2	0.021	125
AuNPs/Ti$_3$C$_2$T$_x$-MXene	Amperometric transistor	Lake water	$1.0 \times 10^{-5}–5 \times 10^3$	1.0×10^{-5}	134
Pd-GCM/GCE	FI amp	N/A	$0.1–4 \times 10^3$	0.03	136
Ag nanoprisms@P-CNTs	SPCE/FI-amp	N/A	$0.01–4 \times 10^3$	0.0032	137
ZrO$_2$@MWCNTs/SPE	Chronoamperometry	Food and water samples	5–100	0.94	143

Table 8 (Contd.)

Sensing element(s)/transducer	Method	Real sample	Detection range (μM)	LOD (μM)	Ref.
FeTMPyP/NbMoO$_6$/GCE	Differential pulse voltammetry	Water samples	40–670	7.4	100
C$_{60}$-Ag$_2$SNP-HPC-Nafion/GCE	Differential pulse voltammetry	Processed meat and river water	4.0–148	0.09	102
ZIF-8@ZIF-67/Au	Differential pulse voltammetry	Water, sausages, and deli meat	$6.4 \times 10^{-3} - 2.214 \times 10^4$	0.002	111
BP/MoS$_2$–Co/GCE	Differential pulse voltammetry	Pond and sea water	$100–2 \times 10^3$	4.1	101
CB/Cu-MOF/SPCE	Linear sweep voltammetry	Waste water	1.0–200.0	0.084	109
Ag–Bi$_2$O$_3$–rGO	Linear sweep voltammetry	KCl electrolyte	$100–1.2 \times 10^3$	19.792	105
CoTLMethPc/MWCNTs/GCE	Cyclic voltammetry and differential pulse voltammetry	Beetroot gravy vegetable	CV: 0.05–0.75 DPV: 0.05–1.05	CV: 0.03 DPV: 0.035	106
CoTMePhCAPc/MWCNTs/GCE	Cyclic voltammetry and differential pulse voltammetry	Drinking water and butter leaf lettuce	CV and DPV: 0.05–0.75	CV and DPV: 0.0105	107
AuNPs/MnO$_x$-VO$_x$/ERGO/GCE	Linear sweep voltammetry and amperometry	Sausages and river water	LSV: $30–1 \times 10^3$ AMP: 1–100	LSV: 10 AMP: 0.33	104
CeO$_2$ NSs/CuO NFs/CC p–n heterostructure	Amperometry	Food samples	$0.1–4 \times 10^3$	0.037	135

4.4. Electrochemical impedance spectroscopy (EIS)

EIS can be used to quantify target analytes in electrochemical systems by analyzing changes in electrical properties like charge transfer resistance, so researchers can quantify nitrite.[138] In this regard, on-site detection of nitrite was achieved using a self-assembled monolayer embedded with an ion-imprinted polymer (IIP).[139] The selectivity originates from the ion recognition sites of the IIP polymer surface that captures nitrite. The IIP-electrode was more sensitive to nitrite at lower applied frequencies. The EIS spectra showed NO_2^- saturation after 30 ppm. Luo[140] introduced another EIS approach based on a nanogold film integrated with a high-affinity chrome-black T. A sensitive and selective EIS sensor for nitrite was developed by Wang.[141] The sensor used a modified Griess reaction between naphthylethylenediamine (NEA) and sulphanilic acid (SA) on a gold electrode surface. The modified reaction produced negative self-assembled monolayers (SAMs) that acted as a barrier for electron transfer between the electrode and the redox probe $[Fe(CN)_6]^{3-/4-}$. The impedance signals increased with nitrite concentration, and the proposed electrodes showed an LOD of 20 nM. SA reacted with nitrite ions to form a diazo derivative, facilitating charge transfer through negative charges. The Au-modified electrode had a larger charge transfer impedance than the NEA/Au-modified electrode, suggesting that NEA facilitated electron transfer between the redox probe and electrode. The impedance response improved in the presence of SA, as the negative charges of SA resisted the redox couple's access to the electrode surface. A modified Randle's equivalent circuit was used to fit the impedance spectra and determine electrical parameters for each step.

In another study reported by Terbouche,[142] EIS was used to examine changes in charge transfer resistance (R) on a carbon paste electrode that was modified with a ternary Ru(III)–1,3-bis(salicylideneamino)propan-2-olpolydentate Schiff base (BSAP) and 3-picolylamine (PLA) (BSAP-PLA) complex. A non-ideal capacitor phase element was monitored. As the potential and temperature increased, the charge transfer resistance decreased, leading to better nitrite accumulation on the electrode's surface. The modified electrode CPE/Ru(III)-BSAP-PL experienced a surface barrier effect, which was confirmed by the increase in charge transfer resistance at higher anodic potentials, indicating the presence of Warburg impedance. However, the charge transfer resistance decreased, possibly due to electrostatic interaction between the complex and negatively charged NO_2^- ions. EIS offers advantages like sensitivity (LOD down to 20 nM) and selectivity through tailored surface modification; however, interpreting EIS data can be challenging due to the involvement of complex electrical models and fitting procedures. Expertise in electrochemistry and impedance spectroscopy is often required. To sum up the contents of this section, Table 8 has been prepared.

5 Bio-electrochemical nitrite sensors

Bio-electrochemical sensors are a class of analytical devices that integrate a biological recognition element (bioreceptor) with an

electrochemical transducer to detect specific target analytes in complex samples with high selectivity and sensitivity. These bioreceptors, such as enzymes, antibodies, DNA, or whole cells, provide the inherent specificity for nitrite, while the electrochemical transducer converts the biological recognition event into a measurable electrical signal. Recent advancements in this field have focused on enhancing sensor performance through the integration of novel materials, particularly nanomaterials, and optimizing sensor architecture for real-world applications.

5.1. Enzyme-based sensors

Enzyme-based biosensors utilize the catalytic activity of specific enzymes to facilitate the electrochemical detection of nitrite. These enzymes often catalyze reactions involving nitrite, leading to a measurable change in current or potential. For instance, Santharaman[144] investigated a bio-composite of cytochrome c reductase, polypyrrole, and a gold nanocomposite for nitrite biosensing in cardiac cells. This bio-composite was applied to a screen-printed carbon electrode (SPCE) surface and coupled with gold nanoparticles via N-hydroxysuccinimide (NHS) and N-(3-dimethylaminopropyl)-N′-ethylcarbodiimide hydrochloride (EDS), demonstrating a highly sensitive platform for nitrite in complex biological fluids. The biosensor showed a wide linear range from 0.1 to 1600 μM and a detection limit of 60 nM (0.06 μM). The authors also developed an ARM microcontroller-based portable electrochemical analyzer, which was successfully used to measure nitrite levels in hypoxia-induced H9c2 cardiac cells, with results in agreement with standard laboratory instruments. This highlights the potential for on-site analysis in complex biological matrices.

Another approach involved the immobilization of horseradish peroxidase (HRP) enzyme with Co_3O_4 and reduced graphene oxide (rGO) to develop a mediator-free bio-composite.[145] The presence of Co_3O_4 provided a protective microenvironment for the enzymatic stability of HRP, thus enhancing the active surface area of the nanocomposite and improving the electrocatalytic oxidation of nitrite. This biosensor displayed a wide linear range of 1–5400 μM and a low detection limit of 0.21 μM. Similarly, Zazoua[146] reported on the modification of a gold electrode with a catalase bio-membrane for impedimetric detection of nitrite. This study monitored the catalytic activity of the catalase enzyme, which is inhibited by nitrite. The resulting nitrite–catalase complex showed sensitive Electrochemical Impedance Spectroscopy (EIS) responses to nitrite in the presence of O_2, eliminating the need for an external mediator. The sensor achieved a very low detection limit of 8×10^{-11} M (0.00008 μM) in a phosphate buffer at pH 7.3, demonstrating high sensitivity, though real-world sample application details were not specified.

To address challenges in enzyme stability and analyte specificity, Erdoğan[147] prepared a liposome-based nitrite biosensor by encapsulating the nitrite reductase NirB enzyme and embedding the nitrite-specific NirC channels in the liposome structure. The proteoliposomes were coated on a glassy carbon electrode modified with a multi-walled carbon nanotube/chitosan matrix. The incorporation of NirC channels was crucial

for the passage of charged nitrite ions into the liposome, enabling nitrite measurement and significantly increasing the specificity of the electrode towards nitrite in the presence of unexpected oxidation responses from high concentrations of sulfate and formate. This highlights a novel strategy for improving selectivity by controlling analyte access to the enzyme. The sensor showed a linear response between 1 and 500 μM nitrite concentrations. While the sensitivity was slightly lower than that of an unentrapped enzyme, the entrapment of the enzyme in the liposome preserved the electrode activity by 55% over 30 days, addressing a key challenge of enzyme stability in biosensors.

Shi[148] fabricated a novel electrochemical horseradish peroxidase (HRP) biosensor by immobilizing HRP on a multi-walled carbon nanotubes-black phosphorene (MWCNTs-BP) nanocomposite modified carbon ionic liquid electrode (CILE). This sensor was designed for the simultaneous detection of trichloroacetic acid (TCA) and nitrite. The MWCNTs-BP composite significantly enhanced electron transfer and interfacial conductivity, facilitating efficient direct communication between HRP and the electrode. The biosensor exhibited excellent sensitivity for $NaNO_2$ detection with a linear range of 0.1–13.6 mmol L^{-1} (100–13 600 μM) and an LOD of 0.03 mmol L^{-1} (30 μM). It was successfully applied to detect NO_2 content in brine samples from pickled vegetables with recoveries ranging from 97.0% to 102.0% and RSD lower than 5.5%, demonstrating its strong practical applicability in complex food matrices.

5.2. Whole-cell biosensors

Whole-cell biosensors utilize living microorganisms, such as bacteria, as the biological recognition element. These systems leverage the metabolic activity of the cells in response to nitrite.

For example, Li[149] developed a highly specific and sensitive biofilm sensor based on nitrite-oxidizing bacteria (NOB) for the bio-electrochemical detection of nitrite in water. The mechanism relies on the competition for oxygen between aerobic respiration of NOB and cathode oxygen reduction on a carbon felt electrode, resulting in a decrease in current proportional to nitrite concentration. This sensor showed a linear relationship for nitrite in the range of 0.1 to 1 mg L^{-1} and 1 to 10 mg L^{-1} (approx. 2.17 to 21.74 μM and 21.74 to 217.4 μM, respectively), with an LOD of 0.033 mg L^{-1} (0.72 μM). It was successfully applied to actual nitrified wastewater, demonstrating its capability in complex environmental matrices. Crucially, to address the challenge of ammonia-oxidizing bacteria (AOB) interference, allylthiourea (ATU) was effectively used to inhibit AOB activity, maintaining the high selectivity of the biofilm sensor during long-term detection in real water. However, its selectivity could be affected by (AOB); allylthiourea (ATU) was used as a mitigation strategy to inhibit AOB activity and maintain selectivity, directly addressing a common biological interference challenge in wastewater analysis.

Focusing on rapid and robust environmental detection, Wang[150] developed another novel, rapidly responding, high

sensitivity (958.6 μA μM^{-1} cm^{-2}), wide detection range, and anti-interference electrochemical biosensor based on electro-active nitrite-oxidizing bacteria. This biosensor could accurately detect nitrite in the range of 0.3–100 mg L^{-1} (approx. 6.5–2174 μM) within 3 minutes by cyclic voltammetry (CV). The specificity of the biosensor for detecting nitrite was demonstrated by the presence of nitrite oxidizing bacteria (NOB) and nitrite oxidase enzyme (NXR) on the electrode biofilm. The bioelectrode could perform stable detection of nitrite over 200 cycles. The biosensor performed well in wetlands and rivers, with an RSD <14.8% in the detection of nitrite at low concentrations, further revealing the occurrence of nitrification. This highlights its practical application for long-term monitoring and ecological function assessment in diverse surface water bodies.

Another bio-cathode sensor by Lin[151] suggested a novel, rapidly preparable, and easily maintainable biocathode electrochemical biosensor (BEB) using nitrite-reducing bacteria as detectors for continuous nitrite monitoring in wastewater. This BEB could detect nitrite in the range of 0.1–16.0 mg NO_2^-–N per L (approx. 2.17 to 347.8 μM) within 1.7 minutes. The use of nitrite reductase found in these bacteria proved to be a helpful tool in monitoring nitrite levels in water and wastewater. The BEB was successfully used to detect nitrite in real wastewater with a relative error <4.0% and a relative standard deviation <5.8%, demonstrating its robustness in complex environmental matrices. Furthermore, the BEB could be easily maintained by operating in an MFC mode, ensuring stable detection for at least 150 tests, which addresses long-term stability and reusability challenges. Another bio-cathode sensor by Lin was based on a metronidazole-treated biocathode (MT-NBEB) for nitrite detection in wastewater.[152] This MT-NBEB could detect nitrite in the range of 0.0001–8 mg NO_2^-–N per L (approx. 0.002 to 173.9 μM) within 1.7 minutes and maintained stable detection for over 50 continuous cycles (RSD < 2.4%). Notably, its response signals were not affected by common inorganic salts (nitrate, ammonia) and organic matter (acetate), highlighting its high selectivity in complex wastewater matrices. The metronidazole treatment selectively removed interfering electroactive bacteria to achieve this enhanced selectivity, providing a direct mitigation strategy for matrix interferences.

Cheng[153] proposed a novel dual-function electrochemical biosensor (DFEB) that could perform fast, simultaneous detection of nitrite and dissolved BOD. This DFEB utilized a mixed-bacteria bioelectrode with bidirectional electron transfer ability, prepared by culturing the anode of a microbial fuel cell (MFC) in a heterotrophic environment. The sensor accurately measured dissolved BOD in the range of 5–100 mg BOD per L and nitrite in the range of 0.05–16 mg NO_2^-–N per L (approx. 1.09–347.8 μM) within 20 minutes, maintaining stable performance over 200 tests. Crucially, the competition between bio-electrochemical acetate oxidation and nitrite reduction processes was restrained by regulating the operating electrode potential at non-overlapping intervals (−0.5 V and −0.2 V vs. Ag/AgCl), a key strategy for multi-analyte detection. The DFEB performed well in artificial wastewater, aquatic wastewater, anaerobic tank effluent, and anammox effluent, with relative errors <15.7% for nitrite and <16.8% for BOD, showcasing its robustness in various

complex wastewater matrices. This approach holds promise for self-powered and potentially regenerative biosensors, offering a sustainable solution for continuous monitoring in complex wastewater.

Another proposed novel approach was constructed to rapidly fabricate an electrochemically active biofilm (EAB) biosensor for nitrite detection by coating bioinks with varying conductive materials onto graphite sheets.[154] This method significantly shortened the incubation time and improved reproducibility, addressing challenges in large-scale production. Incorporating conductive materials, particularly carbon nanofibers, remarkably enhanced the maximum voltage of the bio-electrode and amplified the nitrite reduction current by a factor of 2.97 due to enhanced extracellular electron transfer (EET). The developed nitrite biosensor exhibited a detection range of 0.1–15 mg NO_2^-–N per L (approx. 2.17 to 326.1 μM), with a high sensitivity of 610.8 μA mM^{-1} cm^{-2}, and a stabilization operation time of at least 280 cycles. This approach offers a practical solution for rapid preparation, scale production, and optimization of highly sensitive and stable EAB sensors.

Yang[155] developed an antiterminator microbial whole-cell biosensor (MWCB) based on *Bacteroides thetaiotaomicron* for *in vivo* diagnosis of colitis. This engineered probiotic responds to nitrate and nitrite, which are elevated in inflammatory environments like colitis. The nitrate/nitrite-inducible promoter was optimized for sensitive and specific response. A preliminary *in vitro* assessment confirmed the functionality, and its *in vivo* sensing ability was evaluated in a chemically induced mouse model of ulcerative colitis (UC). The MWCB exhibited a robust response to colitis, with a notable positive correlation between the intensity of the response and the level of inflammation. This represents a significant advancement in *in vivo* biosensing for diagnostic applications, where the biological matrix is highly dynamic and complex, and sample preparation is virtually non-existent as the sensor operates directly within the living system.

Fan[156] designed a novel biosensor for the simultaneous detection of nitrate and nitrite using self-assembled hydrogel bioelectrodes with reduced graphene oxide (rGO) and genetically engineered electroactive *Shewanella* species. The highly conductive rGO drastically improved reverse electron transfer from the electrode to *Shewanella*, enabling a sensitive and quantitative response. The genetically engineered *Shewanella* allowed for efficient differentiation of nitrate and nitrite detection in a single system, achieving a sensitivity of 888.48 μA mM^{-1} cm^{-2} to nitrite with a low detection limit of 0.72 μM. The whole-cell biohydrogel-based biosensor also demonstrated excellent anti-interference properties and long-term storability, making it suitable for plug-and-play applications in practical environmental monitoring. This work highlights the power of genetic engineering in bacteria for dual-analyte detection in complex environments.

5.3. Aptasensors and immunosensors

Aptasensors and immunosensors employ highly specific recognition elements like aptamers (single-stranded DNA or RNA molecules) or antibodies, respectively, to bind to nitrite.

The principle involves the binding event triggering an electrochemical change. Seo[157] developed a biosensor for nitrite ion on an ITO electrode surface modified with M13 viruses and gold nanostructures. Gold dendritic nanostructures (Au-DNs) were electrochemically co-deposited from a 4E peptide engineered M13 virus (M134E) mixed electrolyte. The M134E specifically nucleated gold precursors, enabling the efficient growth of dendritic nanostructures. This system demonstrated improved sensitivity and selectivity toward nitrite ions from possible interferences, including NO_3^-, Na^+, Ca^{2+}, glucose, and ascorbic acid. The use of biologically engineered viruses provides a highly specific recognition element, contributing significantly to the sensor's ability to overcome matrix effects. Chen[158] developed a simple electrochemical biosensor based on HS-β-cyclodextrin coordinated methanobactin/gold nanoparticles (HS-β-CD@Mb/AuNPs) modified onto a gold electrode. Methanobactin (Mb), a small bioactive peptide, was used for *in situ* reduction of gold nanoparticles (AuNPs). HS-β-cyclodextrin (HS-β-CD), with its supramolecular recognition function, was coordinated with Mb/AuNPs *via* an Au–S bond. This biosensor achieved a low detection limit of 0.013 μM within a linear range of 0.1–10 000 μM. The selectivity of the sensor was demonstrated by anti-interference experiments, and it showed good recoveries (96.53–102.54%) when successfully applied to the detection of nitrite in real samples, particularly in the context of food safety. This work highlights the potential of combining bioactive peptides and supramolecular recognition for highly sensitive and selective nitrite detection.

5.4. Integration of nanomaterials in bio-electrochemical sensors

The integration of nanomaterials is a cornerstone of modern bio-electrochemical nitrite sensors, significantly enhancing their performance by providing high surface area, improved conductivity, and excellent platforms for bioreceptor immobilization, as shown in Scheme 3.

5.4.1. Carbon-based nanomaterials. Zhang[159] developed a conductive laser-induced graphene (LIG) electrode by using a nail polish (NP) embedded in the chitosan (CS) layer to construct a CS/NP-LIG sensor. The nail polish acted as a precursor of the laser-induced graphene LIG. A polyethylene terephthalate (PET) sheet was drop-cast with nail polish and dried, then it was laser scribed using a 405 nm laser engraving machine. The CS layer had a strong accumulation ability on the LIG surface due to its porosity, thus enhancing its sensing capabilities for nitrite in tap and lake water. Nitrite electrochemical measurements were carried out in phosphate buffer (pH 4.0) using cyclic voltammetry and DPV techniques. Salhi[160] suggested a cysteine-based biosensor. By combining cysteine with carbon black nanomaterials and performing an electrodeposition on poly 1,8-DAN (1,8-diaminonaphthalene), the biosensor showed a strong catalytic effect on nitrite oxidation. The combination of thiol and amine groups with carbon black resulted in superior sensing performance. The biosensor successfully detected nitrite in tap water samples with an RSD of 1.8–3.7% and demonstrated sensitivity of 0.126 and 0.94 μA μM^{-1} by amperometry and differential pulse techniques, respectively. Pan[161] modified L-cystine with gold nanoparticles and graphene oxide (AuNPs/GO-SH), where the graphene oxide was functionalized with mercapto-SH for higher ion stability, improving the electrochemical response of nitrite. This sensor was successfully used for nitrite determination in pickled radish, a complex food matrix, demonstrating its promising application in food safety. The electrode showed an LOD of 0.25 μM and a wide range of 5 to 1000 μM. Liu utilized Co_3O_4 and reduced graphene oxide (rGO) to immobilize horseradish peroxidase (HRP), creating a mediator-free bio-composite.[145] Co_3O_4 provided a protective microenvironment for HRP's enzymatic stability, thus enhancing the nanocomposite's active surface area and improving the electrocatalytic oxidation of nitrite in environmental samples.

5.4.2. Metal and metal oxide nanoparticles. Wang[162] reported the use of nano TiO_2 and $Ti_3C_2T_x$, containing chitosan and CTAB, in a glassy carbon electrode. This composite TiO_2-Ti$3C_2TX$-CS-CTAB/GCE showed a linear range of 0.003 μM to 1.25 mM and an LOD of 85 μM. The usage of MXene improved the catalytic and electrochemical properties of the electrode as it showed electrochemical conductivity of 4600 S cm^{-1}. The modified electrode was tested on milk and water. The
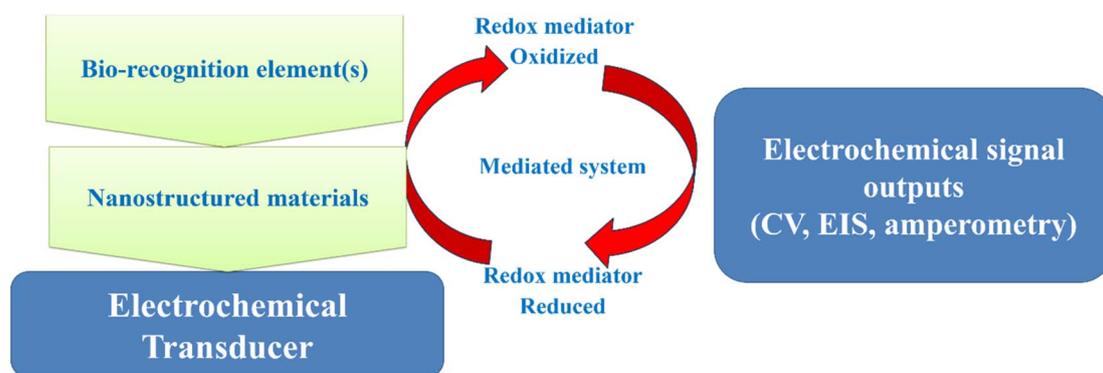
Scheme 3 Bio-electrochemical setup showing the main components including the transducer (electrode) modified with a layer of nanomaterial(s), followed by a layer of bio-recognition element(s) used for the selective analysis. The signal readouts could be obtained through the EIS, CV or/and amperometric techniques.

compatibility between unconventional materials, biorecognition elements, and the overall sensor architecture needs careful evaluation. Additionally, the long-term stability and reusability of sensors incorporating unconventional materials require further investigation.

Focusing on the immobilization of sensing elements on magnetic nanoparticles, Riahifar[163] immobilized cysteine on the nano metal oxide Fe_3O_4, modified with gold and rGO on a glassy carbon electrode (Fe_3O_4@Au@Cys/rGO/GCE), which enhanced the nitrite catalytic response. This sensor was successfully applied for the quantitative measurement of nitrite in human serum, urine, and water, demonstrating high stability and reproducible behavior in these complex biological and environmental fluids. Mohd Taib[164] constructed a biosensor for nitrite detection based on Au nanoparticles that were modified with the extract of *Hibiscus sabdariffa* leaves by a green biosynthetic route. *H. sabdariffa* leaves contained chlorogenic acid that reduced the Au^{3+} ions. The bio-composite was prepared by mixing $HAuCl_4 \cdot 3H_2O$ with *H. sabdariffa* aqueous extract and distilled water with continuous stirring at 600 rpm till the color of the mixed solution turned from pale orange to purple, which is an indicator of Au-NP formation. The electro-oxidation of nitrite was evaluated by cyclic voltammetry, and it showed a limit of detection of 0.11 mM with a linear range of 0.37–10 mM.

Exploring enhanced stability and wide detection ranges using polymer-modified copper nanoparticles, Chu[165] prepared a new nanocomposite by modifying polyaniline–carboxymethyl cellulose nanorods (PANI–CMC) with copper nanoparticles (PANI–CMC@Cu NPs/GCE).[22] Carboxymethyl cellulose (CMC) was used as a template for polyaniline polymerization, forming PANI–CMC nanorods, and also provided an antioxidant film (approx. 2.5 nm thick) around the copper nanoparticles, effectively slowing down their oxidation rate and preventing aggregation. This enhanced stability is crucial for the long-term performance of the sensor. The PANI–CMC@Cu NPs/GCE sensor showed good current response to nitrite with linear detection ranges of 3–15 000 μM and 15 000–29 000 μM, and an LOD of 0.170 μM. It retained 91.3% of its initial sensitivity after 25 days, demonstrating good stability, and was successfully applied to real tap water samples with good recovery rates (102–110%), indicating its accuracy and robustness in a common environmental matrix. To investigate the use of plant extracts for nanoparticle synthesis, Rajith Kumar[166] synthesized NiO nanoparticles using the extract of *Calotropis gigantea* to trace nitrite electro-analytically. The biosensor was modified with nickel oxide, which showed photodegradation of cationic methylene blue (MB) dye using a 250 W UV-light irradiation source. The antibacterial activity of the composite was tested against *S. aureus* and *E. coli* by the Agar well diffusion method, and the NiO NPs inhibited the antibacterial activity of both bacterial strains. The electrochemical calibration curve of nitrite additions was recorded and studied by differential pulse voltammetry in acetate buffer. While the nitrite detection utilized differential pulse voltammetry in acetate buffer, further exploration is needed to optimize its performance.

A green and sustainable approach for nitrite sensing and reducing biomass wastes in water was developed based on egg membrane wastes. To create a cost-effective and highly conductive sensing material from biomass waste, Cao[167] used the waste of egg membrane (ESM) to adsorb Cu^{2+}, which was converted by rapid pyrolysis into Cu^+ biochar. This biochar system had excellent properties such as high conductivity, a 3D porous network, and a large active surface area that was ideal for the electrochemical oxidation of nitrite. The electrode's performance was evaluated by cyclic voltammetry in phosphate buffer (pH 5–7) using a glassy carbon electrode. This approach was successfully applied to water and food samples. This sensor demonstrated superior electrochemical sensing abilities with a broad linear range (1–300 μM), ultralow detection limit (0.63 μM), and high sensitivity. It also showed excellent stability, good reproducibility, and strong anti-interference performance, and was successfully applied to detect nitrite in tap water, mineral water, and sausage samples with high recovery rates, highlighting its versatility and the dual benefit of waste valorization and pollution monitoring.

Mu[168] reported the synthesis of Ti_3C_2 nanosheets functionalized with apoferritin (ApoF)-biomimetic platinum (Pt) nanoparticle (Pt@ApoF/Ti_3C_2) composite materials. ApoF was used as a template for protein-inspired biomineralization of Pt nanoparticles. This nanohybrid exhibits excellent electrochemical sensing performance towards nitrite ($NaNO_2$), where Pt@ApoF catalyzes the conversion of nitrites into nitrates. The biosensor demonstrated a wide detection range of 0.001–9 mM (1–9000 μM) with a low detection limit of 0.425 μM. It also possesses high selectivity and sensitivity while maintaining a relatively stable electrochemical sensing performance over 7 days, enabling the monitoring of $NaNO_2$ in complex environments. This work provides a new approach for constructing efficient electrochemical biosensors, offering a simple and rapid method for detecting $NaNO_2$ in complex environments. Aldosari and Koh[169] developed a flexible nanoporous gold film electrode (NPGFE) by upcycling recordable compact disks (CDs) for nitrite biosensing. This cost-effective and sustainable fabrication method involved mechanical tailoring and electrochemical deposition of nanoporous gold onto the CD film. The NPGFE showed a significant increase in active surface area and minimized electron transfer resistance. It exhibited a linear range of 0.5 μM to 9 mM (9000 μM) with a sensitivity of 20 nA μM^{-1} cm^{-2} and a low detection limit of 0.5 μM. The sensor demonstrated remarkable reproducibility and highly satisfactory reusability. Selectivity studies showed a significant current increase with nitrite, ascorbic acid, and sodium sulfite, but no remarkable changes with other interferents. Importantly, the NPGFE retained 99% of its initial current response after six months of storage, indicating excellent long-term stability and service life. This highlights a promising platform for flexible and robust biosensors in various biomedical applications.

Introducing a novel visual detection method for food safety, Guan[170] developed a novel nanozyme-based electrochemical-driven electrochromic visual biosensor for rapid detection of nitrite in food samples. The system uses Fe_3O_4@Au-Cu/MOF as the nanozyme, which exhibits remarkable catalytic efficiency for

Table 9 Developed bio-electrochemical systems used for the nitrite ions in biological and environmental matrices

Electrode material	Bio-element	Detection method	Sample matrix	Range (μM)	Electrolyte	pH	LOD (μM)	Ref.
CS/NP-LIG	Chitosan	Differential pulse voltammetry	Tap and lake water	$2.0-1 \times 10^3$	N/A	N/A	0.9	159
Gold electrode	Catalase	EIS	N/A	$45-3 \times 10^4$	3 mM phosphate buffer	7.3	8×10^{-5}	146
Dual-function electrochemical biosensor (DFEB) (DFEB)	Microbial fuel cell (MFC)	Cyclic voltammetry	Wastewater	1.09–347.75	Phosphate buffer pH 7.2		N/A	153
ITO/Au$_{4E}$ electrode gold nanoparticles and electrodeposited on Co by the usage of ITO electrodes	M13 viruses engineered into 4E peptides M13 (M13$_{4E}$)	Linear sweep voltammetry	N/A	100–800			N/A	157
Poly 1,8-DAN/CB/GCE (1,8-diaminonaphthalene) and carbon black nanomaterials on a glassy carbon electrode	Cysteine	Amperometry and differential pulse voltammetry	Tap water	Amp: 1–40 DPV: 20–210	Phosphate buffer	7.2	0.25	160
Fe$_3$O$_4$@Au core–shell-rGO on a glassy carbon electrode	Cysteine	Differential pulse voltammetry	Urine & human serum	$0.03-2.215 \times 10^3$		3	0.008	163
Gold and graphene oxide	Cysteine	Cyclic voltammetry	Food samples	$5-1 \times 10^3$	Phosphate buffer pH 7.4		0.25	161
N-LC/CoS$_2$-MoS$_2$	Lignocellulose	Cyclic voltammetry	Human urine	$0.5-5.16 \times 10^3$			0.20	175
CNO/GCE electrode	Carbon nano onions (CNOs) from castor oil	Chronoamperometry	N/A	1–90	Phosphate buffer	6	0.75	174
Dual-chamber biocathode electrochemical biosensor BES	Nitrite reductase	Linear sweep voltammetry	Water and waste water	2.17–347.75	Phosphate buffer	6	N/A	151
Co$_3$O$_4$-HRP/rGO/GCE	Horseradish peroxidase	Amperometry	Environmental samples	$1-5.4 \times 10^3$		5.5	0.21	145
NOB biofilm on a carbon felt (CF) surface	Nitrite-oxidizing bacteria (NOB)	Amperometry	Real water	2.17–217.34		7.5	0.72	149
CcR-SAMGNP-PPy-SPCE Gold nanoparticles	Cytochrome c reductase	Cyclic voltammetry	Normoxia and hypoxia induced cardiac cells	$0.1-1.6 \times 10^3$	Phosphate buffer pH 7		0.06	144
TiO$_2$-Ti$_3$C$_2$T$_x$/CTAB-GCE	Chitosan	Differential pulse voltammetry	Milk & water	$0.003-1.25 \times 10^3$			85	162
3D printed graphene	Polylactic acid	Amperometry	Urine and saliva	0.5–250			0.03	176
Au-NPs/GCE	Hibiscus sabdariffa leaves	Amperometry	Tap & mineral water	$370-1 \times 10^4$	KCl	7	110	164
PANI–CMC@Cu NPs/GCE	Cellulose	Amperometry	Real water	$3-2.9 \times 10^4$	Phosphate buffer	5	0.170	165
Cu^{2+}-Cu$^+$/GCE	Biochar egg membrane waste ESM	Cyclic voltammetry	Water & food samples	1–300	Phosphate buffer	5–7	0.63	167
NiO/GCE	C. gigantea	Differential pulse voltammetry	N/A	$8-1.7 \times 10^3$	Acetate buffer	4	1.2	166
Metronidazole biocathode MT-NBEB	Nitrite reducing bacteria	Linear sweep voltammetry	Wastewater	0.00217–173.88	N/A	N/A	N/A	177
Liposome-based biosensor (NirB enzyme, NirC channels) on MWCNTs/chitosan modified GCE	Nitrite reductase (NirB) enzyme, NirC channels	Electrochemical (implied)	N/A	1–500	N/A	N/A	N/A	147
MWCNTs-BP nanocomposite modified CILE	Horseradish peroxidase (HRP) enzyme	Electrochemical (implied)	Pickled vegetable soaking water	$100-1.36 \times 10^4$	N/A	N/A	30	148
Electroactive nitrite-oxidizing bacteria biosensor	Nitrite-oxidizing bacteria (NOB)	Cyclic voltammetry	Wetlands, rivers	$7.14-1.07 \times 10^3$	N/A	N/A	N/A	150

Table 9 (*Contd.*)

Electrode material	Bio-element	Detection method	Sample matrix	Range (μM)	Electrolyte	pH	LOD (μM)	Ref.
Electrochemically active biofilm (EAB) biosensor on graphite sheets	Electrochemically active biofilm (EAB)	Electrochemical (implied)	N/A	7.14–1070.89	N/A	N/A	N/A	154
Antiterminator microbial whole-cell biosensor (MWCB)	*Bacteroides thetaiotaomicron*	Optical/fluorescence (*in vivo*)	Mouse model of ulcerative colitis (*in vivo*)	N/A	N/A	N/A	0.72	155
Self-assembled hydrogel bioelectrodes (*Shewanella*) with rGO	Genetically engineered electroactive *Shewanella* species	Electrochemical (implied)	Environmental (general)	0.1–1×10^4	HEPES buffer solution	N/A	0.72	156
HS-β-cyclodextrin coordination methanobactin/gold nanoparticles (HS-β-CD@Mb/AuNPs) modified gold electrode	Methanobactin (Mb)	Electrochemical (implied)	Food (general)	1–9×10^3	N/A	N/A	0.425	158
Ti$_3$C$_2$ nanosheets functionalized with ApoF-Pt nanoparticles (Pt@ApoF/Ti$_3$C$_2$)	Apoferritin (ApoF)	Electrochemical (implied)	Complex environments	0.5–9×10^3	N/A	N/A	0.5	168
Flexible nanoporous gold film electrode (NPGFE) from upcycled CDs	N/A (material-based detection)	Electrochemical (implied)	N/A	10–1×10^5	N/A	N/A	3.37	169
Nanozyme-based electrochemical-driven electrochromic visual biosensor (Fe$_3$O$_4$@Au-Cu/MOF, PEDOT:PSS/RGO)	Fe$_3$O$_4$@Au-Cu/MOF (nanozyme)	Electrochemical-driven electrochromic visual	Food samples	10–100×10^3	N/A	N/A	3.37	170
PEDOT doped with graphene oxide-Fe$_3$O$_4$ (GO–Fe$_3$O$_4$) nanocomposite	N/A (material-based detection, catalytic activity)	Electrochemical (implied)	Human serum (for microRNA)	5–45	N/A	N/A	0.15	171
Manganese-based MOF (UoZ-6) as the oxidase nanozyme	UoZ-6 (nanozyme)	Ratiometric colorimetric and visual-mode	Processed meat, water	10^{-9}–10	N/A	N/A	CC: 5.18×10^{-9} i-t: 7.36×10^{-9}	172

Table 10 Comparative table of nitrite detection methodologies

Method category	Sub-method examples	Typical LOD range (μM)	Typical sensitivity (qualitative/metric)	Typical specificity (qualitative)	Typical sample volume (μL mL^{-1})	Typical analysis time	Cost (qualitative)	Portability/field applicability (qualitative)	Key advantages	Key limitations/ challenges
Spectroscopic methods	Colorimetry/UV-vis (*e.g.*, Griess variants, CD-based)	0.02–10	Medium	Medium (often susceptible to color/turbidity)	mL	Minutes (1–10 min)	Low	Medium (can be miniaturized, smartphone-based)	Simplicity, low cost, visual detection, high throughput with automation	Matrix interferences (color, turbidity), sample preparation, reagent stability
	Fluorescence (*e.g.*, CD-based, MOF-based, specific probes)	0.005–50	High	Medium-high (depends on probe)	μL–mL	Minutes (2–15 min)	Medium	Medium (some smartphone-based)	High sensitivity (low LODs), good selectivity with specific probes	Complex probe design, potential interferences from fluorescent matrices, photobleaching
	IR/FTIR (*e.g.*, NIR + chemometrics, VPG-FTIR)	1–700	Low-medium	Medium (chemometrics/VPG needed for complex)	μL–mL	Seconds to minutes	High	Low (lab-based, some portability exists)	Non-destructive, provides molecular information, rapid	High matrix interference, lower sensitivity for trace analysis, expensive instrumentation
	Raman/SERS (*e.g.*, AuNPs, AgNPs, MOF-SERS)	0.00001–5	Very high	High (fingerprinting, specific reactions)	μL	Seconds to minutes	High	Low-medium (progress in miniaturization)	Ultra-high sensitivity (very low LODs), high molecular specificity, rapid	High instrumentation cost, substrate reproducibility, matrix interference (quenching), portability
	Chemiluminescence (CL) (*e.g.*, gas-phase, luminol-based)	0.0006–5	Very high	Medium-high (depends on the reaction)	μL–mL	Seconds to minutes	Medium	Medium	Exceptionally low detection limits (high sensitivity), wide linear range	Requires specific oxidizing agents, potential interferences, careful optimization
Chromatographic methods	Gas chromatography (GC) (*e.g.*, GC-MS, HS-GC)	0.000001–0.1	High	Very high (separation-based)	μL	Minutes to tens of minutes	High	Low (lab-based)	High separation efficiency, high sensitivity, robust for volatile analytes	Requires derivatization for non-volatile nitrite, complex instrumentation, long analysis time

Table 10 (Contd.)

Method category	Sub-method examples	Typical LOD range (μM)	Typical sensitivity (qualitative/metric)	Typical specificity (qualitative)	Typical sample volume (μL mL^{-1})	Typical analysis time	Cost (qualitative)	Portability/field applicability (qualitative)	Key advantages	Key limitations/challenges
	Liquid chromatography (LC/HPLC)	0.06–20	High	Very high (separation-based)	μL–mL	Minutes to tens of minutes	High	Low (lab-based)	High sensitivity, excellent separation of complex mixtures, good reproducibility	High instrumentation cost, extensive sample preparation, solvent consumption
	Ion chromatography (IC)	0.01–20	High	High (separation-based for inorganic ions)	μL–mL	Minutes to tens of minutes	Medium	Medium-high (portable ICs available)	Good for inorganic ions, simultaneous multi-ion detection, good sensitivity	Matrix effects from high salt/organic content, requires specific columns
	Capillary electrophoresis (CE)	0.0006–20	Medium-high	High (separation-based)	nL–μL	Seconds to minutes	Medium	High (microchip CE, portable)	Rapid analysis, high separation efficiency, low sample/reagent consumption, minimal waste	Lower sensitivity than some other methods, potential interferences, requires skilled operation
Flow injection analysis (FIA)	Spectrophotometric FIA	0.0000065–1	Medium	Medium-high	μL–mL	Seconds to minutes (high throughput)	Medium	Medium-high	High throughput, automation, low reagent consumption, rapid response	Potential interferences from sample components, sensitivity might be lower than that of HPLC
	Amperometric FIA	0.00001–9	High	Medium-high	μL–mL	Seconds to minutes	Medium	Medium-high	High sensitivity, real-time monitoring, automation	Electrode fouling, interferences from other electroactive analytes
Electrochemical methods	Potentiometric	0.02–10	Medium	Medium (ion-selective membrane dependent)	μL–mL	Seconds to minutes	Low-medium	High (can be miniaturized, handheld)	Simple setup, rapid response, low cost, potential for miniaturization	Susceptibility to interferences from other ions, limited selectivity without specific ionophores, leaching issues

Table 10 (*Contd.*)

Method category	Sub-method examples	Typical LOD range (μM)	Typical sensitivity (qualitative/metric)	Typical specificity (qualitative)	Typical sample volume (μL mL^{-1})	Typical analysis time	Cost (qualitative)	Portability/field applicability (qualitative)	Key advantages	Key limitations/challenges
	Voltammetric	0.002–10	High	Medium-high (nanomaterial dependent)	μL–mL	Seconds to minutes	Medium	Medium (some portable potentiostats)	High sensitivity, provides mechanistic information, versatile with nanomaterial modification	Matrix interferences, electrode fouling, requires skilled operation
	Amperometric	0.00001–1	High	Medium-high (nanomaterial dependent)	μL–mL	Seconds to minutes	Medium	Medium-High (portable potentiostats, SPEs)	High sensitivity, real-time monitoring, simplicity of measurement	Electrode fouling, interferences from other electroactive species, requires constant potential
	Electrochemical impedance spectroscopy (EIS)	0.02–10	Medium	Medium-high	μL–mL	Minutes	Medium	Low-medium	Highly sensitive to surface changes, provides kinetic and mechanistic information	Complex data interpretation, requires specialized equipment, susceptible to noise
Bio-electrochemical systems	Enzyme-based biosensors	0.00008–30	High	Very high (enzymatic specificity)	μL–mL	Minutes	Medium-High	Medium-high	High specificity due to enzymatic recognition, good sensitivity	Enzyme stability, cost of enzymes, potential for denaturation, limited shelf-life
	Whole-cell biosensors	0.7–20	Medium	Very high (microbial specificity)	μL–mL	Minutes to tens of minutes	Medium	Medium	High specificity (metabolic response), robust in complex matrices, long-term stability	Response time can be slower, susceptibility to toxins affecting cell viability, potential for AOB interference
	Aptasensors & immunosensors	0.01–10	High	Very high (high affinity binding)	μL	Minutes	High	Medium	Ultra-high specificity, high affinity binding, good sensitivity	High cost of aptamers/antibodies, stability of biorecognition elements, complex immobilization

nitrite conversion, and a PEDOT:PSS/RGO thin film as the counter electrode, known for its outstanding electron transport and electrochromic properties. The color of the PEDOT:PSS/RGO film changes in response to the electronic current generated by nitrite oxidation, allowing for visual detection. This electrochromic sensor combined with smartphone-based colorimetry enables instant and visual detection. Under ideal conditions, the sensor detected nitrite within a linear range of 0.01 to 100 mmol L^{-1} (10–100 000 μM) and exhibited a detection limit of 3.37 μM. This method demonstrated no significant difference compared to electrochemical results and was effectively employed for the detection of nitrite in real samples (food). It is highlighted for minimizing the interference of humidity, human operational errors, and instrument stability, offering high stability, low cost, and ease of operation for food safety monitoring.

Sun[171] constructed a dual-mode electrochemical biosensing platform for microRNA detection, based on a poly(3,4-ethylenedioxythiophene) (PEDOT) doped with graphene oxide–Fe_3O_4 (GO–Fe_3O_4) nanocomposite. While the primary application is microRNA detection, the GO–Fe_3O_4/PEDOT composite demonstrated strong catalytic ability towards nitrite with a distinct oxidation peak. This catalytic activity was then utilized as a signal amplification strategy for microRNA detection. The biosensor was successfully used for microRNA analysis in human serum, demonstrating the material's robust performance in complex biological matrices and its potential for precise and sensitive biosensing. This highlights the utility of such nanomaterials in facilitating nitrite-related electrochemical reactions, even when nitrite itself is not the primary analyte. Ameen and Omer[172] synthesized a novel manganese-based MOF (UoZ-6) that functions as a cold/hot compatible (0–100 °C) and recyclable oxidase nanozyme for nitrite ion detection.[43] This multi-functional MOF was developed for both ratiometric-based colorimetric and color tonality visual-mode detection of nitrite. The mechanism involves nitrite ions promoting the diazotization process of the oxTMB product, leading to a decay in absorbance at 652 nm and the emergence of a new signal at 461 nm. This dual-absorbance ratiometric platform functions effectively across a wide temperature range, offering a linear detection range of 5–45 μM with a detection limit of 0.15 μM using visual-mode. This approach is sensitive, reliable, and selective, making it effective for detecting nitrite ions in processed meat and water. The magnetic property of UoZ-6 also allows it to be reused up to seven times, emphasizing its sustainability and cost-effectiveness.

5.4.3. Novel nanomaterial architecture. The innovative designs and structures of nanomaterials offer new avenues for highly sensitive and selective nitrite detection. Such architecture often leverages unique material properties and assembly methods to enhance sensor performance.[173] Shaikh[174] managed to perform the electrochemical determination of nitrite. Castor natural oil (CNO) was prepared by a flame synthesis method, in which a soaked cotton wick in castor oil was ignited, and the black powder produced was collected as a CNO nanoparticle product with no further purification. CNOs have a structural defect that works as active sites for nitrite adsorption, thus

enhancing the electro-catalytic activity in nitrite determination. The evaluation of CNOs for the electrocatalytic activity towards nitrite was performed by the cyclic voltammetry technique in PBS solution (pH 6.0), and a well-defined peak of nitrite appeared at 0.85 V. On the other hand, the calibration curve was obtained by chronoamperometry and resulted in an LOD of 0.75 μM and a sensitivity of 214.29 μA mM^{-1} cm^{-2} for nitrite sensing. Developing amperometric biosensors capable of detecting multiple analytes simultaneously, particularly those relevant to specific applications (*e.g.*, nitrite and nitrate in food analysis), can offer significant advantages by streamlining workflows and reducing analysis time.

Zhang[175] developed a bio-composite consisting of binary metal sulfide (CoS_2–MoS_2) modified with N-doped lignocellulose on a glassy carbon electrode.[23] The N-doped lignocellulose (N-LC) acts as a substrate, improving surface area and electrical conductivity, while the synergistic effects of CoS_2 and MoS_2 enhance catalytic performance. This system demonstrated a wide linear range of 0.5–5160 μM and an LOD of 0.20 μM for nitrite. It also displayed good anti-interference properties against common co-existing analytes like dopamine (DA) and ascorbic acid (AA), and good stability, making it suitable for applications in complex biological fluids such as human urine.

Furthermore, Cardoso[176] demonstrated the development of (bio)sensors for the analysis of biological fluids using 3D printing. Fused deposition modeling was used to fabricate (bio)sensing platforms from commercially available filaments made of polylactic acid containing graphene (G-PLA). The surface treatment of the 3D-printed sensor (mechanical polishing followed by solvent immersion) was shown to provide improved electrochemical properties. This enabled the direct detection of nitrite and uric acid in saliva and urine with high precision (RSD < 2.1%) and low LODs (0.03 μM for nitrite). This highlights a practical approach for multi-analyte detection in complex biological matrices and the advantages of 3D printing for rapid prototyping and customizable sensor geometries.

Overall, bio-electrochemical sensors offer high specificity due to their biological recognition elements and can achieve very low detection limits, often in the nanomolar range. They are particularly adept at handling complex biological and environmental matrices, with many studies demonstrating successful application in real samples like urine, serum, milk, pickled radish, tap water, mineral water, various types of wastewaters, food samples, and even *in vivo* in animal models. While sample preparation is often minimized due to the inherent selectivity, challenges can arise from matrix-induced fouling or interference from co-existing species, which are often addressed through careful sensor design, selective bioreceptor choice, or the use of inhibiting agents. To sum up the contents of this section, Table 9 has been prepared.

5.5. Overview of nitrite detection methodologies

Following a comprehensive exposition of the diverse methodologies employed for nitrite detection in Table 10, encompassing established spectrophotometric and chromatographic

techniques alongside advanced electrochemical and bio-electrochemical systems, a systematic synthesis of their practical attributes and limitations is warranted. Although each analytical approach offers distinct merits pertaining to sensitivity, selectivity, and operational applicability, significant variability exists in their performance characteristics and resource demands. The ensuing comparative table provides a concise overview, delineating key analytical parameters such as typical detection limits, sensitivity, specificity, requisite sample volumes, analysis duration, approximate financial outlay, and inherent portability. This consolidated presentation aims to facilitate a holistic understanding of their respective trade-offs and suitability across a spectrum of real-world monitoring contexts.

6. Emerging trends and technologies in nitrite detection

The accurate and sensitive detection of nitrite remains a critical area of research due to its pervasive presence as an environmental pollutant and a food additive with potential health implications. While significant advancements have been made across various analytical techniques, this section highlights promising avenues for the next generation of nitrite sensing technologies.

6.1. Integration of artificial intelligence and machine learning

The combination of Artificial Intelligence (AI) and Machine Learning (ML) algorithms provides a disruptive new trend in chemical sensing, including nitrite detection. These computational methods can dramatically improve sensor performance, data interpretation, and decision-making. ML techniques can be used to achieve advanced signal processing, filter out noise, and extract subtle patterns from complex data. They can also create more robust calibration models that adapt to changes in sample matrices or sensor degradation over time, and use them for predictive modeling. For example, a portable and autonomous device for real-time colorimetric detection of phosphorus and nitrite was developed by Pal.[178] It established the groundwork for AI/ML integration. The device's increased capability includes comprehensive data storage, retrieval, and real-time monitoring capabilities, although the usage of AI/ML algorithms is not stated directly. The authors emphasize that future applications "may also include prediction and control of various parameters in diverse domains". This continuous data acquisition capability, as well as the vision for predictive analytics, are critical prerequisites for the successful deployment of AI and ML models capable of analyzing these datasets to identify trends, predict concentrations, and optimize control strategies in environmental monitoring.

More directly, Akhter (2021)[179] established an IoT-enabled portable sensor device for detecting nitrate in water that explicitly uses AI. In their system, a machine learning method is used to teach the microcontroller-based system. This training allows the system to reliably determine temperature and nitrate

concentrations in actual water samples, to show how machine learning can be integrated directly into sensor platforms to enhance the reliability and accuracy of water quality measurements. Given the chemical similarity and co-occurrence of nitrate and nitrite in many environmental samples, this method is highly beneficial for nitrite detection. Further building on this, Akhter (2023)[180] presented an IoT-enabled portable water quality monitoring system with a MWCNTs/PDMS multifunctional sensor. This advanced system also includes a machine learning algorithm for training Arduino-based systems. This ML component is critical for determining temperature, nitrate, phosphate, and pH levels in real water samples. The use of ML in such a multifunctional system demonstrates its effectiveness in managing a wide range of sensor inputs and delivering complete, intelligent insights on water quality, which can be easily extended to include nitrite. The ability of machine learning (ML) to analyze numerous correlated factors at the same time improves the sensing system's accuracy and applicability in complicated, real-world circumstances, allowing for intelligent data processing and more reliable measurements. Further showcasing this trend, Nguyen (2023)[181] developed an autonomous system for assessing and predicting nitrite levels in aquaculture water. This system makes use of machine learning techniques, including Decision Tree (DT) and Artificial Neural Network (ANN) algorithms, to generate robust prediction models. These models are implemented on an embedded computer (Raspberry Pi 3), which also collects image data and controls peripheral devices. The system automates the process of collecting water samples, mixing them with reagents to produce a colorimetric response indicating nitrite content, and then assessing and categorizing current nitrite levels (e.g., "good," "tolerable," "harmful," "dangerous," or "toxic"). The study found that the ANN algorithm yielded higher accuracy on both training and test datasets, demonstrating the superior predictive power of neural networks in this application. The system's connectivity to an IoT platform for transmitting prediction results to a mobile application further highlights its practical, real-time applicability in aquaculture management.

In the field of food safety, Son (2024)[182] investigated the innovative application of hyperspectral imaging combined with machine learning algorithms for rapid and non-destructive monitoring of residual nitrite in emulsified pork sausages. This study utilized various ML models, including XGBoost, CATboost, and LightGBM, to analyze hyperspectral data. The findings revealed that higher nitrite concentrations influenced the protein matrix and hydrogen-bonding capacities, leading to increased reflectance at specific wavelengths (approximately 1080 nm and 1280 nm). Among the tested models, XGBoost demonstrated the best performance, achieving an R^2 of 0.999 and a root mean square error (RMSE) of 0.095, indicating exceptionally high predictive accuracy. This integration offers a powerful, non-destructive, and real-time method for quality control in the meat industry, with potential for streamlining industrial operations. Similarly, Abbas (2024)[183] used machine learning to modify experimental settings for an electrochemical sensor meant to precisely detect nitrite levels in pickled vegetables. Their sensor, made of poly(3,4-ethylenedioxythiophene)

functionalized carbon matrix suspended Cu nanoparticles (PEDOT-C@Cu-NPs), profited from machine learning-driven tuning of pH, drying time, and concentrations. The ML-assisted technique improved sensor performance for complex food matrices, resulting in high sensitivity ($0.6372~\mu A~\mu M^{-1}~cm^{-2}$), selectivity, low detection limit (3.91 μM), and wide linear range (5–580 μM).

For environmental monitoring, Li (2024)[184] proposed a sophisticated stacked extreme learning machine model based on information entropy weight for the accurate detection of nitrite–nitrogen concentration in surface water using ultraviolet-visible spectroscopy. This model was developed to address challenges in surface water pollution monitoring, offering an effective method for online and *in situ* detection. Experimental results demonstrated that this stacked extreme learning machine model surpassed traditional models in measurement accuracy, highlighting its capability for quick and precise nitrite–nitrogen detection in environmental samples. Rafiq (2024)[185] applied ML techniques to predict nitrite accumulation in sulfide-dosed partial nitrification processes in wastewater treatment, a complex biological system. They conducted a comparative analysis of three ML models: Gaussian Process Regression (GPR), Support Vector Machine (SVM), and Ensemble Regression Tree (ER). The study aimed to identify the most influential parameters for nitrite accumulation, considering pH, HS^-/N, and H_2S/N as input parameters. GPR emerged as the superior performer with an $R^2 = 0.95$, RMSE = 0.19, and MAE = 0.14, indicating its effectiveness in providing accurate predictions. This research underscores ML's crucial role in optimizing biological nitrogen removal processes in real-world wastewater treatment applications, addressing both operational challenges and environmental concerns. Presenting a cutting-edge smartphone-integrated device for complex sample analysis, Bai (2025)[186] presented a smartphone-integrated microfluidic paper-based device (μPAD) for nitrite detection, where machine learning (ML) through an Artificial Neural Network (ANN) algorithm played a pivotal role. This ML component facilitated high accuracy and selectivity in complex samples, enabling both nitrite concentration prediction and antioxidant additive discrimination. This platform showcases ML's ability to enhance biosensing in challenging matrices, providing innovative solutions for reliable nitrite detection. Furthermore, while focusing on ammonia-nitrogen, Qiu (2024)[187] demonstrated the application of soft sensor models (Linear Regression, Neural Networks, and Random Forest Regression, including Recurrent Neural Networks) for prediction and optimization in domestic wastewater treatment. Their RNN-based model exhibited excellent performance in NH_3–N monitoring and process optimization, indicating the broader applicability of AI and ML in enhancing the interpretability, accuracy, and adaptability of sensing and control systems in environmental contexts. This study highlights the potential for ML-driven soft sensors to improve energy efficiency and sustainability in wastewater treatment by optimizing process cycles based on predicted pollutant levels.

To evaluate an IoT device for long-term monitoring in real-world wastewater treatment plants, Navarro (2024)[188]

constructed an Internet-of-Things (IoT) device for long-term monitoring and detection of nitrate and nitrite in wastewater treatment plants (WWTPs). This device, integrated into an IoT system, combines an ion chromatography (IC) sensor with mechanical elements for water sample acquisition and electronic circuits for control. The system's capability to "store, analyze, and visualize the obtained water quality metrics" through a cloud software platform, and its "satisfactory validation against standardized laboratory values" with a coefficient of determination of 96.7% on average, strongly implies the use of sophisticated data processing and analytical techniques that often leverage ML for robust performance and long-term reliability in complex, real-world environments. While reporting on continuous monitoring in aquaculture systems, Butinyac (2024)[189] reported on continuous nitrite and nitrate monitoring in recirculating aquaculture systems (RAS) using a deployable ion chromatography-based analyzer. This system, which delivers real-time concentration data *via* a cellular IoT module and cloud-based dashboard, demonstrated analytical performance comparable to accredited lab-based instrumentation. The continuous data stream and the need for reliable performance in dynamic aquaculture environments suggest a strong potential for AI/ML integration for predictive maintenance, anomaly detection, and optimization of aquaculture conditions.

Furthermore, Pal *et al.* (2022)[190] advanced their IoT-enabled microfluidic colorimetric detection platform for continuous monitoring of nitrite and phosphate in soil. This miniaturized device, incorporating optoelectronic components and a PDMS microfluidic device, uses IoT and Bluetooth modules with an Arduino microcontroller for online data monitoring and storage in remote locations. While the article focuses on the hardware and connectivity, the continuous data generation and remote monitoring capabilities are ideal for applying ML algorithms to analyze soil nutrient trends, predict deficiencies or excesses, and inform precision agriculture strategies, thereby optimizing resource use and preventing pollution. Ye (2024)[191] designed an intelligent artificial sensing platform (OPTY) for the discrimination of formaldehyde and nitrite in food. This portable sensing chip, combined with a smartphone, utilizes distinct fluorescence responses to detect these compounds. Meanwhile, Huang (2017)[70] demonstrated the determination of total nitrogen, ammonia nitrogen, and nitrite nitrogen in river water using near-infrared spectroscopy (NIRS) coupled with chemometrics, specifically a back-propagation neural network (BPNN). NIRS spectra were obtained from 138 river water samples, and principal component analysis (PCA) was used for preprocessing to eliminate redundant information. The BPNN models showed high correlation coefficients ($R^2 = 0.9562$ for nitrite nitrogen) and low root-mean-square errors of prediction (RMSEP = 0.04157 for nitrite nitrogen), indicating accurate determination. This study highlights the power of combining spectroscopic techniques with advanced neural network models for precise and accurate multi-parameter analysis in complex environmental samples.

6.2. Miniaturization, portability, and on-site analysis

6.2.1. Colorimetric devices with optical sensors. The demand for rapid, straightforward, and cost-effective nitrite detection outside of traditional laboratory settings has resulted in major advances in sensor downsizing and portability. Portable devices that use color shifts as a detection mechanism are frequently paired with optical sensors for quantitative analysis. These systems are ideal for on-site applications due to their simplicity and ease of interpretation. Cadeado (2022)[192] developed a palm-sized wireless device for colorimetric nitrite determination in water based on the Griess method. The sensor was a battery-powered (lithium-ion), low reagent demand (20 μL) device, with wireless data sharing to smartphones/computers. The Griess method involves a diazotization–coupling reaction where nitrite reacts with a Griess reagent to form a colored azo dye. The intensity of this color is proportional to the nitrite concentration. The device uses an RGB sensor (APDS 9960) as a detector and a green LED ($\lambda_{max} = 530$ nm) as the light source. The green channel signal, which is most sensitive to the red-purple color produced by the Griess reaction, is monitored. An ESP32 board handles signal processing and wireless data transfer (acting as a router).

To enhance measurement stability and accuracy in a portable format, Feng (2025)[193] designed a portable dual-channel analysis device for on-site nitrite determination in surface water, also based on the Griess method. The design is a 3D-printed compact housing, low weight, low power consumption (0.13 W), designed for on-site analysis. It incorporates a beam splitter prism to create a dual-channel optical path, enhancing measurement stability and accuracy. The device's housing is produced using 3D printing technology, significantly reducing its size and weight (552.6 g). Data processing involves a median average method of five absorbance readings. Liang (2024)[194] developed a metal–organic framework (MOF)-based ratiometric POCT platform for quantitative visual detection of nitrite. It's a novel fluorescent nanoprobe (Ru@MOF-NH$_2$) that exhibits a distinct color change from blue to red in the presence of nitrite due to a diazo-reaction between the amino group of UiO-66-NH$_2$ and nitrite. The red emission from $[Ru(bpy)_3]^{2+}$ serves as a reference signal for ratiometric detection. The color change is observable by the naked eye, and quantitative detection is achieved by using a personal smartphone as the detection device to read the color hue. The system depends on visual detection and smartphone integration, and is designed for on-site monitoring in food and environmental safety.

Aiming for enhanced accuracy and on-site screening, Zhao[195] constructed portable hydrogel kits with self-ratio optical bimodal detection and smartphone imaging for on-site nitrite screening. The kit co-assembles upconversion nanoparticles (Er:Tm@Yb:Tm) and nitrogen-doped carbon platinum nanomaterials (Pt/CN) in a sodium alginate (SA) hydrogel. Nitrite mediates the diazotization of oxidized 3,3′,5,5′-tetramethylbenzidine (oxTMB), triggering a change in absorption signals and a ratiometric fluorescence response from the upconversion nanoparticles. An image processing algorithm

analyzes the nitrite-induced signal change captured by a smartphone (vivo X70 Pro+). The bimodal optical response (absorption and fluorescence ratio) enhances accuracy. Ye (2025)[196] designed an intelligent sensing platform for the discrimination of formaldehyde and nitrite in food. It's based on a fluorescent probe (OPTY) that undergoes distinct fluorescence changes upon reaction with nitrite (intramolecular cyclization cascade reaction, boasting bright green fluorescence). The probe was fabricated into a portable sensing chip combined with a smartphone to form a portable sensing platform. This allows for on-site visual detection.

An innovative approach using gas pressure for rapid nitrite sensing was developed. Xiao[197] introduced a portable gas pressure meter for rapid and selective nitrite detection in ham sausage and water samples. This method relies on the specific reaction between nitrite (NO_2^-) and sodium cyclamate under acidic conditions, which generates gaseous products (cyclohexene and nitrogen). The increase in gas pressure within a sealed reaction bottle is directly proportional to the nitrite concentration. The mechanism is based on a miniaturized pressure meter that is used as the detector to measure the pressure changes. The specificity of the reaction with sodium cyclamate helps to avoid interferences from other coexisting ions. Leveraging nanotechnology and smartphone integration for trace nitrite detection, Das[198] reported a carbon nanodot-neutral red (C-dots-NR)-based photometric and fluorescence mode sensing for trace nitrite detection in water and soil using a smartphone. The sensing scheme utilizes a Förster Resonance Energy Transfer (FRET) process between C-dots (donor) and NR (acceptor). The presence of nitrite affects this FRET process, causing a decrease in absorption at 560 nm and an increase in fluorescence intensity at 563 nm (upon 375 nm excitation). These changes are correlated to quantify nitrite concentration. The handheld compact sensing platform developed on a smartphone captures and analyzes these optical variations. The device is low-cost, field-portable, and convenient to handle, making it suitable for on-site assessment of nitrite in water and soil samples. Pei[199] proposed a low-cost and high-precision nitrite detection method for mariculture water based on an improved Residual Network (ResNet). This method combines a chemical color development reaction (likely Griess-based) with machine vision recognition using an improved deep learning model. After the colorimetric reaction, images of the water samples are captured. An improved ResNet (ResNet18 with ResNeXt and attention mechanisms like SE and CBAM) is used to process these images and determine nitrite concentration. The residual blocks and multi-branch structures enhance feature extraction and prevent network degradation. The device is simple, with the machine vision component being adaptable to embedded systems or smartphones for on-site analysis, offering a high-accuracy, low-cost solution for aquaculture.

6.2.2. Electrochemical sensors. Silva[200] presented a 3D-printed electrochemical sensor for nitrite determination. The sensor utilizes differential-pulse voltammetry (DPV), an electroanalytical technique that measures current as a function of potential, allowing for sensitive detection of redox-active species like nitrite. The entire device, including the set of three

electrodes (working, counter, pseudo-reference), is 3D printed using a carbon black-based filament. The electrode surface is treated to enhance conductivity and electrochemical performance. The sensors are designed for on-site environmental and clinical monitoring.

A pioneering versatile dual-mode detection on a single portable device was developed by Tiawpisitpong.[201] The miniaturized nitrite sensor depended on a single portable paper-based device (PAD). It combines colorimetric and electrochemical detection. Colorimetry (using $KMnO_4$ as a chromogenic agent) is used for high nitrite concentrations, while electrochemical detection (DPV) with a cellulose acetate-modified screen-printed electrode (CA/SPCE) is used for low concentrations. High nitrite levels produce a faded color (smartphone-analyzed), triggering electrochemical analysis for enhanced precision at lower levels. Kusonpan[202] developed a manually rotated paper-based analytical device (μPAD) with electrochemical sensors for the simultaneous determination of nitrite and nitrate. Nitrite is directly detected electrochemically. Nitrate is measured after reduction to nitrite using zinc dust. The device features a circular paper disc with screen-printed carbon electrodes modified with N-doped multiwalled carbon nanotubes (N-MWCNTs) and copper(II) phthalocyanine (CuPc) to enhance sensitivity. Manual rotation facilitates mixing. Regarding portability, it's a user-friendly rotational μPAD with integrated electrochemical sensors and is designed for rapid on-site determination in food samples. Madani & Hatamie[203] designed a portable mini-electrochemical cell integrating microsampling and micro-electroanalysis. It depends on the direct micro-electroanalysis of nitrite ions. A modified Au microelectrode (Au/Au NPs) and an Ag/AgCl reference electrode are integrated within a micropipette tip. This allows for microvolume sampling (20–40 μL or a single droplet) and direct analysis without additional reagents or complex sampling steps. It's suitable for clinical, forensic, and environmental samples.

6.2.3. Ion chromatography (IC). Mikhail (2024)[204] demonstrated the successful implementation of a mixed-mode ion chromatography method to a portable ion chromatography system (Aquamonitrix analyser) for the simultaneous separation and detection of monochloramine, nitrite, and nitrate. The mixed-mode IC combines ion exchange and ion exclusion for separation. Detection is *via* UV absorbance. A benchtop method was successfully transferred to the portable Aquamonitrix analyser, which uses an LED-based UV absorbance detector. The system is a fully portable IC system, capable of on-site monitoring of municipal water supplies with a total run time of less than 10 minutes. Debruille (2024)[205] presented a portable IC system with dual LED-based absorbance detectors and a 3D-printed post-column heated micro-reactor for the simultaneous determination of ammonium, nitrite, and nitrate. The system separates ions using ion chromatography. Nitrite and nitrate are detected directly by UV absorbance. Ammonium (a cation) is detected post-column using a modified Berthelot reaction, which requires heating to accelerate color development. The core is a commercial portable ion chromatograph (Aquamonitrix). A novel 3D-printed micro-reactor chip with an integrated heater (initially a Peltier chip, later a PCB heating plate) is used for the post-column colorimetric detection of ammonium. This allows for rapid heating (70 °C in 40 s) and efficient mixing within a serpentine microchannel. Dual LED-based absorbance detectors (*e.g.*, 660 nm for ammonium, and others for nitrite/nitrate) enable multi-analyte detection. It's a fully integrated and self-contained portable analyzer, designed for field deployment and autonomous water quality monitoring in natural and industrial waters (which can have high nitrogen content). The 3D printing significantly contributes to miniaturization and integration.

The primary challenge for these portable devices lies in maintaining high analytical performance (sensitivity, accuracy, selectivity) while ensuring robustness, ease of use, and cost-effectiveness outside of controlled laboratory environments. Factors like power consumption, shelf-life of reagents, interference from environmental conditions (temperature, humidity), and the need for minimal user training are critical considerations for widespread adoption. The increasing trend of sodium nitrite in suicides further highlights the urgent societal need for highly reliable and accessible on-site detection methods in emergency and forensic contexts, underscoring the practical challenges in rapid analysis outside traditional lab settings.

6.3. Smartphone-based detection systems

The widespread availability and advanced capabilities of smartphones offer a compelling platform for developing highly accessible, portable, and user-friendly nitrite detection systems. This trend directly addresses the need for convenient and real-time monitoring. Smartphones, equipped with high-resolution cameras and powerful processors, can capture images of colorimetric reactions or even analyze electrochemical signals *via* integrated peripherals. For example, Zhang[206] designed a fast, cost-effective, and adaptable on-site testing approach that uses a smartphone and a self-designed 3D-printed portable equipment to detect nitrite, ammonia nitrogen, and total phosphorus in ambient water. This method uses the smartphone's color recognition capability and an adaptive deconvolution algorithm to identify many parameters with a six-channel device. This method offers a quick, precise, and sensitive alternative to traditional analysis, reducing analysis time while minimizing sample contamination and errors, making it ideal for rapid water quality detection. Similarly, focusing on citizen science initiatives for environmental monitoring, Zheng[207] reported a simple on-site detection method for ammonium and nitrite, specifically designed for citizen science initiatives. This method is based on the classic Griess reaction and modified indophenol blue reaction. Digital image colorimetry is carried out using a smartphone with a custom-made WeChat mini-program or free built-in applications (APPs). The robustness of the method was demonstrated across different smartphones, applications, and operators, yielding excellent accuracy in the field analysis of ammonium and nitrite in a wastewater treatment plant and a local river. This highlights the potential for widespread public engagement in environmental monitoring.

Achieving accurate on-site detection for water quality assessment, Fang (2021)[208] achieved real on-site detection of nitrate plus nitrite in natural water samples using a smartphone-based detector. Their method, based on the VCl_3 reduction–Griess reaction, showed a good linear relationship between the intensity of the green channel and nitrate concentration. The results obtained with the smartphone were not significantly different from those obtained with a benchtop spectrophotometer, demonstrating the accuracy and practical applicability of smartphone-based detection for environmental water quality assessment. Zhan (2025)[209] developed a sensitive strategy for nitrite detection using a read-out photoresponsive colorimetric platform based on a smartphone APP. This biosensing platform utilizes the colorimetric reaction of 3,3′,5,5′-tetramethylbenzidine (TMB) by photooxidation, where the color changes from blue to green and finally to yellow upon nitrite addition. The reaction is carried out on low-cost filter paper modified with chitosan, and the color imaging is collected using a smartphone APP coded on Android Studio. This multichannel color analysis APP enables quantitative nitrite analysis, offering a low-cost and portable solution with broad application prospects in drug quality safety supervision.

Meanwhile, Khachornsakkul (2024)[210] presented a gold nanomaterial-based microfluidic paper analytical device (μPAD) for the simultaneous quantification of Gram-negative bacteria and nitrite ions in water samples. The color changes resulting from aggregation and anti-aggregation reactions on the μPAD are measured using a smartphone application. This cost-effective μPAD provides real-time analysis of both contaminants, making it suitable for assessing water quality in resource-limited settings. The sensor also showed acceptable recovery for monitoring nitrite in drinking water samples and human urine, further expanding the utility of smartphone-integrated devices. Chen (2021)[60] developed a quantitative image analysis method based on a cyanine dye-upconversion nanoparticle (UCNP) composite luminescent nanoprobe for nitrite detection. This method utilized an upconversion luminescence total internal reflection image platform. The system achieved a fast response (~0.1 s) and low sample consumption (10 μL), with powerful data support from 550 frame time series images. This quantitative image analysis method was successfully applied for nitrite analysis in environmental water and food samples, demonstrating its potential for rapid and precise detection by leveraging image processing capabilities. Additionally, Liu[211] designed a multipurpose optical fiber smartphone spectrometer (MOSS) as a point-of-care testing platform for on-site biochemical sensing. This compact device integrates absorption, emission, and surface plasmon resonance (SPR) spectroscopy and has been successfully applied to nitrite, mercury ion, and sucrose sensing. Equipped with an inner power supply and a user-friendly smartphone application, the MOSS is particularly suited for on-site applications, offering high-quality multipurpose spectral detection using compact and cost-effective components.

Zhao (2024)[195] constructed portable hydrogel kits with self-ratio optical bimodal detection and smartphone imaging for on-site nitrite screening. These kits embed upconversion nanoparticles and nitrogen-doped carbon platinum nanomaterials in a sodium alginate hydrogel. An image processing algorithm analyzes the nitrite-induced signal change, resulting in detection limits of 0.63 μM. The integration with smartphone imaging enhances the portability and user-friendliness of this system, making it suitable for point-of-care applications due to its reliability, long-term stability, accuracy, and sensitivity. These examples collectively demonstrate the rapid growth and versatility of smartphone-based detection systems, transforming nitrite analysis into a more accessible, portable, and user-friendly process for diverse applications.

6.4. Point of care nitrite sensors

The development of point-of-care (POC) nitrite sensors is a crucial trend, driven by the need for rapid, on-site, and decentralized analysis in various settings, including environmental monitoring, food safety, and clinical diagnostics. POC sensors aim to provide immediate results without the need for complex laboratory infrastructure or highly trained personnel. To demonstrate smart sensing of salivary biomarkers for health assessment, Bharwani[212] developed a point-of-care kit for the rapid detection of hydrogen peroxide and nitrite in adulterated cow milk. For nitrite detection, a modified Griess assay was used, where the Griess reagent was coated on reusable polystyrene strips with polyethylene glycol (PEG) as a stabilizer. This kit could identify nitrite concentrations of 32 μg mL^{-1} and above, demonstrating an accuracy of up to 95% in cow milk samples. The nitrite strips were stable for 10 days and reusable twice, highlighting their practical utility for on-site screening in food safety. Moving into advanced biomedical applications, Zeng (2024)[213] developed multifunctional nanoenzyme-assisted ion-selective and oxidation catalysis SERS biosensors for point-of-care nitrite testing (POCT). These biosensors, based on VB12-modified ZIF-67 loaded with a gold colloidal complex, demonstrated high sensitivity with a detection limit of 1.67 nM and a wide linear response range (1 M to 100 nM). The presence of distinct biomimetic Co in the biosensors enabled ion-selective capture of nitrite. The sensors were evaluated using real salivary samples under varied activities (working, eating, exercising, and sleeping) and compared with commercial nitrite kits, showing superior performance and promising potential for POCT and healthcare applications, particularly for non-invasive detection. Wei[214] presented a ferrocene-based polymeric photonic crystal sensor for semi-quantitative visual detection of sodium nitrite in food. This sensor platform aims to address the lack of portable systems for rapid, real-time visual analysis in field settings. It achieved a minimum response concentration of 0.72 μM, and rapid response within 60 seconds. Distinct structural color transitions (orange-red to green) correlated with different nitrite concentrations, enabling visual detection. The method is facile, insensitive to pH variations, rapid, and exhibits high sensitivity, stability, broad adaptability, and robust anti-interference capability, with promising preliminary application in real food samples. Kusonpan[202] developed a simple manually rotated paper-based analytical device (μPAD) with electrochemical sensors for the determination of nitrite and nitrate.
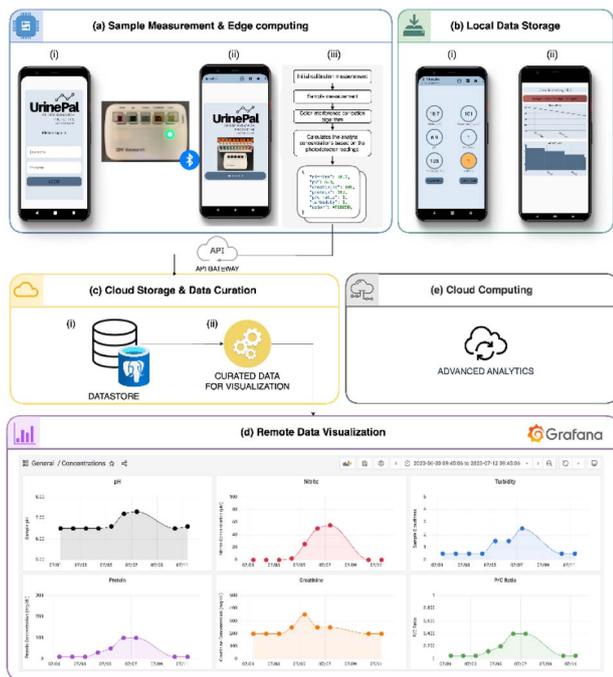
Fig. 5 Scheme representing data architecture (a–e) in POC nitrite sensing systems (reproduced from: V. S. Siu, M. Lu, K. Y. Hsieh, B. Wen, I. Buleje, N. Hinds, K. Patel, B. Dang and R. Budd, *Biosensors* (*Basel*), 2024, **14**), open access with permission from MDPI. Licensed under CC BY 4.0, 2024.

This user-friendly, rotational device, designed for portability, allows for the simultaneous detection of both ions. The sensing electrodes, screen-printed carbon electrodes modified with N-doped multiwalled carbon nanotubes (N-MWCNTs) and copper(II) phthalocyanine (CuPc), enhanced sensitivity for nitrite oxidation. The device provides a linear range of 50–1000 μM for the simultaneous determination of nitrite and nitrate, with detection limits of 10.0 and 20.0 μM, respectively. The analytical protocol was successfully applied to meat samples, demonstrating its great potential for rapid, on-site determination of nitrite and nitrate ions in food.

A cost-effective and highly sensitive solution for clinical diagnostics was offered. Siu[215] developed a cost-effective, quantitative, point-of-care solution for urinalysis screening, specifically targeting nitrite as a crucial biomarker for urinary tract infections (UTIs), alongside protein, creatinine, and pH. They designed a portable, transmission-based colorimeter using readily available components (costing less than $80), which is controllable *via* a smartphone application through Bluetooth. This device successfully detected nitrite within its clinically relevant range (6.25–200 μM) in salt buffer, artificial urine, and human urine samples, as shown in Fig. 5. Notably, its detection limit in artificial urine (1.6 μM) was approximately 16 times more sensitive than commercial dipstick reflectance analyzers, enabling earlier detection of urinary infections. The colorimeter also offers versatile data storage options (local or cloud) and facilitates the visualization of time-series analyte measurements in a web-based dashboard, allowing for

longitudinal tracking of urinalysis results to identify trends and potential infections earlier. Further refining their approach to urine analysis, Siu[216] elaborated on this quantitative colorimeter specifically for nitrite detection in urine, highlighting its ability to provide quantitative results beyond the semi-quantitative nature of traditional dipsticks, thus improving the overall sensitivity and specificity for UTI diagnosis. Paramasivam[217] demonstrated smart sensing of salivary nitrite (NO_2^-) levels through a point-of-care (POC) electrochemical approach. Their sensor utilized copper chlorophyllin (CuCP) as an enzyme mimic electrodeposited onto multi-walled carbon nanotube (MWCNT)-functionalized screen-printed carbon electrodes (SPCEs). This modified sensor allowed sensitive electrochemical detection of nitrite over a wide range of concentrations (10 μM to 10 mM) in both standard solutions and real human saliva samples. The practical applicability of this enzyme mimic-based platform for POC measurement was validated by comparing its results with a commercial Griess reagent test, confirming its utility for identifying individuals with oral diseases and other clinical conditions related to nitric oxide biology.

In a broader context of non-invasive diagnostics, Pittman[218] provided a comprehensive review on saliva-based microfluidic point-of-care diagnostics. While not detailing a specific nitrite sensor, this review emphasizes the growing interest in using saliva as an ideal non-invasive biofluid for detecting biomarkers due to its ready availability and the correlation of its analyte levels with those in blood. The authors highlighted that next-generation POC devices are leveraging microfluidic technologies to perform additional sample processing steps, leading to more sensitive and selective analysis of biomarkers in biological fluids in a non-invasive manner. This context is crucial for understanding the broader push towards non-invasive POC nitrite detection, particularly in clinical settings.[3] Zhao[219] developed a method for the point-of-care detection of salivary nitrite based on a surface plasmon-assisted catalytic coupling reaction of aromatic amines. This rapid quantification method, which utilizes gold nanoparticles (GNPs) under light illumination, can detect nitrite in the range of 1–100 μM with a detection limit of 1 μM. The facile nature of this method suggests its suitability for on-site fast screening and POC applications, with potential implications for understanding and managing conditions like periodontitis. Tseng[220] prepared an electrochemical conducting polymer-based biosensor for the simultaneous detection of leukocyte esterase (LE) and nitrite (NIT), both crucial biomarkers for diagnosing urinary tract infections (UTIs). This sensor, based on an LE antibody conjugated to a carboxylic acid-functionalized poly(3,4-ethylenedioxythiophene) (PEDOT-COOH) modified glassy carbon electrode, was designed as a fast and versatile multi-analyte biosensor. In a pilot study, it successfully analyzed NIT and LE in clinical urine samples, demonstrating high diagnostic sensitivity (100%) and specificity (87.5%) for identifying UTI patients. This highlights its potential as a comprehensive POC tool for UTI diagnosis. Stephenson[221] reported on the increasing use of sodium nitrite in suicides, highlighting it as an emerging

Table 11 Qualitative assessment and cost/performance ranking of nanomaterials for nitrite sensing applications

Nanomaterial type	Platform	Fabrication complexity (qualitative)	Cost (qualitative)	Fouling resistance (qualitative)	Stability/shelf-life (qualitative)	Overall performance score (1–5)	Cost/performance ratio (lower = better)	Ref.
Carbon dots (CDs)	PAA-CDs (from m-phenylenediamine)	Medium (one-step solvothermal)	Low-medium (2)	High (5)	High (5)	5	0.4	11
	NETH-CDs (from N-(1-naphthalene)-ethylenediamine)	Medium (electrolysis)	Low-medium (2)	Medium (3)	Medium-high (4)	4.1	0.49	12
	N-CDs (from chitosan)	Low (one-step hydrothermal)	Low (1)	Medium (3)	High (5)	4.4	0.23	224
	Blue-green fluorescent CDs (from p-aminobenzenesulfonic acid)	Medium (one-step solvothermal)	Low-medium (2)	Medium (3)	Medium (3)	3.2	0.63	66
	C-Dots-NR (carbon nanodots-neutral red)	Medium	Low-medium (2)	Medium (3)	Medium (3)	3.2	0.63	198
	Fluorine and nitrogen co-doped NIR-CDs	Medium (one-step hydrothermal)	Low-medium (2)	Medium (3)	Medium (3)	3.2	0.63	226
Gold nanoparticles (AuNPs)	p-Aminothiophenol-capped gold nanorods + 1,8-diaminonaphthalene-modified gold nanoparticles	High (complex synthesis/functionalization)	High (5)	Medium (3)	Medium (3)	3.2	1.56	19
	CTAB@AuNPs	Medium	Medium (3)	Medium (3)	Medium (3)	3.2	0.94	67
	Fe$_3$O$_4$@SiO$_2$/Au MNPs	High (multi-component synthesis)	High (5)	High (5)	High (5)	5	1	80
	Plasmonic gold nanostars + silver nanopyramid array	High (complex nanostructure fabrication)	High (5)	Medium-high (4)	Medium (3)	3.7	1.35	20
	SH-β-CD@AuNPs	High (functionalization)	High (5)	High (5)	High (5)	5	1	83
	Au@COF composite	High (MOF synthesis + AuNP doping)	High (5)	Medium-high (4)	High (5)	4.7	1.06	81
	Au@Ag nanoparticles	Medium-high	Medium-high (4)	Medium-high (4)	High (5)	4.3	0.93	87
	AuNP-CeO$_2$ NP@GO catalytic nanohybrid	High (multi-component nanohybrid)	Medium-high (4)	Medium (3)	High (5)	4.1	0.98	22
	ZIF-8@ZIF-67//Au nanocomposite	High (MOF synthesis + AuNP modification)	High (5)	Medium (3)	Medium-high (4)	3.7	1.35	111
	Au nanoparticles modified with Hibiscus sabdariffa extract	Low-medium (biogenic synthesis)	Low-medium (2)	Medium (3)	Medium (3)	3.2	0.63	164
	Flexible nanoporous gold film electrode (NPGFE) from upcycled CDs	Medium (electrochemical deposition on recycled material)	Low-medium (2)	High (5)	High (5)	5	0.4	169
Metal-organic frameworks (MOFs)	VB12-modified ZIF-67 loaded with gold colloidal complex	High (complex functionalization)	High (5)	Medium (3)	Medium (3)	3.2	1.56	213
	UiO-66-NH$_2$	High (solvothermal synthesis)	High (5)	Medium (3)	High (5)	4.1	1.22	64
	Nano-porous terbium luminescent metal–organic framework	High (solvothermal synthesis)	High (5)	Medium (3)	High (5)	4.1	1.22	57
	CB/Cu-MOF	High (multi-component synthesis)	Medium-high (4)	Medium (3)	Medium (3)	3.2	1.25	109

Table 11 (*Contd.*)

Nanomaterial type	Platform	Fabrication complexity (qualitative)	Cost (qualitative)	Fouling resistance (qualitative)	Stability/shelf-life (qualitative)	Overall performance score (1–5)	Cost/performance ratio (lower = better)	Ref.
	Ir-UiO-66 nanocomposite	High	High (5)	Medium (3)	Medium (3)	3.2	1.56	114
	Co@N-doped carbon nanorods/nanosheets (from Co-ZIF-L)	High (carbonization of the MOF precursor)	Medium-high (4)	Medium (3)	High (5)	4.1	0.98	116
	Ru@MOF-NH$_2$	High	High (5)	Medium (3)	High (5)	4.1	1.22	194
	Fe$_3$O$_4$@Au-Cu/MOF nanozyme	High (multi-component nanozyme)	High (5)	Medium-high (4)	High (5)	4.7	1.06	170
MXenes	Manganese-based MOF (UoZ-6)	High (biogenic synthesis)	Medium-high (4)	Medium-high (4)	High (5)	4.3	0.93	172
	TiO$_2$-Ti$_3$C$_2$TX-CS-CTAB/GCE	Medium-high (multi-component synthesis)	Medium (3)	Medium (3)	Medium (3)	3.2	0.94	162
	Ultrathin (Ti$_3$C$_2$T$_x$-MXene) doped with Au nanoparticles	High (etching + doping)	Medium-high (4)	Medium (3)	Medium (3)	3.2	1.25	134
	Ti$_3$C$_2$ nanosheets functionalized with ApoF-Pt nanoparticles (Pt@ApoF/Ti$_3$C$_2$)	High (complex bioconjugation)	High (5)	Medium (3)	Medium (3)	3.2	1.56	168
Graphene/graphene oxide (GO/rGO)	Reduced graphene oxide (rGO) + MnO$_x$-VO$_x$-AuNPs	Medium-high (multi-component composite)	Medium (3)	Medium (3)	Medium (3)	3.2	0.94	104
	rGO + Bi$_2$O$_3$ + Ag nanoparticles (Ag–Bi$_2$O$_3$–rGO)	Medium-high	Medium (3)	Medium (3)	Medium (3)	3.2	0.94	105
	MWCNTs-black phosphorene (MWCNTs-BP) nanocomposite	High (multi-component nanocomposite)	Medium-high (4)	Medium (3)	Medium (3)	3.2	1.25	148
	Co$_3$O$_4$-HRP/rGO bio-composite	High (enzyme immobilization)	Medium-high (4)	Medium (3)	Medium (3)	3.2	1.25	145
	LIG (laser-induced graphene) electrode (CS/NP-LIG)	Low (laser scribing)	Low (1)	Medium (3)	High (5)	4.4	0.23	159
	GO modified with PANI and Au nanoparticles	Medium	Medium (3)	Medium (3)	Medium (3)	3.2	0.94	126
	PEDOT-rGO	Medium	Low-medium (2)	Medium (3)	Medium (3)	3.2	0.63	127
	Co$_3$O$_4$-rGO@CNTs	Medium-high	Medium (3)	High (5)	High (5)	4.7	0.85	129
	ZIF-67C@RGO/NiNPs	High	Medium-high (4)	Medium (3)	Medium (3)	3.2	1.25	130
	Self-assembled hydrogel bioelectrodes with rGO + engineered *Shewanella*	High (genetic engineering + hydrogel)	High (5)	High (5)	High (5)	5	1	156
	PEDOT doped with graphene oxide-Fe$_3$O$_4$ (GO-Fe$_3$O$_4$) nanocomposite	Medium-high	Medium (3)	Medium (3)	High (5)	4.1	0.73	171
Metal oxide nanoparticles	α-MnO$_2$ nanorods (FLR@ α-MnO$_2$ NRs)	Medium	Medium (3)	Medium (3)	Medium (3)	3.2	0.94	62
	Cobalt oxide nanoparticle-based carbon electrode	Medium	Low-medium (2)	Medium (3)	Medium (3)	3.2	0.63	228
	Hollow ZnO@Ag nanosphere	High (complex hollow structure)	High (5)	Medium (3)	Medium (3)	3.2	1.56	79
	ZrO$_2$@MWCNT nanocomposite	Medium	Medium (3)	Medium (3)	Medium (3)	3.2	0.94	119
	Bi$_2$Se$_3$@MWCNTs-COOH	Medium	Medium (3)	Medium (3)	Medium (3)	3.2	0.94	120
	CuO, NiO, SnO$_2$ on FTO electrode	Medium	Low-medium (2)	Medium (3)	Medium (3)	3.2	0.63	121

Table 11 (Contd.)

Nanomaterial type	Platform	Fabrication complexity (qualitative)	Cost (qualitative)	Fouling resistance (qualitative)	Stability/shelf-life (qualitative)	Overall performance score (1–5)	Cost/performance ratio (lower = better)	Ref.
	ZnO modified with a conductive copolymer	Medium	Low-medium (2)	Medium (3)	Medium (3)	3.2	0.63	122
	Co$_3$O$_4$ and MoO$_3$ hybrid coupling	Medium	Medium (3)	Medium (3)	Medium (3)	3.2	0.94	123
	CeO$_2$ doped with Sn	Low-medium (facile precipitation)	Low (1)	Medium (3)	Medium (3)	3.2	0.31	124
	ZnO conjugated with tetra-amino-cobalt(II) phthalocyanine + PANI	Medium	Medium (3)	Medium (3)	Medium (3)	3.2	0.94	125
	Strontium ferrite (SF) nanochain architecture	Medium	Medium (3)	Medium (3)	Medium (3)	3.2	0.94	132
	3D CeO$_2$ NSs/CuO NFs p–n heterostructure on carbon cloth	High (complex 3D architecture, electrodeposition)	Medium-high (4)	High (5)	High (5)	5	0.8	135
	Fe$_3$O$_4$@Au@Cys/rGO/GCE	High (multi-component functionalization)	Medium-high (4)	Medium (3)	High (5)	4.1	0.98	163
	NiO nanoparticles (from *Calotropis gigantea* extract)	Low (biogenic synthesis)	Low (1)	Medium (3)	Medium (3)	3.2	0.31	166
	Cu$^+$ biochar (from egg membrane wastes)	Low (rapid pyrolysis of waste)	Low (1)	High (5)	High (5)	5	0.2	167
	Binary metal sulfide (CoS$_2$–MoS$_2$) modified with N-doped lignocellulose	Medium-high	Medium (3)	High (5)	High (5)	4.7	0.85	175
	Mn NPs (from *Pinus brutia* pine needles)	Low (biogenic synthesis)	Low (1)	Medium (3)	Medium (3)	3.2	0.31	227
Conducting polymers	Poly(1-vinylimidazole-*co*-ethylene dimethacrylate) (VIM-EDMA) monolithic capillary	Medium (monolithic column synthesis)	Medium (3)	High (5)	High (5)	5	0.6	29
	PANI–CMC@Cu NPs	Medium	Medium (3)	Medium-high (4)	High (5)	4.4	0.68	165
	PEDOT:PSS/RGO thin film	Medium	Low-medium (2)	Medium (3)	Medium (3)	3.2	0.63	170
	PEDOT-COOH modified glassy carbon electrode	Medium	Low-medium (2)	Medium (3)	Medium (3)	3.2	0.63	220
	Carbon black-based filament for a 3D-printed electrochemical sensor	Low-medium (3D printing)	Low (1)	Medium (3)	Medium (3)	3.2	0.31	200
Carbon nanotubes (CNTs)	MWCNTs-CS-modified sensor	Medium	Medium (3)	Medium (3)	Medium (3)	3.2	0.94	229
	MWCNTs-BP nanocomposite	High (multi-component nanocomposite)	Medium-high (4)	Medium (3)	Medium (3)	3.2	1.25	148
	MWCNTs (in CoTL-MethPc composite)	Medium	Medium (3)	Medium (3)	High (5)	4.1	0.73	106
	MWCNTs (in CoTMePhCAPc composite)	Medium	Medium (3)	Medium (3)	High (5)	4.1	0.73	107
	Co$_3$O$_4$-rGO@CNTs	Medium-high	Medium (3)	High (5)	High (5)	4.7	0.85	129
	AgNPr@P-CNTs/SPCE	Medium-high	Medium (3)	Medium (3)	Medium (3)	3.2	1.25	137
	MWCNTs-functionalized SPCEs (with CuCP)	Medium	Medium (3)	Medium (3)	Medium (3)	3.2	0.94	217

Table 11 (Contd.)

Nanomaterial type	Platform	Fabrication complexity (qualitative)	Cost (qualitative)	Fouling resistance (qualitative)	Stability/shelf-life (qualitative)	Overall performance score (1–5)	Cost/performance ratio (lower = better)	Ref.
	N-Doped multiwalled carbon nanotubes (N-MWCNTs) with CuPc	Medium	Medium (3)	Medium (3)	Medium (3)	3.2	0.94	202
Other nanomaterials/nanostructures	Silver nanopyramid array (coupled with Au nanostars)	High (complex nanostructure fabrication)	High (5)	Medium-high (4)	Medium (3)	3.7	1.35	20
	Silicon-based electrode	Medium (microfabrication)	Medium (3)	Medium (3)	High (5)	4.1	0.73	131
	Carbon nano-onions (CNOs) from castor oil	Low (flame synthesis from waste)	Low (1)	Medium (3)	Medium (3)	3.2	0.31	174
	3D printed graphene (G-PLA)	Low-medium (3D printing)	Low-medium (2)	Medium (3)	Medium (3)	3.2	0.63	176
	Superabsorbent cellulose hydrogel	Medium	Low (1)	High (5)	Medium (3)	4.1	0.24	230
	Silicon carbide (SiC) nanoparticles (NH$_2$-IL/SiC)	Medium	Medium (3)	Medium (3)	Medium (3)	3.2	0.94	51
	FeTMPyP/NbMoO$_6$ sandwich-shaped sensor	Medium	Medium (3)	Medium (3)	Medium (3)	3.2	0.94	100
	Black phosphorus/molybdenum disulfide (BP/MoS$_2$) doped with Ni and Co	High	High (5)	Medium (3)	Medium (3)	3.2	1.56	101
	Tetra L-methionine cobalt(II) phthalocyanine (CoTL-MethPc)	Medium-high	Medium (3)	Medium (3)	High (5)	4.1	0.73	106
	Tetra-4-(2-methoxyphenoxy) carboxamide cobalt(II) with amide-bridged phthalocyanine (CoTMePhCAPc)	Medium-high	Medium (3)	Medium (3)	High (5)	4.1	0.73	107
	Pd and glassy carbon microspheres (GCMs)	Medium	Medium (3)	Medium (3)	Medium (3)	3.2	0.94	137
	Ion-imprinted polymer (IIP)	Medium	Medium (3)	Medium (3)	Medium (3)	3.2	0.94	139
	High-affinity chrome-black T (with nanogold Au film)	Medium	Medium (3)	Medium (3)	Medium (3)	3.2	0.94	140
	Ru(II)-(BSAP-PLA) complex (on carbon paste electrode)	Medium	Medium (3)	Medium (3)	Medium (3)	3.2	0.94	142
	Cytochrome c reductase, polypyrrole, and gold nanocomposite	High (bio-conjugation)	High (5)	Medium (3)	Medium (3)	3.2	1.56	144
	Liposome-based nitrite biosensor (NirB enzyme, NirC channels)	High (complex bio-assembly)	High (5)	High (5)	High (5)	5	1	147
	M13 viruses and gold nanostructures	High (viral modification)	High (5)	Medium (3)	Medium (3)	3.2	1.56	157
	HS-β-cyclodextrin coordination methanobactin/gold nanoparticles (HS-β-CD@Mb/AuNPs)	High (complex bioconjugation)	High (5)	High (5)	High (5)	5	1	158

trend and noting significant analytical limitations in evaluating suspected cases. It underscores the critical need for rapid and accurate nitrite detection, particularly in forensic and emergency medical contexts. The challenges in post-mortem analysis (e.g., conversion of nitrite to nitrate) as discussed by Kim (2022)[222] and Tomsia[223] further emphasized the value of real-time, on-site detection methods that could potentially aid in earlier intervention or more accurate forensic assessment. Kim[222] developed an ion chromatography method to quantify nitrite and nitrate in postmortem blood. Due to nitrite's postmortem conversion to nitrate, nitrite levels were low (e.g., 32.4 ± 29.5 mg L^{-1} in peripheral blood), while nitrate levels were high (e.g., 298.0 ± 25.6 mg L^{-1}). Therefore, both nitrite and nitrate concentrations are crucial for diagnosing sodium nitrite poisoning, especially in postmortem samples.

6.5. Green chemistry approaches in nitrite sensing

Embracing green chemistry principles in the development of nitrite sensors is an increasingly important trend, driven by environmental consciousness and the desire for sustainable analytical solutions. This involves using environmentally benign precursors, reducing hazardous waste generation, and employing energy-efficient synthesis routes. Waste valorization, such as transforming waste materials into valuable sensing components, is a prime example of green chemistry in this field. Sun[224] successfully synthesized N-doped carbon dots (N-CDs) via a simple one-step hydrothermal carbonization using chitosan as carbon and nitrogen sources. Chitosan, a natural polysaccharide with high nitrogen content, is a promising and green precursor for N-CDs. These N-CDs exhibited strong blue fluorescence and were applied as a fluorescent sensor for nitrite determination in real tap water and lake water samples. This approach exemplifies green chemistry by utilizing a natural, abundant, and biodegradable polymer (chitosan) to create a highly sensitive and selective sensor, minimizing the use of hazardous chemicals and complex synthesis steps. Wang (2016)[225] developed a simple and non-enzymatic electrochemical sensor for nitrite based on a TEMPO oxidized straw cellulose/molybdenum sulfide (TOSC-MoS$_2$) nanocomposite. This composite was synthesized via a hydrothermal method, using straw cellulose as a natural, abundant, and renewable substrate. The use of straw cellulose, a common agricultural waste product, aligns with green chemistry principles by valorizing biomass into a functional material for sensing. The electrochemical approach itself is considered environmentally friendly as it "requires no additional chemical loading". Ning[226] established a fluorescence "on–off–on" strategy for nitrite determination using fluorine and nitrogen co-doped near-infrared carbon dots (NIR-CDs). These NIR-CDs were prepared via a one-step hydrothermal method using N-(4-aminophenyl)-acetamide and 4,5-difluorobenzene-1,2-diamine as precursors. While the precursors are synthetic, the one-step hydrothermal method is generally considered a greener synthesis approach compared to multi-step, high-energy processes, reducing reaction time and solvent use. The method showed good applicability for nitrite determination in soil extract, human urine, and water samples. Mohammed Ameen[227] synthesized manganese nanoparticles (Mn NPs) using a cost-effective and eco-friendly biogenic approach with Pinus brutia pine needles. These pine needle-derived Mn NPs exhibited remarkable oxidase-like activity, catalyzing the oxidation of TMB for visual and colorimetric nitrite detection. This approach is a strong example of green chemistry due to its biogenic synthesis, utilizing a natural, abundant, and renewable biomass source (pine needles) to produce a sustainable nanozyme. The method combines simplicity, cost-effectiveness, and eco-friendliness, ensuring accurate, portable, and instrument-free nitrite detection, ideal for real-world food testing applications. The use of natural materials and a straightforward synthesis route significantly reduces the environmental footprint of sensor fabrication. These examples collectively demonstrate the rapid growth and versatility of point-of-care nitrite sensors, transforming nitrite analysis into a more accessible, portable, and user-friendly process for diverse applications, including food safety, environmental monitoring, and clinical diagnostics. The increasing focus on non-invasive samples like saliva and urine, coupled with integrated technologies, is a key driver in this field.

6.6. Qualitative assessment and cost/performance ranking of nanomaterials for nitrite sensing applications

Table 11, provides a qualitative assessment and a derived cost/performance ranking of various nanomaterial-based platforms utilized for nitrite sensing. It synthesizes information on fabrication complexity, qualitative cost, resistance to fouling, and stability/shelf-life, along with a calculated overall performance score and a cost/performance ratio to facilitate comparative evaluation. All qualitative assessments (low, medium, high) are converted to numerical scores (1–5, where 5 is the highest) for calculation, with the "Overall Performance Score" being a weighted average of the qualitative advantages, fouling resistance, and stability/shelf-life. A lower "Cost/Performance Ratio" indicates greater cost-effectiveness.

7. Challenges and limitations in nitrite sensing

7.1. Complex matrix interferences in high-nitrogen and sludge samples

Nitrite detection in matrices with high nitrogen content, such as agricultural soils, manures, and wastewater sludge, presents unique challenges due to the presence of various nitrogen species (ammonium, nitrate, organic nitrogen) and other complex organic and inorganic components.

The accurate detection of nitrite in highly complex matrices, such as those found in high-nitrogen wastewaters and various sludge samples, presents a significant analytical challenge. These matrices are characterized by a rich and diverse composition of co-existing chemical species, including various nitrogen compounds (e.g., ammonia, nitrate, and organic nitrogen), heavy metals, suspended solids, organic matter, and

microbial communities. These components can severely interfere with nitrite sensing by causing signal suppression or enhancement, electrochemical fouling, or non-specific reactions, thereby compromising the selectivity, sensitivity, and reliability of the detection methods. Addressing these interferences is paramount for developing robust and accurate nitrite sensors suitable for real-world environmental and industrial applications. To illustrate these challenges, Malley[231] investigated the use of a field-portable near-infrared spectrometer (NIRS) for compositional measurement of cattle dung while composting. While NIRS was effective for measuring total C, organic C, total N, C:N, S, K, and pH, calibrations for nitrate + nitrite were unsuccessful. This demonstrates a considerable issue in reliably distinguishing these specific nitrogen species in extremely heterogeneous and complex organic matrices such as manure, most likely due to overlapping spectral signals or insufficient sensitivity for the various forms of nitrogen. The study emphasized the need for further research using moist, "as is" manure and compost samples for on-site application, underscoring the difficulties of direct analysis without extensive sample preparation. Puspalak[228] developed a cobalt oxide nanoparticle-based carbon electrode for detecting residual nitrite in agricultural field soil. While the electrode showed good sensitivity (LOD 0.3 μM) and a wider linear range, the inherent complexity of soil as a matrix (varying composition, pH, organic matter) still poses challenges for direct, interference-free measurement.

Furthermore, specifically confronting the issue of interferences in soil, Wang[232] addressed the challenges of on-site nitrite detection in soil by developing a 3D porous conductive matrix with excellent antifouling ability. Their sensor, based on phase-transitioning BSA and covalent coupling-stabilized transitioning ZnS-CNTs, exhibited remarkable resistance to interferences from pH variations, microbial presence, and organic pollutants commonly found in the soil. This allowed for effective direct detection of nitrite in real soil suspensions without complex pretreatments, demonstrating a significant step towards overcoming matrix interferences in challenging soil environments. Gurban[229] also developed flexible miniaturized electrochemical sensors for nitrite in soil solutions extracted from corn fields and vegetable gardens. They specifically noted the need to dry, mortar, sieve, and suspend the soil samples in ultrapure water, and homogenize, decant, and filter them for spectrophotometric validation, illustrating the extensive preparation required to isolate analytes from the solid soil matrix. Their MWCNT-CS-modified sensor, however, was dedicated to direct detection in soil solutions collected using suction lysimeters, indicating an advancement in on-site analysis of the liquid phase of soil. Zhao[233] further highlighted the complexity of soil solutions as a "classic complex chemical system" and proposed a new modified spectrometer technology (MST) combining high-throughput experiments and machine learning to simultaneously quantify multiple chemical properties. This approach, achieving high accuracy ($R^2 = 0.996$) for eight indicators, including potential nitrogen species, underscores the power of advanced computational methods in handling the multi-component interference in the soil. From a review

perspective, Hossain[234] reviewed the development of electrochemical sensors for NPK (nitrogen, phosphorus, potassium) ions in soil and water. They emphasized that while electrochemical sensors are promising for rapid detection, the complexity of soil matrices necessitates advanced sensor designs and often some level of sample preparation (e.g., obtaining soil solutions via lysimeters or suspensions) to overcome interferences. Their review highlights the ongoing challenge of achieving direct, interference-free measurements in such complex environments, reinforcing the need for smart and portable solutions to reduce excess fertilizer use.

Mai[235] applied a portable IC system for real-time on-site analysis of nitrite and nitrate in soils and soil pore waters. They developed a field-applicable ultrasonic-assisted extraction method for soil samples and demonstrated the potential of portable IC for analyzing high organic matter soil (e.g., sheep manure samples). For soil pore-water sampling, they prepared a "sludge" by mixing soil with deionized water to ensure good contact between the sampler and the soil, which is a form of on-site sample preparation for a challenging matrix. This study explicitly addresses the challenges of complex solid and semi-solid matrices, demonstrating methods to extract analytes for portable analysis. Gauthama[230] also described spectrophotometric determination of nitrite and nitrate in water and soil samples using in situ azo dye formation. They noted the need to remove the formed azo dye using a superabsorbent cellulose hydrogel to "reduce organic load in the test samples," indicating that even after the reaction, organic interferences can remain and require further treatment. Similarly, Ji[236] revealed the considerable issue of reliably estimating dissolved organic nitrogen (DON) due to cumulative analytical errors caused by removing dissolved inorganic nitrogen species (DIN, such as nitrite and nitrate) from total dissolved nitrogen (TDN). They stated that "poor separations between DON and DIN species" and "severe interferences from nitrite or nitrate on the analysis of DON fractions" are ongoing issues, particularly at high DIN/TDN ratios. To address this, they created an improved Size Exclusion Chromatography system with an Organic Nitrogen Detector (SEC-OND). While their system improved separation and achieved complete oxidation of N species to nitrate using an independent vacuum ultraviolet (VUV) oxidation device, the inherent complexity of separating and quantifying multiple nitrogen forms in various aquatic samples (river water, lake water, wastewater effluent, groundwater, landfill leachate) remains a challenge. This method, while powerful, requires careful optimization of oxidation time, injection mass, and mobile phase conditions to ensure sufficient N recoveries and minimize interferences from co-eluting species. Despite advancements, many solutions for complex matrices still have limitations. Improved interference resistance often adds device complexity, increases manufacturing costs, or reduces portability, undermining on-site analysis goals. Crucially, "sample preparation" steps frequently reappear subtly, merely shifting the burden. The unpredictable nature of high-nitrogen and sludge samples means a universal solution remains elusive. Future research should prioritize integrating robust, autonomous sample pretreatment modules directly into portable

devices. This, combined with sophisticated AI/ML algorithms to intelligently compensate for unavoidable matrix effects, is essential for maintaining accuracy and ease of use without compromise.

7.2. Limitations regarding nitrite sensing methods

While significant advancements have been made in nitrite sensing, each method faces specific limitations, particularly in complex matrices. Near-infrared spectrometry (NIRS), for instance, struggles with reliably distinguishing specific nitrogen species in highly heterogeneous organic samples like cattle dung, often due to overlapping spectral signals or insufficient sensitivity to various nitrogen forms, highlighting the need for further research with "as is" samples for on-site application.[231] Electrochemical methods, while promising, are susceptible to severe interferences from high-organic-content samples, leading to signal suppression or enhancement, electrochemical fouling, and compromised selectivity.[228,234] Despite developments like 3D porous conductive matrices to enhance antifouling,[232] these methods often still necessitate some level of sample preparation, such as obtaining soil solutions *via* lysimeters or suspensions, to overcome interferences.[229,234] Chromatographic techniques, like portable IC systems, despite their potential for real-time on-site analysis, may still require initial extraction methods for solid or semi-solid matrices, as seen with ultrasonic-assisted extraction for soil or mixing soil with deionized water to create "sludge" for pore-water sampling.[235] Furthermore, accurately estimating dissolved organic nitrogen (DON) using chromatographic methods can be challenging due to cumulative analytical errors from removing dissolved inorganic nitrogen species (DIN) and "poor separations".[236] Spectrophotometric methods, even when employing *in situ* azo dye formation, can require additional treatment steps to remove organic load from test samples to mitigate interferences.[230] In summary, improving interference resistance often adds device complexity, increases manufacturing costs, or reduces portability, thereby challenging the goals of truly on-site and autonomous analysis. The unpredictable nature of high-nitrogen and sludge samples means that a universal, compromise-free solution remains elusive, indicating that sample preparation burdens are often merely shifted rather than entirely eliminated.

8. Market demand, societal relevance, and regulatory landscape

The demand for accurate, rapid, and cost-effective nitrite detection extends across numerous sectors, driven by critical societal needs related to health, environment, and food safety. This section highlights the market drivers, key industrial applications, and the regulatory frameworks that shape the development and adoption of nitrite sensing technologies.

8.1. Market drivers and societal relevance

The global market for nitrite detection is robust and growing, fueled by increasing awareness of its impact on human health and environmental quality. Nitrite's toxicity, particularly its role in methemoglobinemia (blue baby syndrome) in infants and its potential to form carcinogenic *N*-nitrosamines in food, necessitates stringent monitoring.[237] Also, nitrite is a critical intermediate in the nitrogen cycle, and its accumulation in water bodies (eutrophication) can lead to oxygen depletion and harm aquatic life.[238] Monitoring nitrite levels is essential for assessing water quality in rivers, lakes, oceans, and groundwater, and for managing nutrient pollution. Regarding food safety and quality, nitrite is widely used as a curing agent in meat products to preserve color, inhibit microbial growth (especially *Clostridium botulinum*), and enhance flavor. However, residual nitrite levels must be carefully controlled to prevent health risks.[239] The demand for "nitrite-free" or "clean label" products also drives innovation in alternative preservation methods and the need for accurate nitrite detection in these products.[240] In agriculture, nitrite is part of the nitrogen cycle in soils. Excessive use of nitrogen fertilizers can lead to nitrite accumulation, impacting soil health, crop yield, and contributing to water pollution through runoff.[241] Efficient monitoring helps optimize fertilizer use, reduce environmental impact, and support sustainable farming practices. Finally, in industrial processes, nitrite monitoring is crucial in wastewater treatment plants (WWTPs), where precise control of nitrification and denitrification processes is vital for efficient nitrogen removal and regulatory compliance.[242]

8.2. Key social/industrial applications

Nitrite detection technologies find application across a diverse range of industries:

Continuous, real-time monitoring of nitrite is essential for optimizing biological nutrient removal (BNR) processes in WWTPs. Fault detection and diagnosis in sensors are critical to ensure operational efficiency, reduce energy consumption, and minimize greenhouse gas emissions.[243] Portable systems are increasingly valuable for field assessments and decentralized treatment facilities.[244] Quality control and safety assurance in the meat, dairy, and processed food industries heavily rely on accurate nitrite measurement. This includes monitoring curing processes, ensuring compliance with residual nitrite limits, and validating "nitrite-free" claims.[245] Moreover, farmers and agricultural researchers use nitrite sensors to assess soil nutrient status, optimize fertilizer application, and monitor runoff into water sources. Portable sensors are particularly beneficial for on-site soil analysis and precision agriculture.[246,247] Additionally, maintaining optimal water quality in fish farms and other aquaculture systems is paramount for the health and productivity of aquatic organisms. Nitrite levels, even at low concentrations, can be toxic, necessitating continuous and sensitive monitoring.[248,249] Finally, regarding the clinical diagnostics and forensics, nitrite detection is relevant in specific medical contexts (*e.g.*, urinary tract infections[250]) and is critically important in forensic investigations involving nitrite poisoning.[251,252] The development of portable, rapid diagnostic tools for these applications is a growing area of interest.[9]

8.3. Regulatory limits and compliance

Regulatory bodies and environmental organizations worldwide establish strict limits and guidelines for nitrite concentrations across various matrices to protect public health and the environment. Compliance with these regulations is a major driver for the adoption of reliable detection technologies.

8.3.1. International guidelines. The WHO provides guidelines for drinking water quality, often recommending a guideline value for nitrite to protect against methemoglobinemia. These guidelines serve as a basis for national regulations globally. For instance, the WHO's Guidelines for Drinking-water Quality typically recommend a guideline value of 3 mg L^{-1} (as NO_2^-) or 0.9 mg L^{-1} (as NO_2^-–N) to prevent health effects from short-term exposure, especially in infants.[253] The U.S. Environmental Protection Agency (EPA) sets a legally enforceable maximum contaminant level (MCL) for nitrite in drinking water at 1 mg L^{-1} (as nitrite-N), equivalent to approximately 3.28 mg L^{-1} as NO_2^- or 71.4 μM. The EPA also issues guidelines and analytical methods for monitoring nitrogen compounds in wastewater and surface waters under the Clean Water Act, influencing discharge permits for industrial and municipal facilities.[203] Moreover, the European Union (EU) Drinking Water Directive (Directive 98/83/EC, and its revision Directive (EU) 2020/2184) sets a maximum concentration for nitrite in drinking water at 0.50 mg L^{-1} as NO_2^-.[254] For wastewater, the Urban Wastewater Treatment Directive (91/271/EEC) and the Water Framework Directive (2000/60/EC) establish frameworks for monitoring and controlling nitrogen discharges, including nitrite, to prevent eutrophication and ensure good ecological status of water bodies.[255]

8.3.2. Specific regulatory applications. The European Union and the U.S. (USDA and FDA) heavily regulate residual nitrite and nitrate levels in cured meat products to prevent the formation of carcinogenic *N*-nitrosamines while still ensuring protection against foodborne pathogens like *Clostridium botulinum*.[256] The EU, for instance, has historically set limits such as 50 mg kg^{-1} for cooked ham and recently, with Regulation 2023/2108, introduced significantly stricter limits for nitrites and nitrates as food additives. This new EU legislation, effective from October 9, 2025, mandates lower maximum added amounts and, for the first time, sets mandatory residual nitrite limits (with indicative nitrate levels), reflecting scientific assessments of nitrosamine risks. Similarly, the USDA and FDA regulate maximum allowable amounts and labeling, with the USDA's FSIS having indicated plans to prohibit "No Nitrate or Nitrite Added" claims on products processed with any source of these compounds, including natural ones like celery powder, and to classify natural sources as curing agents.[257] These regulations necessitate rigorous analytical methods and quality control across the food industry to ensure consumer safety. The discharge limits for nitrogen species, including nitrite, are imposed on WWTPs to prevent eutrophication of receiving water bodies.[258] These limits vary depending on local regulations and the sensitivity of the receiving environment. Continuous monitoring and accurate sensor data are crucial for demonstrating compliance, as highlighted by studies on sensor fault detection and diagnosis in WWTPs.[243] While direct regulatory limits for nitrite in soil are less common, regulations on fertilizer use and nutrient management plans indirectly drive the need for soil nitrite monitoring to prevent runoff and groundwater contamination.[259] Agricultural ministries and environmental agencies often provide best practice guidelines for nutrient application to minimize environmental impact.

9 Conclusion

This comprehensive review has highlighted the remarkable advancements in the chemical analysis of nitrite across a diverse array of instrumental methods, including sophisticated spectroscopic, chromatographic, flow injection, electrochemical, and bio-electrochemical techniques. Innovative approaches, particularly those integrating nanomaterials and novel reaction chemistries, have been detailed, and these techniques have significantly pushed the boundaries of sensitivity, selectivity, and stability in nitrite detection. The emergence of dual-mode sensing platforms, the achievement of ultrafast reaction kinetics through nanointerface engineering, and the increasing focus on green chemistry principles underscore the dynamic evolution of this field. Despite these significant strides, the widespread adoption and real-world impact of many cutting-edge nitrite sensing technologies hinge upon overcoming several critical, interconnected challenges. The primary hurdle remains bridging the translational gap from laboratory-scale proof-of-concept to robust, reliable, and commercially viable solutions. This encompasses the inherent complexity of real-world matrices, such as high-nitrogen agricultural soils, wastewater sludge, and intricate biological fluids—which frequently introduce interfering species and demand extensive sample preparation, often compromising sensor performance. Equally crucial are the issues of standardization and rigorous validation. The rapid proliferation of novel materials and methods, while innovative, often lacks universally accepted fabrication protocols and comprehensive validation across diverse sample types and environmental conditions. Establishing such standards is paramount to ensuring reproducibility, comparability of results across different platforms, and ultimately, regulatory acceptance, thereby fostering trust in novel nitrite detection technologies. Furthermore, the commercial viability and cost scalability of advanced nitrite sensors present a significant barrier. While high-performance nanomaterials offer unprecedented analytical figures of merit, their complex synthesis and the overall cost-effectiveness of the final device must be addressed for large-scale manufacturing and market competitiveness. The drive towards truly portable, user-friendly, and durable devices hinges not only on miniaturization but also on sustainable and economically feasible production methods with extended shelf-lives. Looking ahead, the future of nitrite sensing demands an integrated, interdisciplinary approach. Future research must prioritize the development of inherently robust sensors capable of autonomous, real-time, and on-site analysis with minimal pre-treatment. This necessitates continued innovation in AI-integrated platforms for intelligent data processing, adaptive calibration, and predictive analytics, enabling smart sensors to compensate for matrix effects and identify trends. In addition, novel

nanomaterial architectures that offer enhanced selectivity, superior anti-fouling capabilities, and long-term stability in harsh environments. Also, sustainable and green manufacturing processes for sensors are needed for reducing environmental impact and promoting cost-effective, scalable production. Thus, by focusing on standardization, rigorous real-world validation, and addressing the economic and practical aspects of commercialization, the next generation of nitrite sensors can fulfill the urgent societal need for accurate, accessible, and reliable environmental, food safety, and clinical monitoring globally. This sustained innovation will be critical for safeguarding public health, promoting sustainable agriculture, and ensuring environmental quality in an increasingly complex world.

Author contributions

Nadeen Rajab, Ahmed Youssef and Rabeay Y. A. Hassan designed the objectives and scope of the review article. All authors here contributed in writing and revision of the current version of the review article.

Conflicts of interest

Authors declare no conflict of interest.

Data availability

No primary research results, software or code have been included and no new data were generated or analysed as part of this review.

Acknowledgements

References

1 D. Pang, C. Ma, D. Chen, Y. Shen, W. Zhu, J. Gao, H. Song, X. Zhang and S. Zhang, *Org. Electron.*, 2019, **75**, 105374.

2 N. Jaiswal, I. Tiwari, C. W. Foster and C. E. Banks, *Electrochim. Acta*, 2017, **227**, 255–266.

3 H. Rao, Y. Liu, J. Zhong, Z. Zhang, X. Zhao, X. Liu, Y. Jiang, P. Zou, X. Wang and Y. Wang, *ACS Sustain. Chem. Eng.*, 2017, **5**, 10926–10939.

4 A. Kalezic, B. Macanovic, E. Garalejic, A. Korac, V. Otasevic and B. Korac, *Chem. Biol. Interact.*, 2018, **291**, 264–270.

5 Y. Liu, K. D. Croft, J. M. Hodgson, T. Mori and N. C. Ward, *J. Funct. Foods*, 2021, **80**, 104447.

6 L. Xie, S. Chen, C. Yao, D. Li, L. Li and R. Tang, *Aquaculture*, 2019, **507**, 275–281.

7 Y. Wang, Z. Zeng, J. Qiao, S. Dong, Q. Liang and S. Shao, *Talanta*, 2021, **221**, 121605.

8 H. Shi, L. Fu, F. Chen, S. Zhao and G. Lai, *Environ. Res.*, 2022, **209**, 112747.

9 S. Kumar, J. B. Kaushal and H. P. Lee, *Biosensors*, 2024, **14**, 300.

10 D. Tsikas, *J. Chromatogr. B*, 2007, **851**, 51–70.

11 Y. Hao, Z. Yang, W. Dong, Y. Liu, S. Song, Q. Hu, S. Shuang, C. Dong and X. Gong, *J. Hazard. Mater.*, 2022, **430**, 128393.

12 J. Sun, T. Long, Z. Chen, H. Luo, J. Cao, D. Xu and Z. Yuan, *Anal. Chim. Acta*, 2025, **1336**, 343524.

13 P. Singhaphan and F. Unob, *Sens. Actuators, B*, 2021, **327**, 128938.

14 T. Taweekarn, W. Wongniramaikul, C. Boonkanon, K. Phatthanawiwat, P. Pasitsuparoad, R. J. Ritchie and A. Choodum, *Food Chem.*, 2022, **389**, 133085.

15 Y.-T. Tai, C.-Y. Cheng, Y.-S. Chen and F.-H. Ko, *Sens. Actuators, B*, 2022, **369**, 132298.

16 M. H. Ibrahim, Z. Xue, M. I. Shinger, H. I. Abdu, L. Xiong, D. Shan and X. Lu, *Spectrochim. Acta, Part A*, 2019, **210**, 398–404.

17 R. Catalan-Carrio, J. Saez, L. Á. Fernández Cuadrado, G. Arana, L. Basabe-Desmonts and F. Benito-Lopez, *Anal. Chim. Acta*, 2022, **1205**, 339753.

18 A. Das, S. I. Sanakal, G. Sivakumar, A. Babu and S. Maji, *Mater. Adv.*, 2025, **6**, 5045–5055.

19 Z. Li, M. Li, C. Wang, X. Zhou, J. Li and D. Li, *Sens. Actuators, B*, 2019, **297**, 126757.

20 P. Zheng, S. Kasani, X. Shi, A. E. Boryczka, F. Yang, H. Tang, M. Li, W. Zheng, D. E. Elswick and N. Wu, *Anal. Chim. Acta*, 2018, **1040**, 158–165.

21 N. Pourreza, M. R. Fat'hi and A. Hatami, *Microchem. J.*, 2012, **104**, 22–25.

22 O. Adegoke, S. Zolotovskaya, A. Abdolvand and N. N. Daeid, *Talanta*, 2021, **224**, 121875.

23 A. T. Mubarak, A. A. Mohamed, K. F. Fawy and A. S. Al-Shihry, *Microchim. Acta*, 2007, **157**, 99–105.

24 Y. S. Li, C. L. Zhao, B. L. Li and X. F. Gao, *Food Chem.*, 2020, **330**, 127151.

25 S. Aslani and D. W. Armstrong, *J. Chromatogr. A*, 2022, 463255, DOI: 10.1016/j.chroma.2022.463255.

26 J. V. Seeley and S. K. Seeley, *Anal. Chem.*, 2013, **85**, 557–578.

27 M. Akyüz and Ş. Ata, *Talanta*, 2009, **79**, 900–904.

28 S.-X. Zhang, R. Peng, R. Jiang, X.-S. Chai and D. G. Barnes, *J. Chromatogr. A*, 2018, **1538**, 104–107.

29 S. L. Lin, J. W. Hsu and M. R. Fuh, *Talanta*, 2019, **205**, 120082.

30 P. Yenda, N. K. Katari, T. Dongala, G. Vyas, L. N. R. Katakam and S. K. Ettaboina, *Biomed. Chromatogr.*, 2022, **36**, e5269.

31 K. Zhang, S. Li, C. Liu, Q. Wang, Y. Wang and J. Fan, *J. Sep. Sci.*, 2019, **42**, 574–581.

32 E. Murray, P. Roche, K. Harrington, M. McCaul, B. Moore, A. Morrin, D. Diamond and B. Paull, *J. Chromatogr. A*, 2019, **1603**, 8–14.

33 R. Mazumdar, M. Sharif, T. Khan, M. Rahman and A. Abdullah, *Food Res.*, 2022, **6**, 145–152.

34 L. Chiesa, F. Arioli, R. Pavlovic, R. Villa and S. Panseri, *Food Chem.*, 2019, **288**, 361–367.

35 T. D'Amore, A. Di Taranto, V. Vita, G. Berardi and M. Iammarino, *Food Anal. Methods*, 2019, **12**, 1813–1822.

36 L. Moravský, P. Troška, M. Klas, M. Masár and Š. Matejčík, *Contrib. Plasma Phys.*, 2020, **60**, e202000014.

37 X. Wang, E. Adams and A. Van Schepdael, *Talanta*, 2012, **97**, 142–144.

38 P. Troška, R. Chudoba, L. Danč, R. Bodor, M. Horčičiak, E. Tesařová and M. Masár, *J. Chromatogr. B*, 2013, **930**, 41–47.

39 F. Della Betta, L. Vitali, R. Fett and A. C. O. Costa, *Talanta*, 2014, **122**, 23–29.

40 C. B. Freitas, R. C. Moreira, M. G. de Oliveira Tavares and W. K. T. Coltro, *Talanta*, 2016, **147**, 335–341.

41 J. M. Siegel, K. M. Schilly, M. B. Wijesinghe, G. Caruso, C. G. Fresta and S. M. Lunte, *Anal. Methods*, 2019, **11**, 148–156.

42 R. Gottardo, F. Taus, N. Pigaiani, F. Bortolotti, D. Lonati, G. Scaravaggi, C. A. Locatelli and F. Tagliaro, *Toxicol. Anal. Clin.*, 2022, **34**, S26.

43 S. B. Lucas, L. M. Duarte, K. C. A. Rezende and W. K. T. Coltro, *Micromachines*, 2022, **13**, 1736.

44 Z. N. Tembo, F. Şeker Aygun and B. Y. Erdoğan, *Sep. Sci. plus*, 2021, **4**, 45–53.

45 Z. Kalaycıoğlu, H. S. Karadeniz and B. Berker, *AURUM J. Eng. Syst. Archit.*, 2021, **5**, 139–148.

46 C. E. López Pasquali, P. Fernández Hernando and J. S. Durand Alegría, *Anal. Chim. Acta*, 2007, **600**, 177–182.

47 X.-F. Yue, Z.-Q. Zhang and H.-T. Yan, *Talanta*, 2004, **62**, 97–101.

48 M. Noroozifar, M. Khorasani-Motlagh, A. Taheri and M. Homayoonfard, *Talanta*, 2007, **71**, 359–364.

49 S. Nouroozi and R. Mirshafian, *Talanta*, 2009, **79**, 1149–1153.

50 S. Feng, M. Zhang, Y. Huang, D. Yuan and Y. Zhu, *Talanta*, 2013, **117**, 456–462.

51 A. Salimi, M. Kurd, H. Teymourian and R. Hallaj, *Sens. Actuators, B*, 2014, **205**, 136–142.

52 L. A. Pradela-Filho, B. C. Oliveira, R. M. Takeuchi and A. L. Santos, *Electrochim. Acta*, 2015, **180**, 939–946.

53 S. Wang, K. Lin, N. Chen, D. Yuan and J. Ma, *Talanta*, 2016, **146**, 744–748.

54 M. A. Tzani, D. K. Gioftsidou, M. G. Kallitsakis, N. V. Pliatsios, N. P. Kalogiouri, P. A. Angaridis, I. N. Lykakis and M. A. Terzidis, *Molecules*, 2021, **26**(24), 1–29.

55 E. Nagababu and J. M. Rifkind, *Free Radicals Biol. Med.*, 2007, **42**, 1146–1154.

56 Z. Fu, W. Gao, T. Yu and L. Bi, *Talanta*, 2019, **195**, 463–471.

57 B. Ding, Y. Cheng, J. Wu, X. M. Wu, H. M. Zhang, Y. Luo, X. F. Shi, X. X. Wu, J. Z. Huo, Y. Y. Liu and Y. Li, *Dyes Pigm.*, 2017, **146**, 455–466.

58 M. Yaqoob, B. Folgado Biot, A. Nabi and P. J. Worsfold, *Luminescence*, 2012, **27**, 419–425.

59 J. Jia, W. Lu, L. Li, Y. Gao, Y. Jiao, H. Han, C. Dong and S. Shuang, *J. Mater. Chem. B*, 2020, **8**(10), 2123–2127.

60 H. Chen, W. Tang, Y. Liu and L. Wang, *Food Chem.*, 2022, **367**, 130660.

61 C. Rosas-Salazar, M. H. Shilts, Z.-Z. Tang, Q. Hong, K. N. Turi, B. M. Snyder, D. A. Wiggins, C. E. Lynch, T. Gebretsadik and R. S. Peebles Jr, *J. Allergy Clin. Immunol.*, 2022, **150**, 612–621.

62 H. R. H. Ali, A. I. Hassan, Y. F. Hassan and M. M. El-Wekil, *Microchem. J.*, 2021, **164**, 105982.

63 M. M. Doroodmand and M. Askari, *Anal. Chim. Acta*, 2017, **968**, 74–84.

64 X. Hao, Y. Liang, H. Zhen, X. Sun, X. Liu, M. Li, A. Shen and Y. Yang, *J. Solid State Chem.*, 2020, **287**, 121323.

65 J. Zhang, F. Pan, Y. Jin, N. Wang, J. He, W. Zhang and W. Zhao, *Dyes Pigm.*, 2018, **155**, 276–283.

66 Y. Deng, J. Qian, Y. Zhou and Y. Niu, *RSC Adv.*, 2021, **11**, 10922–10928.

67 K. Chaiendoo, K. Ngamdee, W. Limbut, C. Saiyasombat, W. Busayaporn, S. Ittisanronnachai, V. Promarak, K. Promsuwan, P. Thavarungkul, P. Kanatharana and W. Ngeontae, *Microchem. J.*, 2021, **168**, 106470.

68 K.-K. Yu, S.-L. Pan, K. Li, L. Shi, Y.-H. Liu, S.-Y. Chen and X.-Q. Yu, *Food Chem.*, 2021, **341**, 128254.

69 Y.-H. Zhan, R. Sun, W.-J. Zhu, Y.-J. Xu and J.-F. Ge, *Sens. Actuators, B*, 2017, **240**, 1283–1290.

70 J. Huang, P.-r. Liu, Q.-y. Sun, H. Zhang, Y. Zhang and K. Wang, *Anal. Lett.*, 2017, **50**, 1620–1629.

71 G. Ma, H. Chen, Q. Zhang, J. Ma, Q. Yu, L. Han, C. Chen and R. Song, *LWT*, 2019, **116**, 108556.

72 S. D. Ebbesen, B. L. Mojet and L. Lefferts, *J. Catal.*, 2008, **256**, 15–23.

73 M. Gallignani, M. Valero, C. Ayala, M. del Rosario Brunetto, A. Sánchez, J. L. Burguera and M. Burguera, *Talanta*, 2004, **64**, 1290–1298.

74 M. Paydar, Y. L. Wong, W. F. Wong, O. A. A. Hamdi, N. A. Kadir and C. Y. Looi, *J. Food Sci.*, 2013, **78**, T1940–T1947.

75 M. D. Yilmaz, *Microchem. J.*, 2024, **196**, 109554.

76 H. Ozmen, F. Polat and A. Cukurovali, *Anal. Lett.*, 2006, **39**, 823–833.

77 H. Yang, Y. Xiang, X. Guo, Y. Wu, Y. Wen and H. Yang, *Sens. Actuators, B*, 2018, **271**, 118–121.

78 P. Wang, Y. Sun, X. Li, J. Shan, Y. Xu and G. Li, *Vib. Spectrosc.*, 2021, **113**, 103221.

79 J. Wang, M. M. Hassan, W. Ahmad, T. Jiao, Y. Xu, H. Li, Q. Ouyang, Z. Guo and Q. Chen, *Sens. Actuators, B*, 2019, **285**, 302–309.

80 J. Chen, S. Pang, L. He and S. R. Nugen, *Biosens. Bioelectron.*, 2016, **85**, 726–733.

81 R. Tan, M. Zeng, Q. Huang, N. Zhou, M. Deng, Y. Li and X. Luo, *Food Chem.*, 2024, **457**, 140166.

82 Y. Gu, P. Fang, Y. Chen, T. Xie, G. Yang and L. Qu, *Microchim. Acta*, 2024, **191**, 595.

83 Z. Li, Y. Hu, L. Wang, H. Liu, T. Ren, C. Wang and D. Li, *Sensors*, 2024, **24**, 1093.

84 P. Zhao, H. Sun, F. Gao, L. Yu, K. Shang, M. Fang, B. Ma, X. Tan, S. Wang and X. Wang, *Adv. Funct. Mater.*, 2025, **35**, 2414319.

85 C. Lai, J. Wen, X. Zhang, X. Chen, H. Tang and J. Xiang, *Phys. Scr.*, 2024, **99**, 055016.

86 F. Liang, Y. Huang, J. Miao and K. Lai, *Analyst*, 2024, **149**, 1518–1526.

87 Y. Wang, C. Zhang, R. Yu, Z. Wu, Y. Wang, W. Wang and Y. Lai, *Spectrochim. Acta, Part A*, 2024, **309**, 123794.

88 R. Y. A. Hassan, *Sensors*, 2022, **22**(19), 1–22.

89 S. S. M. Hassan, S. A. M. Marzouk and H. E. M. Sayour, *Talanta*, 2003, **59**, 1237–1244.

90 M. Shamsipur, M. Javanbakht, A. R. Hassaninejad, H. Sharghi, M. R. Ganjali and M. F. Mousavi, *Electroanalysis*, 2003, **15**, 1251–1259.

91 M. R. Ganjali, S. Shirvani-Arani, P. Norouzi, M. Rezapour and M. Salavati-Niasari, *Microchim. Acta*, 2004, **146**, 35–41.

92 V. Dana, E. Pica, E. Fagadar-Cosma, B. Otilia and C. Viorica, *Leonardo Electron. J. Pract. Technol.*, 2006, **5**(9), 5–16.

93 B. Néel, M. Ghahraman Asfhar, G. A. Crespo, M. Pawlak, D. Dorokhin and E. Bakker, *Electroanalysis*, 2014, **26**, 473–480.

94 S. Feng and T. Dong, *Appl. Mech. Mater.*, 2014, **662**, 225–228.

95 R. R. A. Soares, R. G. Hjort, C. C. Pola, D. Jing, V. S. Cecon, J. C. Claussen and C. L. Gomes, *Microchim. Acta*, 2023, **190**, 43.

96 R. Abdellatef, E. Khaled, H. A. Hendawy and R. Y. A. Hassan, *J. Anal. Test.*, 2021, **5**, 341–349.

97 H. Abd El-Raheem, R. Helim, R. Y. A. Hassan, A. F. A. Youssef, H. Korri-Youssoufi and C. Kraiya, *Microchem. J.*, 2024, **207**, 112086.

98 O. Gamal, M. H. Eldin, A. A. Refaat and R. Y. A. Hassan, *Front. Sens.*, 2024, **5**, 1–14.

99 R. H. Mahmoud, F. A. Samhan, M. K. Ibrahim, G. H. Ali and R. Y. A. Hassan, *Electrochem. Sci. Adv.*, 2022, **2**, e2100071.

100 T. Cao, Y. Zhou, H. Wang, R. Qiao, X. Zhang, J. Ruan, J. Cao and Z. Tong, *Mater. Chem. Phys.*, 2022, **289**, 126501.

101 G. Yanalak, Z. Eroglu, S. Yılmaz, S. Z. Bas, O. Metin and I. H. Patir, *Int. J. Hydrogen Energy*, 2023, **48**(38), 14238–14254.

102 A. Wong, A. M. Santos, A. A. Cardenas-Riojas, A. M. Baena-Moncada and M. Sotomayor, *Food Chem.*, 2022, **383**, 132384.

103 W. Gao, *Graphene Oxide: Reduction Recipes, Spectroscopy, and Applications*, 2015, pp. 61–95.

104 B. Aslışen and S. Koçak, *J. Electroanal. Chem.*, 2022, **904**, 115875.

105 P. C. Nethravathi, M. V. Manjula, S. Devaraja, M. Sakar and D. Suresh, *J. Photochem. Photobiol., A*, 2023, **435**, 114295.

106 Mounesh and K. R. Venugopala Reddy, *Anal. Chim. Acta*, 2020, **1108**, 98–107.

107 Mounesh, J. M. Manriquez, K. R. Venugopala Reddy, K. G. Shilpa and B. M. Nagaraja, *Langmuir*, 2023, **39**, 1665–1676.

108 Z.-X. Cai, Z.-L. Wang, J. Kim and Y. Yamauchi, *Adv. Mater.*, 2019, **31**, 1804903.

109 A. D. Ambaye, M. Muchindu, A. Jijana, S. Mishra and E. Nxumalo, *Mater. Today Commun.*, 2023, 105567.

110 P. Cao, Y. Liu, X. Quan, J. Zhao, S. Chen and H. Yu, *Catal. Today*, 2019, **327**, 366–373.

111 E. Saeb and K. Asadpour-Zeynali, *Electrochim. Acta*, 2022, **417**, 140278.

112 V. Mani, A. P. Periasamy and S.-M. Chen, *Electrochem. Commun.*, 2012, **17**, 75–78.

113 A. Kumar, J. M. Gonçalves, A. Sukeri, K. Araki and M. Bertotti, *Sens. Actuators, B*, 2018, **263**, 237–247.

114 T.-E. Chang, C.-H. Chuang and C.-W. Kung, *Electrochem. Commun.*, 2021, **122**, 106899.

115 Y. Li, J. Qian, Y. Zhang, T. Zeng, Q. Wan and N. Yang, *Adv. Sens. Res.*, 2023, 2200014.

116 Z. Yang, X. Zhou, Y. Yin, H. Xue and W. Fang, *J. Alloys Compd.*, 2022, **911**, 164915.

117 S. I. Dorovskikh, D. D. Klyamer, A. D. Fedorenko, N. B. Morozova and T. V. Basova, *Sensors*, 2022, **22**, 5780.

118 D. P. Saraiva, D. V. Braga, B. Bossard and M. Bertotti, *Molecules*, 2023, **28**, 387.

119 N. Rajab, H. Ibrahim, R. Y. Hassan and A. F. Youssef, *RSC Adv.*, 2023, **13**, 21259–21270.

120 F. Zhu, H. Shi, C. Wang, X. Zhou, X. Zhang and F. Yang, *Sens. Actuators, B*, 2021, **332**, 129454.

121 Y. Li, T. Wang, T. Wang, L. Li, J. Gong, L. Zhang and W. Chen, *Mater. Res. Bull.*, 2022, **149**, 111712.

122 Z. Cheng, H. Song, X. Zhang, X. Cheng, Y. Xu, H. Zhao, S. Gao and L. Huo, *Colloids Surf., B*, 2022, **211**, 112313.

123 T. Zhe, M. Li, F. Li, R. Li, F. Bai, T. Bu, P. Jia and L. Wang, *Food Chem.*, 2022, **367**, 130666.

124 G. Manibalan, G. Murugadoss, S. Hazra, R. Marimuthu, C. Manikandan, R. Jothi Ramalingam and M. Rajesh Kumar, *Inorg. Chem. Commun.*, 2022, **135**, 109096.

125 S. M. Sudhakara, M. C. Devendrachari, F. Khan, S. Thippeshappa and H. M. N. Kotresh, *Surf. Interfaces*, 2023, **36**, 102565.

126 G. Chen and J. Zheng, *Microchem. J.*, 2021, **164**, 106034.

127 A. Meng, X. Hong, Y. Zhang, S. Li, L. Sheng and Z. Li, *J. Colloid Interface Sci.*, 2022, **608**, 131–141.

128 A. M. Kumar, A. Khan, M. A. Hussein, M. Y. Khan, H. Dafalla, B. Suresh and S. Ramakrishna, *Prog. Org. Coat.*, 2022, **170**, 106946.

129 Z. Zhao, J. Zhang, W. Wang, Y. Sun, P. Li, J. Hu, L. Chen and W. Gong, *Appl. Surf. Sci.*, 2019, **485**, 274–282.

130 L. Feng, M. Zou, X. Lv, X. Min, X. Lin and Y. Ni, *Microchem. J.*, 2022, **179**, 107508.

131 J. Yin, W. Gao, Z. Zhang, Y. Mai, A. Luan, H. Jin, J. Jian and Q. Jin, *Electrochim. Acta*, 2020, **335**, 135660.

132 M. Annalakshmi, R. Balaji, S.-M. Chen, T.-W. Chen and Y. C. Huang, *Electrochim. Acta*, 2020, **360**, 136797.

133 H.-M. Luo, D. Liu, Q. Gao and L. Xu, *Inorg. Chem. Commun.*, 2020, **118**, 107996.

134 Z. Cai, B. Tu, R. Zhou, D. Xia, H. He, N. Gao, G. Chang and Y. He, *J. Electroanal. Chem.*, 2023, **928**, 117012.

135 J. Zhang, H. Jiang, J. Gao, C. Zhao and H. Suo, *Anal. Chim. Acta*, 2025, **1336**, 343526.

136 K. Promsuwan, P. Kanatharana, P. Thavarungkul and W. Limbut, *Electrochim. Acta*, 2020, **331**, 135309.

137 K. Promsuwan, J. Saichanapan, A. Soleh, K. Saisahas, K. Samoson, C. H. Phua, S. Wangchuk, P. Kanatharana, P. Thavarungkul and W. Limbut, *Electrochim. Acta*, 2022, **436**, 141439.

138 H. S. Magar, R. Y. A. Hassan and A. Mulchandani, *Sensors*, 2021, **21**, 6578.

139 M. E. E. Alahi, N. Afsarimanesh, S. Mukhopadhyay, L. Burkitt and P. L. Yu, *IEEE*, 2016, 1–5.

140 H. Luo, X. Lin, Z. Peng, Y. Zhou, S. Xu, M. Song, L. Jin and X. Zheng, *Front. Chem.*, 2020, **8**, 366.

141 Z. Wang, X. Liu, M. Yang, S. An, X. Han, W. Zhao, Z. Ji, X. Zhao, N. Xia and X. Yang, *Int. J. Electrochem. Sci.*, 2014, **9**, 1139–1145.

142 A. Terbouche, S. Lameche, C. Ait-Ramdane-Terbouche, D. Guerniche, D. Lerari, K. Bachari and D. Hauchard, *Measurement*, 2016, **92**, 524–533.

143 N. Rajab, H. Ibrahim, R. Y. A. Hassan and A. F. A. Youssef, *RSC Adv.*, 2023, **13**, 21259–21270.

144 P. Santharaman, K. A. Venkatesh, K. Vairamani, A. R. Benjamin, N. K. Sethy, K. Bhargava and C. Karunakaran, *Biosens. Bioelectron.*, 2017, **90**, 410–417.

145 H. Liu, K. Guo, J. Lv, Y. Gao, C. Duan, L. Deng and Z. Zhu, *Sens. Actuators, B*, 2017, **238**, 249–256.

146 A. Zazoua, C. Dernane, I. Kazane, M. Belghobsi, A. Errachid and N. Jaffrezic-Renault, *Sens. Lett.*, 2011, **9**, 2283–2286.

147 E. M. Erdoğan, H. Yılmaz, P. Ergenekon, E. Erhan and M. Özkan, *J. Ind. Eng. Chem.*, 2025, **144**, 565–574.

148 F. Shi, J. Geng, B. Wang, B. Mohan, W. Chen, Y. Bi, L. Jiang, S. Deng, S. Wang, X. Li and W. Sun, *Int. J. Electrochem. Sci.*, 2025, **20**, 101126.

149 X. Li, X. Yang, M. Cui, Y. Liu, J. Wang, L. Zhang and G. Zhan, *Sci. Total Environ.*, 2022, **826**, 154178.

150 J. Wang, G. Zhan, X. Yang, D. Zheng, X. Li, L. Zhang, T. Huang and X. Wang, *Biosens. Bioelectron.*, 2022, **215**, 114573.

151 Z. Lin, S. Cheng, H. Li and L. Li, *Sci. Total Environ.*, 2022, **806**, 150945.

152 Z. Lin, S. Cheng, H. Li, B. Jin and X. He, *Biosens. Bioelectron.*, 2022, **214**, 1–8.

153 S. Cheng, Z. Lin, Y. Sun, H. Li and X. Ren, *Water Res.*, 2022, **213**, 118186.

154 S. Cheng, H. Chen, H. Li, L. Li, Y. Lu, B. Jin and X. He, *Environ. Res.*, 2024, **263**, 120093.

155 X. Yang, X. Ye, F. Wang, X. Yang, X. Gao, J. Yu and W. Liu, *ACS Synth. Biol.*, 2025, **14**, 453–462.

156 Q. Fan, Y. Chen, R.-J. Ma, W. Zhou, E. Zhang, X. Zhao, H. Gao, Y.-C. Yong and Z. Fang, *Anal. Chem.*, 2025, **97**(28), 15146–15152.

157 Y. Seo, S. Manivannan, I. Kang, S. W. Lee and K. Kim, *Biosens. Bioelectron.*, 2017, **94**, 87–93.

158 L. Chen, J. Song, L. Wang, X. Hao, H. Zhang, X. Li and J. Wu, *J. Solid State Electrochem.*, 2024, **28**, 305–316.

159 N. Zhang, J. Yang and C. Hu, *Sens. Actuators, B*, 2022, **357**, 131394.

160 O. Salhi, T. Ez-zine, L. Oularbi and M. El Rhazi, *Arab. J. Chem.*, 2022, **15**, 103820.

161 F. Pan, D. Chen, X. Zhuang, X. Wu, F. Luan, S. Zhang, J. Wei, S. Xia and X. Li, *J. Alloys Compd.*, 2018, **744**, 51–56.

162 X. Wang, M. Li, S. Yang and J. Shan, *Electrochim. Acta*, 2020, **359**, 136938.

163 V. Riahifar, N. Haghnazari, F. Keshavarzi and F. Nasri, *Microchem. J.*, 2021, **166**, 106217.

164 S. H. Mohd Taib, K. Shameli, P. Moozarm Nia, M. Etesami, M. Miyake, R. Rasit Ali, E. Abouzari-Lotf and Z. Izadiyan, *J. Taiwan Inst. Chem. Eng.*, 2019, **95**, 616–626.

165 G.-L. Chu, J.-C. Huang, J.-Q. Yin, Y.-M. Guo, M. Li, Y.-Y. Zhang and X. Sun, *Chin. J. Anal. Chem.*, 2021, **49**, 1–9.

166 C. R. Rajith Kumar, V. S. Betageri, G. Nagaraju, G. H. Pujar, B. P. Suma and M. S. Latha, *J. Sci. Adv. Mater. Devices*, 2020, **5**, 48–55.

167 L. Cao, Z. W. Kang, Q. Ding, X. Zhang, H. Lin, M. Lin and D. P. Yang, *Sci. Total Environ.*, 2020, **723**, 138008.

168 R. Mu, D. Zhu and G. Wei, *Biosensors*, 2024, **14**, 258.

169 M. Aldosari and A. Koh, *IOPscience*, 2024, **245**, 2727–2727.

170 H. Guan, Y. Chen, D. Wang, Q. Liu, J. Zhong, Z. Zhang and D. Lü, *Food Chem.*, 2025, **481**, 143971.

171 L. Sun, Z. Zhang, J. Wang and N. Hui, *Bioelectrochemistry*, 2024, **160**, 108786.

172 S. S. M. Ameen and K. M. Omer, *Food Chem.*, 2025, **462**, 141027.

173 O. Ramadan and R. Y. A. Hassan, *Biosens. Bioelectron.: X*, 2025, **23**, 100596.

174 A. Shaikh, B. K. Singh and S. Parida, *Mater. Chem. Phys.*, 2019, **235**, 121744.

175 Y. Zhang, F. Wen, Z. Huang, J. Tan, Z. Zhou, K. Yuan and H. Wang, *J. Electroanal. Chem.*, 2017, **806**, 150–157.

176 R. M. Cardoso, P. R. L. Silva, A. P. Lima, D. P. Rocha, T. C. Oliveira, T. M. do Prado, E. L. Fava, O. Fatibello-Filho, E. M. Richter and R. A. A. Muñoz, *Sens. Actuators, B*, 2020, **307**, 127621.

177 Z. Lin, S. Cheng, H. Li, B. Jin and X. He, *Biosens. Bioelectron.*, 2022, **214**, 114507.

178 A. Pal, M. B. Kulkarni, H. Gupta, R. Ponnalagu, S. K. Dubey and S. Goel, *Sens. Actuators, A*, 2021, **330**, 112896.

179 F. Akhter, H. Siddiquei, M. E. E. Alahi and S. C. Mukhopadhyay, *Measurement*, 2021, **178**, 109424.

180 F. Akhter, H. R. Siddiquei, M. E. E. Alahi, K. P. Jayasundera and S. C. Mukhopadhyay, *IEEE Internet Things J.*, 2021, **9**, 14307–14316.

181 N. Nguyen, K. Nguyen, N. Dinh and N. Tran, *IEEE*, 2022.

182 W.-Y. Son, M.-H. Kang, J. Hwang, J.-H. Kim, Y. Dixit and H.-W. Kim, *Foods*, 2024, **13**, 3173.

183 W. Abbas, F. Zafar, M. F. Abou Taleb, M. Ameen, A. Sami, M. E. Mazhar, N. Akhtar, M. W. Fazal, M. M. Ibrahim and Z. M. El-Bahy, *Food Chem.*, 2024, **460**, 140395.

184 Q. Li, R. Liu, Y. Shang, Y. Wei and H. Cui, *Int. J. Environ. Sci. Technol.*, 2024, **21**, 6653–6662.

185 M. Rafiq, M. Owaes, K. M. Gani, S. Kumari, M. Seyam and F. Bux, *J. Environ. Eng.*, 2025, **151**, 04025033.

186 P. Bai, J. Zhong, Y. Tang and T. Gu, *J. Hazard. Mater.*, 2025, 138460.

187 C. Qiu, F.-q. Huang, Y.-j. Zhong, J.-z. Wu, Q.-l. Li, C.-h. Zhan, Y.-f. Zhang and L. Wang, *Environ. Technol.*, 2025, **46**, 1959–1980.

188 J. M. Navarro, A. El Aatik, A. Pita, R. Martinez and N. Vela, *IEEE Sens. J.*, 2024, **25**(4), 7145–7153.

189 M. G. Butinyac, V. A. Montaño, J. Downes, N. M. Ruane, E. Ryder, F. Egan, T. Staessen, B. Paull and E. Murray, *Aquac. Int.*, 2024, **32**, 1013–1026.

190 A. Pal, S. K. Dubey and S. Goel, *Comput. Electron. Agric.*, 2022, **195**, 106856.

191 H. Ye, Y. Yang, T. Zhe, M. Lan, L. Jiang and L. Zeng, *SSRN*, 2024, 4971643.

192 A. N. S. Cadeado, C. C. S. Machado, M. Q. Costa and S. G. Silva, *Microchem. J.*, 2022, **183**, 108138.

193 J. Feng, H. Li, J. Zhang, L. Yu, M. Deng and J. Xu, *Environmental Crisis: Pollution and Governance*, 2025, (2024), 118–125.

194 M. Liang, Y. Gao, X. Sun, R.-M. Kong, L. Xia and F. Qu, *J. Hazard. Mater.*, 2024, **469**, 134021.

195 X. Zhao, Y. Lu, J. Wu, Y. Yang, B. Li, H. Li, Y. Sun, X. Yan, X. Liu and G. Lu, *Biosens. Bioelectron.*, 2024, **263**, 116622.

196 H. Ye, Y. Yang, L. Jiang, T. Zhe, J. Xu and L. Zeng, *Chin. Chem. Lett.*, 2025, 110840, DOI: 10.1016/j.cclet.2025.110840.

197 J. Xiao, J. Tang, J. Chen, L. Li, S. Zhang, X. Xiong and Z. Zou, *Sens. Actuators, B*, 2024, **400**, 134914.

198 P. Das, S. Biswas, S. S. Bhattacharya and P. Nath, *ACS Appl. Nano Mater.*, 2022, **5**, 3265–3274.

199 Z. Pei, Z. Cai, J. Meng, Y. Bai, W. Cai and S. Fan, *Electronics*, 2024, **13**, 85.

200 L. R. G. Silva, D. R. Santos-Neto, J. S. Stefano, D. H. de Oliveira, L. S. da Silva, H. S. Pittner, C. L. Handa, R. A. A. Muñoz and D. P. Rocha, *Talanta Open*, 2025, **11**, 100443.

201 P. Tiawpisitpong, T. Warisson, C. Pinyorospathum and K. Charoenkitamorn, *Microchem. J.*, 2024, **207**, 112130.

202 P. Kusonpan, K. Kunpatee, O. Chailapakul, K. Kalcher, A. Ortner, S. Chaiyo and A. Samphao, *Talanta*, 2025, **292**, 127919.

203 S. Madani and A. Hatamie, *Langmuir*, 2024, **40**, 25580–25589.

204 I. E. Mikhail, E. Murray, S. Bluett, S. Astrakhantseva and B. Paull, *Anal. Chim. Acta*, 2024, **1304**, 342557.

205 K. Debruille, Y. Mai, P. Hortin, S. Bluett, E. Murray, V. Gupta and B. Paull, *Anal. Chim. Acta*, 2024, **1304**, 342556.

206 H. Y. Zhang, Y. Zhang, D. Lai, L. Q. Chen, L. Q. Zhou, C. L. Tao, Z. Fang, R. R. Zhu, W. Q. Long, J. W. Liu, Y. C. Fang, J. Zhao, Z. B. Wu, L. Luo and Y. Yang, *Anal. Methods*, 2025, **17**, 5683–5696.

207 S. Zheng, H. Li, T. Fang, G. Bo, D. Yuan and J. Ma, *Sci. Total Environ.*, 2022, **815**, 152613.

208 T. Fang, H. Li, G. Bo, K. Lin, D. Yuan and J. Ma, *Microchem. J.*, 2021, **165**, 106117.

209 Y. Zhan, H. Lin, J. Xiang, B. Zhang, Z. Zhao, J. Lin, J. Li and Y. Cheng, *Microchem. J.*, 2025, **215**, 114365.

210 K. Khachornsakkul, R. Del-Rio-Ruiz, H. Creasey, G. Widmer and S. R. Sonkusale, *ACS Sens.*, 2023, **8**, 4364–4373.

211 T. Liu, J. Huang, Z. Lin, C. Zhan, D. Yi and S. Wang, *IEEE Sens. J.*, 2022, **22**, 21111–21118.

212 H. Bharwani, S. Kapur and S. G. Palani, *RSC Adv.*, 2025, **15**, 1577–1589.

213 M.-h. Zeng, C. Zhang, Q.-h. Yao, J.-w. Jin, T.-X. Ye, X.-m. Chen, Z.-y. Guo and X. Chen, *Sens. Actuators, B*, 2024, **405**, 135352.

214 J. Wei, J. Xu, C. Wang, Y.-F. Yang, Y. Zhang, R. Ni, Y.-Q. Xu, D. Huang and L. Li, *Chem. Eng. J.*, 2025, **515**, 163808.

215 V. S. Siu, M. Lu, K. Y. Hsieh, B. Wen, I. Buleje, N. Hinds, K. Patel, B. Dang and R. Budd, *Biosensors*, 2024, **14**(2), 1–13.

216 V. S. Siu, M. Lu, K. Y. Hsieh, K. Raines, Y. A. Asaad, K. Patel, A. Afzali-Ardakani, B. Wen and R. Budd, *ACS Omega*, 2022, **7**, 11126–11134.

217 S. Paramasivam, S. Mariappan, N. Sethy and P. Manickam, *Mater. Adv.*, 2023, **4**(23), 6223–6232.

218 T. W. Pittman, D. B. Decsi, C. Punyadeera and C. S. Henry, *Theranostics*, 2023, **13**, 1091–1108.

219 C. Zhao, R. Shi, J. Wu, X. Luo and X. Liu, *Biosensors*, 2021, **11**, 223.

220 W.-T. Tseng, Y.-Y. Chou, J.-G. Wu, Y.-C. Wang, T.-N. Tseng, S.-W. Pan, S.-C. Luo and M.-L. Ho, *Microchem. J.*, 2023, **188**, 108493.

221 L. Stephenson, S. Wills, C. van den Heuvel, M. Humphries and R. W. Byard, *Forensic Sci. Med. Pathol.*, 2022, **18**, 311–318.

222 M. Kim, S. Kim, W. Yang and J. Sim, *Forensic Sci. Int.*, 2022, **335**, 111279.

223 M. Tomsia, M. Głaz, J. Nowicka and M. Szczepański, *Journal of forensic and legal medicine*, 2021, **81**, 102186.

224 L. Sun, H. Zhang, Y. Wang, Z. Xiong, X. Zhao and Y. Xia, *Spectrochim. Acta, Part A*, 2021, **251**, 119468.

225 H. Wang, F. Wen, Y. Chen, T. Sun, Y. Meng and Y. Zhang, *Biosens. Bioelectron.*, 2016, **85**, 692–697.

226 G. Ning, P. Mu, B. Li, J. Liu, Q. Xiao and S. Huang, *Microchim. Acta*, 2022, **189**, 230.

227 S. S. Mohammed Ameen, F. Algethami and K. M. Omer, *Microchim. Acta*, 2025, **192**, 146.

228 A. Puspalak, P. Chinnadurai, R. Prathibha, M. P. Kumar, S. G. Manjushree, V. UdayaKumar and P. S. Adarakatti, *Mater. Res. Innovations*, 2023, **27**, 100–109.

229 A.-M. Gurban, L.-G. Zamfir, P. Epure, I.-R. Şuică-Bunghez, R. M. Senin, M.-L. Jecu, M. L. Jinga and M. Doni, *Chemosensors*, 2023, **11**, 224.

230 B. U. Gauthama, B. Narayana, B. K. Sarojini, K. Bello and N. K. Suresh, *SN Appl. Sci.*, 2020, **2**, 1225.

231 D. F. Malley, C. McClure, P. D. Martin, K. Buckley and W. P. McCaughey, *Commun. Soil Sci. Plant Anal.*, 2005, **36**, 455–475.

232 Z. Wang, Y. Wan, Y. Zhang, B. Zhang, M. Li, X. Jin, T. Yang and G. Meng, *J. Hazard. Mater.*, 2024, **472**, 134492.

233 Y. Zhao, Y. Feng, L. Liu, Q. Wan, Z. Guo, J. Lei, W. Wang, F. Liu, Q. Duan and J. Lee, *J. Soils Sediments*, 2024, **24**, 1694–1703.

234 M. I. Hossain, M. A. Khaleque, M. R. Ali, M. S. Bacchu, M. S. Hossain, S. M. F. Shahed, M. A. Saad Aly and M. Z. H. Khan, *RSC Adv.*, 2024, **14**, 9137–9158.

235 Y. Mai, A. Ghiasvand, V. Gupta, S. Edwards, S. Cahoon, K. Debruille, I. Mikhail, E. Murray and B. Paull, *Talanta*, 2024, **274**, 126031.

236 W.-X. Ji, Y.-C. Tian, M.-H. Cai, B.-C. Jiang, S. Cheng, Y. Li, Q. Zhou, B.-Q. Li, B.-Y. Chen, X. Zheng, W.-T. Li and A.-M. Li, *J. Environ. Sci.*, 2023, **125**, 309–318.

237 D. Pjetraj, M. E. Mechri, S. Bacelli, E. Fabiani, L. Caponi, S. Gatti and E. Lionetti, *Ital. J. Pediatr.*, 2025, **51**, 53.

238 W. Wang, M. Li, P. Chen, S. Yuan, K. Wang, S. Wang and X. Jiang, *Environ. Rev.*, 2025, **33**, 1–10.

239 S. Ojha, G. Jairath, S. Bishnoi, G. Mal, M. Verma, M. Gangwar, N. Chauhan and A. K. Pathera, in *Healthier Meat Products*, ed. A. Kumar Pathera, H. Kumar and S. Yadav, Springer Nature Switzerland, Cham, 2025, pp. 373–395, DOI: 10.1007/978-3-031-78215-2_18.

240 M. Kim, S. M. Bae, Y. Yoo, J. Park and J. Y. Jeong, *Foods*, 2025, **14**, 2442.

241 O. Adebanjo-Aina and O. Oludoye, *Pollutants*, 2025, **5**, 21.

242 Y. Yang, X. Wang, Y. Wu, F. Li, Z. Maletskyi, S. Chen, M. Tang and Z. Song, *J. Water Proc. Eng.*, 2025, **72**, 107422.

243 A.-V. Luca, M. Simon-Várhelyi, N.-B. Mihály and V.-M. Cristea, *Environ. Monit. Assess.*, 2025, **197**, 121.

244 J. T. Trimmer, C. Delaire, K. Marshall, R. Khush and R. Peletz, *Environ. Sci. Technol.*, 2024, **58**, 11236–11246.

245 B. Panea and G. Ripoll, *Foods*, 2020, **9**, 803.

246 E. Najdenko, F. Lorenz, K. Dittert and H.-W. Olfs, *Precis. Agric.*, 2024, **25**, 3189–3218.

247 M. Kok, S. Sarjant, S. Verweij, S. F. C. Vaessen and G. H. Ros, *Geoderma*, 2024, **446**, 116903.

248 K. Zhang, Z. Ye, M. Qi, W. Cai, J. L. Saraiva, Y. Wen, G. Liu, Z. Zhu, S. Zhu and J. Zhao, *Rev. Aquacult.*, 2025, **17**, e12985.

249 D.-D. Bian, Y.-X. Shi, X. Zhang, X. Liu, J.-J. Jiang, X.-R. Zhu, D.-Z. Zhang, Q.-N. Liu, B.-J. Zhu and B.-P. Tang, *Rev. Aquacult.*, 2025, **17**, e70062.

250 J. S. Schmitt and L. D. Knight, *Am. J. Forensic Med. Pathol*, 2024, **45**(3), 210–214.

251 D. Andelhofs, W. Van Den Bogaert, B. Lepla, K. Croes and W. Van de Voorde, *Forensic Sci. Med. Pathol.*, 2024, **20**, 949–964.

252 A. E. Cozens, S. D. Johnson and T. C. Lee, *Front. Chem.*, 2025, **13**, 1568867.

253 M. Taghavi, A. Abedi, A. Alami, M. Qasemi and A. Zarei, *Sci. Rep.*, 2025, **15**, 9321.

254 M. Dettori, A. Arghittu, G. Deiana, P. Castiglia and A. Azara, *Environ. Res.*, 2022, **209**, 112773.

255 S. Susmel, F. Girolametti, V. Fonti, F. Figueredo, V. Scognamiglio, A. Antonacci, V. Manna, J. Bilić, V. Soljan, N. De Bortoli, T. Martin, M. Mion, T. Kekez, R. Andricevic, S. Ben Aissa, M. Celussi and A. Annibaldi, *Water*, 2022, **14**, 2460.

256 J. R. G. Molina, J. M. Frías-Celayeta, D. J. Bolton and C. Botinestean, *Foods*, 2024, **13**, 746.

257 R. Owusu-Apenten and E. Vieira, in *Elementary Food Science*, ed. R. Owusu-Apenten and E. R. Vieira, Springer International Publishing, Cham, 2023, pp. 355–376, DOI: 10.1007/978-3-030-65433-7_16.

258 M. Preisner, E. Neverova-Dziopak and Z. Kowalewski, *Ambio*, 2021, **50**, 413–424.

259 P. Krasilnikov, M. A. Taboada and Amanullah, *Agriculture*, 2022, **12**, 462.